ALGORITHMS FOR INVERTING HODGKIN-HUXLEY TYPE NEURON MODELS

A Thesis
Presented to
The Academic Faculty

by

Dylan Shepardson

In Partial Fulfillment
of the Requirements for the Degree
Doctor of Philosophy in
Algorithms, Combinatorics, and Optimization

Algorithms, Combinatorics, and Optimization
Georgia Institute of Technology
December 2009

ALGORITHMS FOR INVERTING HODGKIN-HUXLEY TYPE NEURON MODELS

Approved by:

Professor Craig Tovey, Advisor
School of Industrial and Systems Engineering
Georgia Institute of Technology

Professor Astrid Prinz
Department of Biology
Emory University

Professor Rob Butera
Department of Electrical and Computer Engineering and Laboratory for Neuroengineering
Georgia Institute of Technology

Professor Joel Sokol
School of Industrial and Systems Engineering
Georgia Institute of Technology

Professor Arkadi Nemirovski
School of Industrial and Systems Engineering
Georgia Institute of Technology

Date Approved: August 18, 2009

To my parents, and my brother

ACKNOWLEDGEMENTS

Many thanks to the members of my thesis committee, Craig and Gail Tovey, Gary Parker, Rebeca Sandino, Sean Alu, Burak Karacik, David Lewis, Kapil Gupta, Richa Agarwal, Ashlea Bennett, Clarence Wardell, Daniel Dadush, Randy Shepardson, Amy Adams, Ashwini Bhatia, Tom Eagan, Maggie Villiger, Heidi Rosbe, Alelia Parenteau, Hung-Chung Fang, Buzzy Spain, Heather Laird, Theresa Hwang, Brett Shepardson, and my parents.

TABLE OF CONTENTS

LIST OF TABLES

LIST OF FIGURES

SUMMARY

The study of neurons is of fundamental importance in biology and medicine. Neurons are the most basic unit of information processing in the nervous system of humans and all other vertebrates, and in complex invertebrates. Besides their importance for biology and medicine, networks of neurons (the human brain) are the most sophisticated computational devices known, and the study of neurons individually and working in concert is seen as a step toward understanding consciousness and cognition.

In the 1950's A.L. Hodgkin and A.F. Huxley developed a system of nonlinear ordinary differential equations to describe the behavior of a neuron found in the squid. Equations of this form have since been used to model the behavior of a multitude of neurons and other excitable cells across a broad spectrum of species. Hodgkin-Huxley type neuron models helped lay the foundation for computational neuroscience, and they remain widely used in the study of neuron behavior more than half a century after their development.

Hodgkin-Huxley type models accept a set of parameters as input and generate data describing the electrical activity of the neuron as a function of time. We develop inversion algorithms designed to predict a set of input parameter values from the voltage trace data generated by the model. We test our algorithm on data from the Hodgkin-Huxley equations, and we extend the algorithm to solve the inverse problem associated with a more complex Hodgkin-Huxley type model for a lobster stomatogastric neuron. We find strong empirical evidence that the algorithms produce parameter values that generate a good fit to the target voltage trace, and we

prove that under certain conditions the inversion algorithm for the Hodgkin-Huxley equations converges to a perfect match. To our knowledge this is the first parameter optimization procedure for which convergence has been shown theoretically.

Understanding the relationship between the parameters of a neuron model and its output has important implications for designing effective neuron models (where parameters must be selected to give desired behavior), as well as for explaining the mechanisms by which neurons regulate their behavior. Inversion algorithms for Hodgkin-Huxley type neuron models are an important theoretical and practical step toward understanding the relationship between model parameters and model behavior, and toward the larger problem of inferring neuronal parameters from behavior patterns observed experimentally.

CHAPTER I

INTRODUCTION

The study of neurons is of fundamental importance in biology and medicine, as they play a major role in the transmission of information in living organisms. Neurons are the fundamental unit of information processing in the nervous system of humans and all other vertebrates, and in complex invertebrates like arthropods and worms. Besides their importance for biology and medicine, networks of neurons (the human brain) are the most sophisticated computational devices known, and the study of neurons individually and working in concert is seen as a step toward understanding consciousness and cognition.

The neuron functions by maintaining a voltage difference across its cell membrane. (This transmembrane voltage difference is also called the membrane potential.) Rapid changes in this voltage difference can be initiated in response to external stimuli, including chemical or electrical signals, for example from other neurons, or from photoreceptor cells in the retina. Some neurons also exhibit spontaneous activity, firing regular patterns of electrical impulses even in the absence of external stimulus. Spikes in the transmembrane voltage difference propagate down the length of the neuron (the axon) at a rate of approximately 20 meters per second, allowing rapid transmission of information over macroscopic distances inside an organism.

Despite having been studied by generations of scientists, the detailed processes by which even a single neuron operates are still the subject of intense research. In recent decades, advances in mathematical modeling techniques and computational resources have allowed neuroscientists to begin studying neurons using computer models and simulation while continuing to study actual neurons using increasingly sophisticated

biological, physical, and chemical tools.

1.1 The Hodgkin-Huxley equations and neuronal modeling

Since the 1950's, when A.L. Hodgkin and A.F. Huxley developed a system of equations describing the electrical activity of the squid giant axon [16], neuroscientists have been equipped with a powerful theoretical framework for studying neuronal function and behavior.

Not only are the equations broadly applicable to many classes of neurons, but the internal dynamics of the Hodgkin-Huxley model in many ways closely mirror the physiology of the neuron, making these equations useful tools for studying the mechanisms behind neuronal behavior. Due to the difficulty of working with living neurons, computational neuroscience has become an increasingly important tool for the study of neuronal physiology and behavior in the decades since the development of the Hodgkin-Huxley model.

The fundamental insight of Hodgkin and Huxley, reached after an ingenious series of experiments on the giant axon of the squid, was that the neuronal cell membrane has independent permeability mechanisms for different types of ions, and that the membrane's conductance for each type of ion is a function of time and the transmembrane voltage. Hodgkin and Huxley reproduced the experimental data obtained from the squid giant axon with a quantitative model consisting of a system of nonlinear ordinary differential equations which, given data specifying the internal state of the neuron and its initial conditions, can be solved numerically to simulate the electrical activity of the neuron. The model of Hodgkin and Huxley was the first complete description of the excitability of a single cell [14]. The equations of Hodgkin and Huxley are the basis for almost all ionic current-based neuronal models, and extensions of these equations have been successfully used in the study of neurons playing diverse physiological roles across a broad spectrum of species.

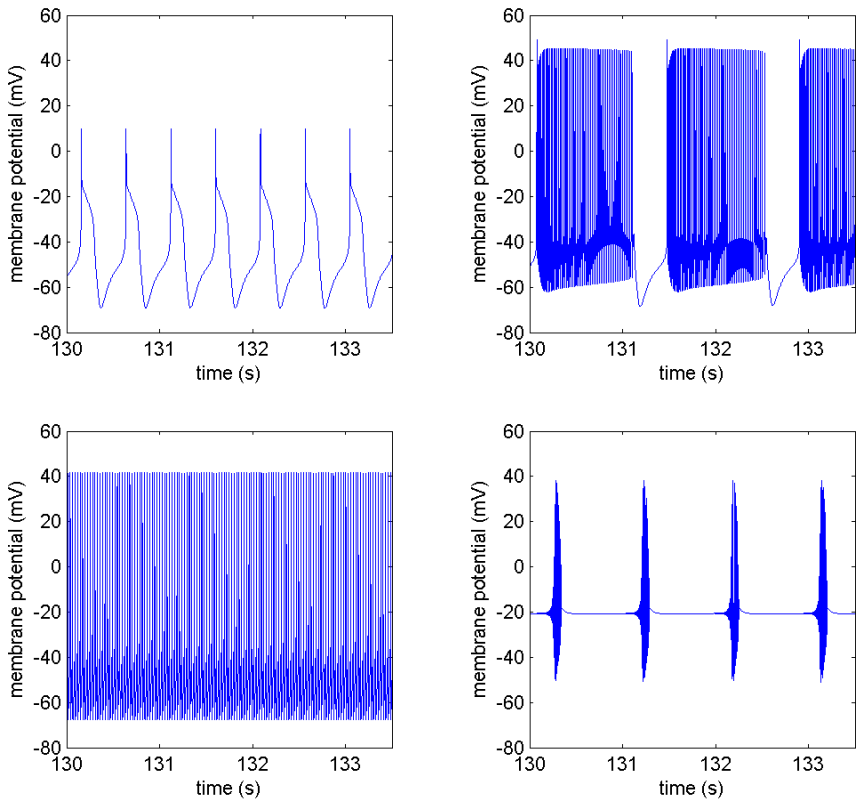

Figure 1: Sample neuron behavior: four voltage traces generated by the same neuron model with different parameter values.

The Hodgkin-Huxley model takes as input a set of parameters specifying the properties of the neuron and outputs a "voltage trace" which gives the voltage difference across the neuron's cell membrane (the membrane potential) as a function of time. A typical Hodgkin-Huxley type neuron model is capable of distinct types of behavior depending on the parameters chosen. Figure 1 shows voltage traces produced by the Hodgkin-Huxley type model for a lobster stomatogastric (STG) neuron introduced in Chapter 3 for four different sets of parameter values.

1.2 Parameter selection

One of the difficulties associated with studying neurons using mathematical models is fixing the parameters of the model to produce the desired behavior. Parameters of neuronal models generally represent physical quantities (for example conductance,

capacitance, or voltage) that can be measured experimentally, but it is almost never the case that all of the parameters needed to specify a neuron model can be measured from the same experimental preparation. In the past, model parameters have been selected by averaging over measurements taken from many neurons of the same type from different animals, or by fixing subsets of the parameters to the measured values obtained from several different animals [23].

Neurons have considerable variability in their internal structure, and neurons of the same type can have very different parameter values [20]. Golowasch et al. showed that building a complete set of model parameters by averaging over measurements taken from many neurons or combining subsets of parameter values measured from different neurons is unreliable for reproducing target behavior [10].

The predominant method for selecting parameters to produce desired behavior in a Hodgkin-Huxley type neuron model is hand-tuning the parameters of the model to obtain a voltage trace resembling the target voltage trace. Besides being difficult, subjective, and time-intensive, there are no guarantees of optimality attached to the solutions found, and failure to find a good set of parameters does not necessarily imply that none exists. Automated alternatives to hand-tuning have been proposed, including evolutionary algorithms [1], gradient descent algorithms [2, 30], algorithms based on bifurcation analysis [11, 12, 30], and systematic exploration of parameter space either by stochastic search [8, 9, 10] or grid search [9, 24]. These studies are discussed in Section 2.2.2. There is currently no widely used alternative to hand-tuning for selecting parameters to give desirable model behavior, and research into automated parameter selection methods is ongoing.

1.3 Inversion of the equations of Hodgkin-Huxley type neuron models

We propose a novel automated technique for selecting parameters to reproduce a given pattern of behavior obtained from the Hodgkin-Huxley equations. We treat the

Hodgkin-Huxley equations as a function that maps a set of parameters to a "voltage trace" that describes the membrane potential of the neuron as a function of time, so that solving the Hodgkin-Huxley equations for a given set of parameters (in practice this means numerically integrating) yields a voltage trace. We develop algorithms for the inverse problem: given a voltage trace from the Hodgkin-Huxley equations, find a set of parameters that generates it.

We test our algorithms on data from the Hodgkin-Huxley equations, and we extend the algorithm to solve the inverse problem associated with a more complex Hodgkin-Huxley type model for a lobster stomatogastric neuron. We find strong empirical evidence that the algorithms produce parameter values that generate a good fit to the target voltage trace, and we prove that under certain conditions the inversion procedure for the Hodgkin-Huxley equations converges to a perfect match. To our knowledge this is the first parameter optimization procedure for which convergence has been shown theoretically.

Algorithms for inverting the equations of Hodgkin-Huxley type neuron models contribute to an understanding of the relationship between neuron behavior (voltage traces) and the parameter space of the neuronal models. Besides its importance for the problem of choosing parameters to obtain a desired model behavior, a detailed understanding of the relationship between the parameters of the model and its behavioral output may be important for answering questions about the mechanisms by which neurons regulate their behavior. Neurons must maintain stable behavioral patterns in a changing environment, and it has been suggested that the parameters governing the maximal membrane conductance to various ions play a central role in the process by which neurons maintain homeostatic equilibrium [19]. Over the past 15 years, many studies have explored the relationship between these maximal conductance values and model neuron behavior [1, 8, 9, 10, 19, 24] by parameter space

exploration. Our inversion algorithms give a direct method for finding a set of maximal conductance parameters to match model neuron behavior, moving us toward an improved understanding of the theoretical relationship between neuronal behavior and the parameters that specify a neuronal model. Finally, algorithms to invert the equations of Hodgkin-Huxley type neuron models represent a step toward the larger problem of inferring the values of neuronal parameters from neuron behavior recorded experimentally.

CHAPTER II

ALGORITHMS FOR INVERTING THE HODGKIN-HUXLEY MODEL

In their 1952 paper [16], Hodgkin and Huxley present a differential equation-based model describing the electrical behavior of the squid giant axon. The model is the culmination of a series of experiments performed on the squid giant axon which indicated that the cell membrane's conductance to ions present in the intracellular and extracellular fluid of the nerve cell is variable over time and voltage-dependent. The squid giant axon is capable of initiating and propagating "action potentials", spikes in the transmembrane voltage difference that are triggered when the voltage difference across the cell membrane reaches a critical threshold level. These electrical impulses enable neurons to transmit information rapidly over large distances and play a major role in neuronal signaling. The squid giant axon was chosen because its unusually large size (it has a length of several centimeters and a diameter of approximately 0.5 mm, much larger than that of most axons) made it ideal for experimental work. The model developed by Hodgkin and Huxley accurately simulates the initiation and propagation of action potentials in the squid giant axon, and the form of the equations has proven to accurately represent the biophysical mechanisms underlying neuronal function. The system of equations developed by Hodgkin and Huxley for the squid giant axon has been shown to be broadly applicable and has been used as the basis for almost all ionic current models of neurons and other excitable cells. The Hodgkin-Huxley equations have been adapted and extended for the study of myelinated axons, striated muscle fibers, and cardiac fibers. The model has been called "the most important model of nerve conduction" [6], and in 1963 Hodgkin and Huxley shared the

Nobel Prize for Physiology and Medicine with John Eccles in recognition of their work.

The neuron, via active transport mechanisms that expend energy to transport ions across the cell membrane, maintains a voltage difference (also called the "membrane potential") across the cell membrane that separates the cytoplasm inside the cell from the extracellular fluid. The sodium-potassium pump, an enzyme found in the cell membrane, is one such active transport mechanism, moving three Na^+ ions out of the cell and two K^+ ions into the cell in each pumping cycle. The net outflow of positive charge under the action of the sodium-potassium pump sets up a steady-state transmembrane voltage difference (the "resting potential") with the inside of the cell electronegative compared to the cell's surroundings. Active transport of ions across the cell membrane also leads to ionic concentration imbalances across the cell membrane. In the intracellular fluid, for example, the concentration of Na^+ ions tends to be lower and the concentration of K^+ ions tends to be higher than in the extracellular fluid as a result of the continuous action of the sodium-potassium pump. The membrane resting potential and the ionic concentration imbalances are the driving forces behind the action potential, allowing the neuron to respond rapidly to stimuli that cause the membrane to become permeable to the flow of ions.

The cell membrane contains many different ionic current pathways ("ion channels") that, when open, allow transmembrane flow of ions of a specific type. These ion channels are "voltage-gated", opening and closing in response to the voltage difference across the cell membrane. Ions flow through these channels in response to electrostatic pressure due to the membrane potential, as well as pressure resulting from intracellular/extracellular concentration imbalances set up by active transport. For each ion there is a "reversal potential" at which these two pressures are balanced and there is no net transmembrane flow. A typical neuron will have several distinct

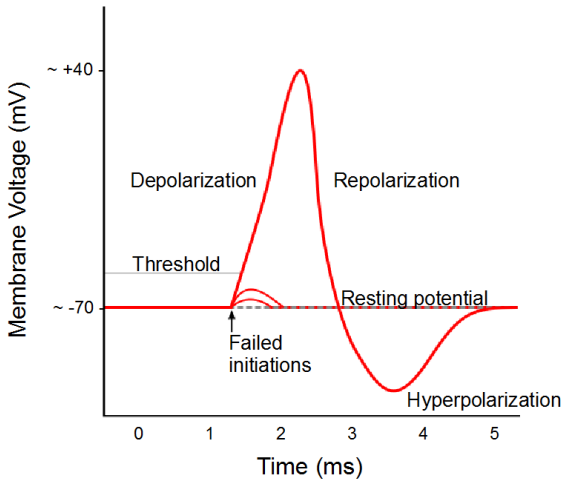

Figure 2: Action potential schematic

types of voltage-gated ion channels, and the interaction between these channels allows an individual neuron to exhibit a range of behaviors, either spontaneously or in response to external stimuli. Ions carry charge, and their flow across the cell membrane influences the membrane potential and hence (via the opening and closing of voltage-gated ion channels) the conductance of the cell membrane to ions of the same type and other types. This enables an intricate system of feedback loops that underlies the neuron's electrical activity. Appendix A shows several examples of behavior generated by a lobster stomatogastric neuron model presented in Chapter 3. This is a Hodgkin-Huxley type model that (unlike the original Hodgkin-Huxley model) exhibits spontaneous activity in the absence of external stimuli.

The neuron's firing of action potentials is central to its role in the rapid transmission of information. An action potential is an all-or-nothing event initiated when the membrane potential rises to a critical threshold value. Figure 2 gives a schematic representation of a neuron action potential. As the membrane potential rises, voltage-gated sodium channels open, allowing Na^+ ions to rush inward in response to electrostatic pressure from the transmembrane voltage difference and diffusion pressure from the transmembrane Na^+ concentration imbalance. The inrush of positively charged

ions drives the membrane potential upward toward zero (the cell becomes further "depolarized", in the parlance of neuroscientists) further increasing the membrane's conductance to Na^+ and creating the conditions for a positive feedback loop. Voltage rises rapidly until, near the peak of the action potential, sodium channels are maximally open, sodium conductance nears its maximal value, and the membrane potential approaches the sodium reversal potential. Potassium channels, which operate on a slower time scale, open later than sodium channels and remain open longer. The outflow of positive charge from K^+ ions leaving the cell in response to the combined diffusion pressure and electrostatic pressure eventually counters the voltage increase due to the incoming Na^+ and the neuron "repolarizes", with the voltage dropping toward the potassium reversal potential and the neuron's resting potential. There is often a brief period of "hyperpolarization" as the neuron overshoots its resting potential. The action of the sodium-potassium pump returns the neuron to its resting state, with an intracellular excess of K^+ and deficit of Na^+. Figure 5 shows the sodium and potassium membrane currents during a simulated action potential for the Hodgkin-Huxley model.

This is a general description of the processes underlying an the action potential as described in the Hodgkin-Huxley model. In biological neurons, there is considerable variability in the ionic current pathways present. Newly developed ionic current-based models tend to be more complicated than the original Hodgkin-Huxley model (we will explore one such model in later chapters), but the form of the underlying equations and the processes they describe generally follow the model developed by Hodgkin and Huxley quite closely.

2.1 Hodgkin-Huxley equations

In a series of experiments, Hodgkin and Huxley deduced that the ionic membrane conductances are variable with time and voltage-dependent, and gave the form of

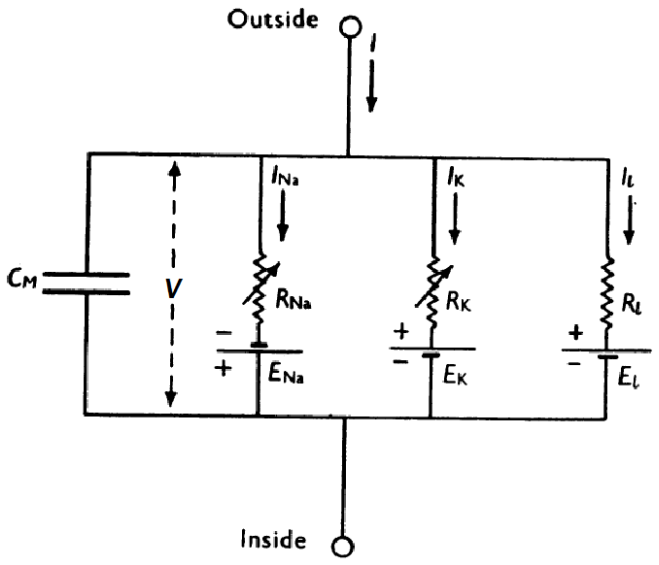

Figure 3: Equivalent circuit for Hodgkin-Huxley model of the squid giant axon, from [16]. $R_{Na} = 1/g_{Na}$, $R_K = 1/g_K$, and $R_L = 1/g_L$. All other quantities are constant.

this voltage-dependence. By treating a segment of the axon as a simple electrical circuit (Figure 3), Hodgkin and Huxley arrived at equations describing the electrical activity of the axon.

The cell membrane, which separates the extracellular medium from the cytoplasm of the cell, acts as a capacitor with capacitance C (Hodgkin and Huxley used a value, based on laboratory measurement, of 10 μF/cm^2 for C). The ionic current channels offer parallel pathways by which charge can pass through the cell membrane. Hodgkin and Huxley use three ionic currents in their description of the squid giant axon; potassium current I_K, sodium current I_{Na}, and a leakage current I_L. The potassium and sodium currents have variable resistances that represent the voltage-gated conductances associated with the membrane ion channels. The total current I is the sum of the ionic currents and the capacitative current which represents the rate of accumulation of charge on opposite sides of the cell membrane. The capacitative current, from electrical circuit theory, is $C\frac{dv}{dt}$, where v is the membrane potential. Hodgkin and Huxley take $v = 0$ to represent the neuron's resting potential, and the

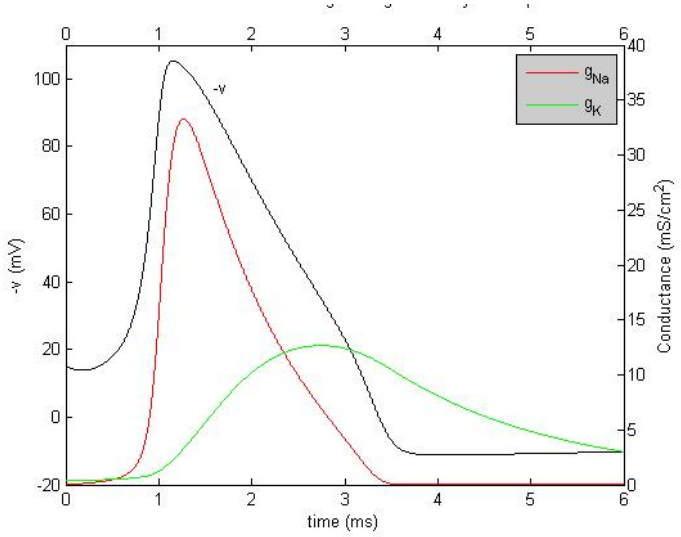

Figure 4: Membrane conductances during a Hodgkin-Huxley action potential. g_L (not shown) is constant.

equations below follow this convention.

$$I = C\frac{dv}{dt} + I_{Na} + I_K + I_L \tag{1}$$

The ionic currents are given by Ohm's law ($I = gV$):

$$\begin{aligned} I_{Na} &= g_{Na} \cdot (v - E_{Na}), \\ I_K &= g_K \cdot (v - E_K), \\ I_L &= g_L \cdot (v - E_L), \end{aligned} \tag{2}$$

where E_{ion} is the reversal potential, and g_{ion} is the ionic membrane conductance. These conductances, in the case of the sodium and potassium currents, are variable and voltage-dependent, representing the voltage-gating of the ion channels. Hodgkin and Huxley deduced from experiment the following forms for the ionic membrane conductances:

$$\begin{aligned} g_{Na} &= x_1 m^3 h, \\ g_K &= x_2 n^4, \\ g_L &= x_3. \end{aligned} \tag{3}$$

Table 1: Parameter values used by Hodgkin and Huxley

Ionic current	Reversal potential (mV)	Maximal conductance (mS/cm^2)
Sodium	$E_{Na} = -115$	$x_1 = 120$
Potassium	$E_K = 12$	$x_2 = 36$
Leakage	$E_L = -10.613$	$x_3 = 0.3$

Here x_1, x_2, and x_3 are the maximal conductance values for the sodium ionic current, the potassium ionic current, and the leakage current, respectively. These quantities are constant. The sodium conductance is controlled by an "activation variable" $m(v,t)$ and an "inactivation variable" $h(v,t)$. The potassium conductance is controlled by an activation variable $n(v,t)$. The variables m, h, and n are each functions of the membrane potential v and vary with time, taking values in the range $[0,1]$. These activation and inactivation variables model the degree to which the relevant ion channels are open. The time course of the membrane conductance to sodium and potassium ions during a Hodgkin-Huxley action potential is shown in Figure 4.

A physical interpretation of the activation and inactivation variables is to consider a sodium ion channel as being open if three independent events of probability m occur simultaneously. The channel is considered blocked if an additional independent event of probability $1-h$ occurs. Accordingly, a sodium channel is considered open and unblocked (activated) with probabability m^3h. The maximal conductance value x_{Na}, determined experimentally by Hodgkin and Huxley, gives the conductance of the membrane to Na^+ ions when all sodium ion channels are activated. A similar interpretation applies to the equation governing the membrane's conductance to potassium ions. Four independent events of probability n must each occur for an ion channel to be open. In the case of potassium channels there is no inactivation variable and no additional blocking mechanism associated with the channels, and a potassium channel is activated with probability n^4. The conductance for the leakage current is constant.

Under this physical interpretation, the three events of probability m that lead

to the opening of a sodium ion channel could involve voltage-driven changes in the conformation of the channel, and an independent voltage-driven change in the conformation of the channel could lead with probability h to the sodium ion channel being blocked. Hodgkin and Huxley, in proposing the model, suggest that "potassium ions can only cross the membrane when four similar particles occupy a certain region of the membrane" [16], basing their speculation on the form of the equations. This physical interpretation is meant to provide insight into the mechanics of the model, but not to give an accurate description of the physiological mechanisms of the voltage-gated ion channels.

The activation and inactivation variables are time-dependent as the membrane potential varies with time, and their values are governed by first-order differential equations:

$$\begin{aligned} \frac{dm}{dt} &= \alpha_m(v)(1-m) - \beta_m(v)m, \\ \frac{dn}{dt} &= \alpha_n(v)(1-n) - \beta_n(v)n, \\ \frac{dh}{dt} &= \alpha_h(v)(1-h) - \beta_h(v)h. \end{aligned} \tag{4}$$

The functions $\alpha(v)$ and $\beta(v)$ have dimensions of [1/time] and govern the rate at which the ion channels transition from the closed state to the open state (α) and vice versa (β). The rate functions are (in units of milliseconds^{-1}, with v in millivolts):

$$\begin{aligned} \alpha_m(v) &= 0.1(v+25)\left[\exp(\frac{v+25}{10}) - 1\right]^{-1} \\ \beta_m(v) &= 4\exp(\frac{v}{18}) \\ \alpha_n(v) &= 0.01(v+10)\left[\exp(\frac{v+10}{10}) - 1\right]^{-1} \\ \beta_n(v) &= 0.125\exp(\frac{v}{80}) \\ \alpha_h(v) &= 0.07\exp(\frac{v}{20}) \\ \beta_h(v) &= \left[\exp(\frac{v+30}{10}) + 1\right]^{-1} \end{aligned} \tag{5}$$

Combining Equations 1, 2, and 3,

$$I = C\frac{dv}{dt} + x_1 m^3 h(v - E_{Na}) + x_2 n^4 (v - E_K) + x_3 (v - E_L). \tag{6}$$

The membrane potential of the neuron as a function of time is determined by integrating the Hodgkin-Huxley equations (4) and (6). The behavior of the neuron under the influence of an applied (time-dependent) stimulus current is studied by setting $I(t)$ to represent the externally applied current. Alternatively, the behavior of the neuron can be simulated for different initial values of v. Figure 5 shows an action potential simulated by numerical integration of the Hodgkin-Huxley equations for zero external current and an initial membrane potential of -15 mV. Hodgkin and Huxley showed an excellent fit between experimental data from the squid giant axon and simulation, including action potentials in response to intial membrane potential exceeding resting membrane potential by more than a threshold of about 7 mV.

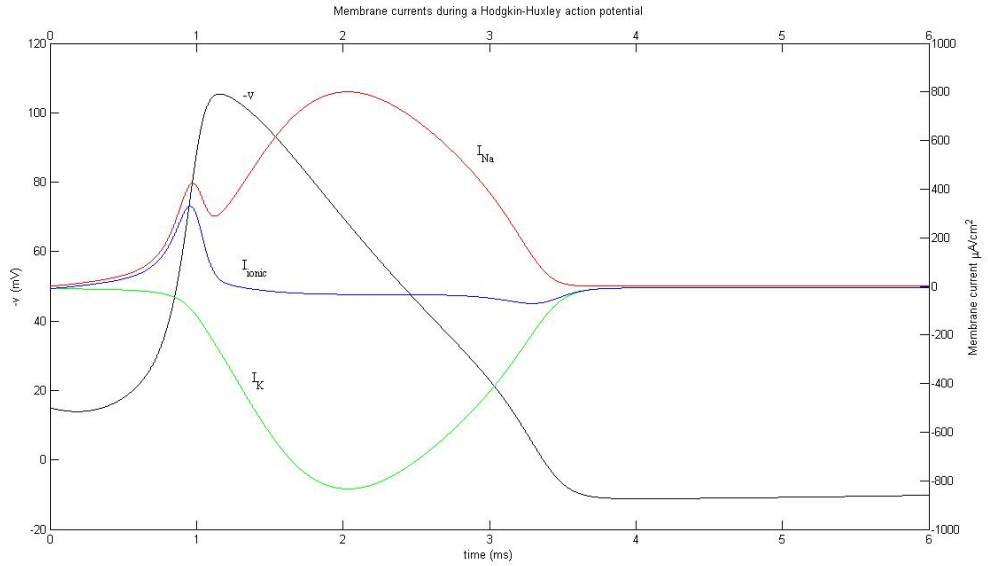

Figure 5: Ionic currents during a Hodgkin-Huxley action potential. Here $I_{ionic} = I_{Na} + I_K$.

For constant membrane potential v, the sodium activation variable m approaches the steady state value

$$m^*(v) = \frac{\alpha_m(v)}{\alpha_m(v) + \beta_m(v)}, \tag{7}$$

from equation (4). Similarly, the variables n and h which also are governed by equation (4) approach steady state values of

$$n^*(v) = \frac{\alpha_n(v)}{\alpha_n(v) + \beta_n(v)} \tag{8}$$

and

$$h^*(v) = \frac{\alpha_h(v)}{\alpha_h(v) + \beta_h(v)} \tag{9}$$

respectively when the membrane potential v remains constant.

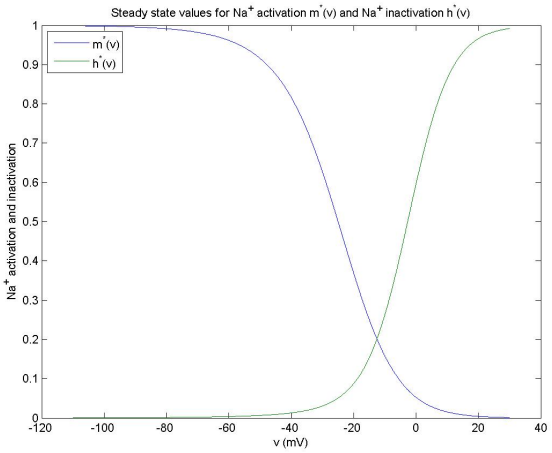

(a) Steady state values $m^*(v)$ and $h^*(v)$ for Na^+ activation and inactivation variables

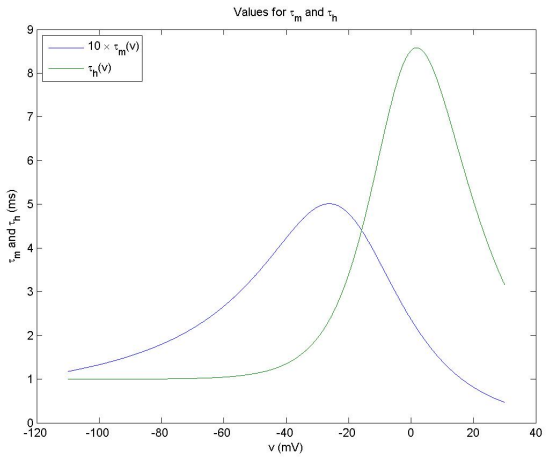

(b) Na^+ activation and inactivation timing variables $\tau_m(v)$ and $\tau_h(v)$

Figure 6: Variables associated with activation and inactivation of Na^+ current

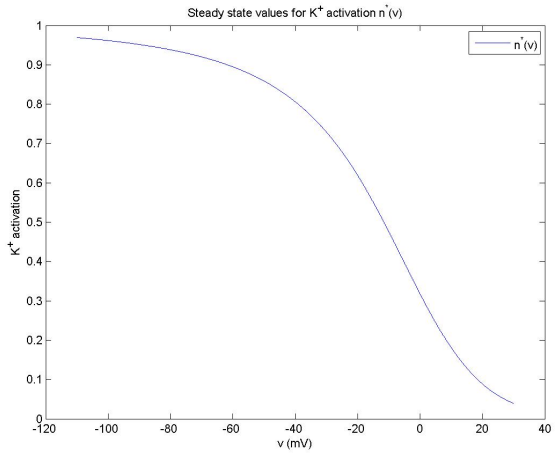

(a) Steady state value $n^*(v)$ for K^+ activation variable

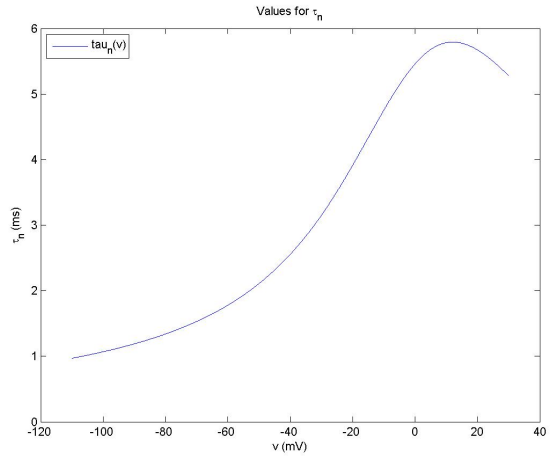

(b) K^+ activation timing variable $\tau_n(v)$

Figure 7: Variables associated with activation of K^+ current

Defining timing variables

$$\begin{aligned} \tau_m(v) &= (\alpha_m(v) + \beta_m(v))^{-1}, \\ \tau_n(v) &= (\alpha_n(v) + \beta_n(v))^{-1}, \\ \tau_h(v) &= (\alpha_h(v) + \beta_h(v))^{-1}, \end{aligned} \tag{10}$$

for membrane potential v, equation (4) can be rewritten as

$$\begin{aligned} \frac{dm}{dt} &= \frac{1}{\tau_m(v)}\left(m^*(v) - m\right), \\ \frac{dn}{dt} &= \frac{1}{\tau_n(v)}\left(n^*(v) - n\right), \\ \frac{dh}{dt} &= \frac{1}{\tau_h(v)}\left(h^*(v) - h\right). \end{aligned} \tag{11}$$

From these equations it is clear that activation and inactivation of the ion channels in the model do not occur instantaneously in response to changes in the membrane potential. At every instant the activation and inactivation variables are each tending toward their steady state values for the instantaneous membrane potential, and τ_m, τ_n, and τ_h govern the rates of change for the respective variables. Since τ_m, τ_n, and τ_h depend on the membrane potential, the rates of activation and inactivation are dependent on v. The voltage dependence of the steady state values for the sodium activation and inactivation variables m and h and their associated timing variables τ_m and τ_h is shown in Figure 6. The voltage dependence of the steady state value for the potassium activation variable n and its timing variable τ_n is shown in Figure 7.

The underlying structure of the Hodgkin-Huxley equations has been applied successfully to the modeling of many different (and more complicated) classes of neurons in the decades since their development. Later chapters treat a Hodgkin-Huxley type model for a lobster stomatogastric (STG) neuron and develop algorithms to invert the Hodgkin-Huxley equations for the STG neuron.

2.2 Background

Ionic current-based models developed by extending and adapting the original Hodgkin-Huxley equations continue to see widespread use by neurobiologists in studying the behavior and physiological processes of neurons and other excitable cells. A difficulty associated with these differential equation-based models is that numerical values must be assigned to each of the parameters and coefficients in order to specify the behavior

of the model. To use the model as a tool for studying the behavior of a particular biological neuron, one must first identify an appropriate choice of numerical values for the parameters of the model to match the behavior of the model neuron to that of the biological neuron.

In general, the problem of identifying a set of parameter values to fully specify a neuron model is a difficult one. It is not normally possible to measure all of the parameters from a single experimental preparation, and there can be significant variability in the properties of the same type of neuron between members of the same species and even within the same animal [20]. Building a complete set of model parameters by averaging over measurements taken from many biological neurons or combining subsets of parameter values measured from different biological neurons has been shown to be unreliable for reproducing target behavior [10].

2.2.1 The problem

The output of the Hodgkin-Huxley equations is a voltage trace $v(t)$ which describes the electrical activity of a model neuron on the domain $t \in [0, \infty)$, giving the voltage across the neuron cell membrane as a function of time. We treat the Hodgkin-Huxley equations as a mapping $H : \mathbb{R}^n \to \mathcal{F}$ from n-dimensional parameter space to a space $\mathcal{F}$ of differentiable functions taking $\mathbb{R}_+$ to $\mathbb{R}$. For a set of input parameters $x \in \mathbb{R}^n$, the Hodgkin-Huxley equations send x to a voltage trace $v_x(t) \in \mathcal{F}$: $H(x) = v_x(t)$. The inverse problem is to consider a voltage trace $H(x^*) = v_{x^*}(t)$ that is the output of the Hodgkin-Huxley equations for an unknown set of parameters $x^* \in \mathbb{R}^n$ and to produce a set of parameter values $x \in \mathbb{R}^n$ so that $H(x) = H(x^*)$.

In the sections that follow, "solving" the Hodgkin-Huxley equations for a set of input parameters refers to integrating the equations in order to obtain the resulting simulated voltage trace. In practice, a closed form solution is not available and the integration must be performed numerically.

"Inverting" the Hodgkin-Huxley equations refers to starting with $v_{x^*}(t)$, a voltage trace generated by solving the Hodgkin-Huxley model for a prespecified set of input parameters x^*, and finding a set of parameters x that generates $v_{x^*}(t)$ when the Hodgkin-Huxley equations are solved with x as input.

2.2.2 Previous work by other researchers

Many previous studies have focused on parameter space exploration, selecting points in parameter space either by hand-tuning, stochastically, or via a systematic enumerative procedure, and reporting on the observed relationship between parameters and the resulting neuron behavior. McCormick and Huguenard [21] study the relationship between membrane conductance and neuron behavior by manipulating single conductances in a thalamocortical relay neuron model, varying maximal conductances individually and reporting the observed effects on model behavior. Goldman et al. [9] systematically vary the maximal conductance values of the 5 ion channels of a neuron model, characterizing the behavior generated by each set of maximal conductances as silent, tonically spiking, or bursting. Prinz et al. [24] use a large scale grid search to assemble a database of neuronal behavior for 1.7 million sets of maximal conductance values for a lobster stomatogastric neuron model. Golowasch et al. [10] randomly generate sets of maximal conductance values for a model with 5 voltage-dependent conductances. From among the set of randomly generated neurons they identify those exhibiting desirable behavior (in this case bursters with a single spike per burst) and show that the space of single-spike bursting neurons is nonconvex. Guckenheimer et al. [11] map the parameter space of a bursting neuron model using bifurcation analysis, identifying boundaries of bifurcation regions with changes in neuron behavior.

Liu et al. [19] take a different approach to the problem of understanding the relationship between parameters and behavior in an attempt to uncover mechanisms

by which neurons regulate their behavior, developing a model neuron whose maximal conductance values are themselves slowly varying with time according to an additional set of differential equations simulating regulatory mechanisms based on calcium currents. The Liu model neuron effectively traces its own path through maximal conductance parameter space with its behavior evolving progressively along this trajectory. The variability of the maximal conductance values represents their role in homeostatic regulation; Liu et al. suggest that the neuron regulates its behavior through variable maximal conductance values.

In addition to parameter space exploration, several researchers have developed parameter search methods to find sets of parameters to match a specific target behavior. Foster et al. [8] use a stochastic technique to search for parameters that produce a match to a target behavior. They search over a parameter space of multiple maximal conductance values, activation voltages, and scaling factors for voltage-dependent timing parameters. The neuron models used are relatively simple, and they measure the similarity of model behavior to target behavior using current-frequency response curves for a range of simulated external stimulus currents. Bhalla and Bower [2] use a method that combines an enumerative grid search with gradient descent, using root mean squared errors in the shape of the voltage trace, length of interspike intervals, and peak to peak amplitude to quantify similarity between model and target (experimental) data. Hayes et al. [15] propose three different objective (error) functions (voltage time series, cumulative voltage integrals, and phase histograms). They investigate the topology induced by these objective functions in regions of parameter space near an optimal solution and conclude that the cumulative voltage integrals and the phase histograms vary smoothly toward a single local minimum in the neighborhood of the optimal solution. The voltage time series objective function is observed to score poorly except in a narrow region surrounding the optimum. Tabak [29] et al. report using gradient methods and the simplex algorithm to minimize aggregate least

squares error in time and frequency domains for a number of target traces. Vanier and Bower [31] compare four automated parameter search methodologies (gradient descent, stochastic search, genetic algorithms, and simulated annealing) and conclude that genetic algorithms and simulated annealing are the most effective for the four models tested. Tien and Guckenheimer [30] use gradient descent methods to fit model burst duration and period to data. They compute parameter sensitivities using automatic differentiation techniques. Achard and De Schutter [1] use an evolutionary algorithm with a fitness function based on phase-plane analysis to obtain a set of 20 distinct models of the cerebellar Purkinje cell, treating maximal conductance values as variable (they emphasize the importance of the maximal conductances in homeostasis) and all other parameters of the model as fixed. Their evolutionary algorithm is quite successful in finding sets of maximal conductances that closely resemble target data for a complex model neuron. Roberge et al. [26] propose using statistical methods to estimate parameters using experimental data giving the values of the peak ionic current and its time of occurrence for a single ion current channel but do not report results.

One of the driving forces that continues to motivate parameter exploration methods is the hope that a deeper understanding of the relationship between the parameters of neuronal models and neuron behavior will lead to insight into neuron function and, in particular, mechanisms of homeostatic regulation. Our inversion algorithms examine the relationship between parameters and behavior from a different perspective by linking the behavior of the model directly to a set of parameters that generates it using the mathematical details of the equations involved. Parameter space exploration methods are generally very computationally intensive. One advantage of the inversion algorithms we develop is their ability to rapidly identify a set of parameters that generates a given behavior (the bulk of the computation time is in the numerical

integration needed to simulate the behavior of the neuron, which parameter exploration methods generally do for each point explored). Inverting the equations of a neuronal model is a step toward understanding the mathematical relationship between parameters and behavior.

Inversion algorithms attempt to solve a related but qualitatively different problem. While parameter search methods attempt to find parameters that generate a good match to a target behavior, algorithms that invert the equations of the model attempt to find a set of parameters that reproduces the target behavior exactly. For some model behaviors, there may not be a unique set of parameter values that generates them, and the inversion algorithm produces one such set of parameters. None of the search techniques given above is an inversion technique. Aside from gradient descent, the search algorithms above do not take advantage of the form of the equations in searching for a solution. Inversion of the equations avoids the difficulties of local minima and nonconvexity that create problems for many of the search algorithms. Ours is also the only algorithm for which a theoretical proof of convergence has been given.

2.3 Solving the Hodgkin-Huxley equations

In practice, the Hodgkin-Huxley equations must be solved numerically and the voltage trace $v(t)$ is replaced by a discrete approximation V_i to the values $v(t_i)$, for a finite set of times $t_i = 1, \ldots, t_N$. Once a numerical integration technique, duration, step size, and initial conditions are specified, numerically solving the Hodgkin-Huxley equations gives a well-defined mapping from a set of maximal conductance parameters $x \in \mathbb{R}^3$ to a discrete voltage trace $V \in \mathbb{R}^N$.

The Hodgkin-Huxley equations are solved by numerically integrating equations (4) and (6). With the Euler method for numerical integration with constant step size

Δt, the value m_{i+1} of the sodium activation variable at time t_{i+1} is computed using

$$m_{i+1} = m_i + \left.\frac{dm}{dt}\right|_i \cdot \Delta t \tag{12}$$

where, from equation (4),

$$\left.\frac{dm}{dt}\right|_i = \alpha_m(V_i)(1 - m_i) - \beta_m(V_i)m_i. \tag{13}$$

The values of n_i and h_i are found similarly.

The voltage at time step $i + 1$ is computed (again by the Euler method) using

$$V_{i+1} = V_i + \left.\frac{dV}{dt}\right|_i \cdot \Delta t \tag{14}$$

and from equation (6)

$$\left.\frac{dV}{dt}\right|_i = \frac{1}{C}\left[I(t_i) - x_{Na}m_i^3h_i(V_i - E_{Na}) - x_K n_i^4(V_i - E_K) - x_L(V_i - E_L)\right]. \tag{15}$$

Unless otherwise specified, the activation and inactivation variables m, n, and h are set initially to their respective steady state values $m^*(0)$, $n^*(0)$, and $h^*(0)$ for the membrane resting potential ($v = 0$) as defined in equations (7-9). (This corresponds to an assumption that the neuron is at rest prior to the beginning of the simulation period.) The initial value V_1 for the membrane potential is assumed known and the external current $I(t)$ is assumed known for all t. By selecting values for the initial membrane potential V_1 and the external current $I(t)$ it is possible to simulate the neuron's response to external stimuli.

2.4 An inversion algorithm for the Hodgkin-Huxley equations

We consider the case where the maximal conductance values are unknown, and all other parameters of the model are as given in Section 2.1. We are given a voltage trace $v_{x^*}(t)$ on some interval $0 \le t \le T$, that is the solution to the Hodgkin-Huxley equations in Section 2.1 with maximal conductance values $x^*=(x_1^*, x_2^*, x_3^*)$. The applied

current $I(t)$ is known for all $t \leq T$, and the initial values for the variables excepting the unknown maximal conductances are known at time $t = 0$. The goal is to produce a set of maximal conductance values $x = (x_1, x_2, x_3)$ so that $v_x(t) = v_{x^*}(t)$. In this section $v(t)$ will be used in place of $v_{x^*}(t)$ to denote the given voltage trace resulting from the Hodgkin-Huxley equations with maximal conductance values x^*.

We are searching for a set of maximal conductance values that reproduces the voltage trace given by the maximal conductances x^*. Since equation (6) is linear in the unknowns x_1, x_2, and x_3, if the values for the activation and inactivation variables m, n, and h are known for a set of times t_i, then computing values for x amounts to solving a system of linear equations. The exact values of the activation and inactivation variables are not directly accessible from the given voltage trace data, but they can be approximated for any t by numerically integrating the equations (4), using the exact membrane potential values $v(t)$ from the given voltage trace. Our inversion procedure is to

1. numerically integrate the Hodgkin-Huxley equations while treating the maximal conductance values as unknown in order to approximate m, n, and h for a finite set of times t_i, and

2. select three times at random and find a set of maximal conductance values that solves a system of three linear equations in three unknowns.

In Step 1, the maximal conductance values are treated as unknown, and the exact membrane potential values $v(t)$, available from the given voltage trace, are used in solving for the activation and inactivation variables by numerical integration of the

equations

$$\begin{aligned}
\frac{dm}{dt} &= \alpha_m(v)(1-m) - \beta_m(v)m, \\
\frac{dn}{dt} &= \alpha_n(v)(1-n) - \beta_n(v)n, \\
\frac{dh}{dt} &= \alpha_h(v)(1-h) - \beta_h(v)h,
\end{aligned} \tag{4}$$

with the functions $\alpha(v)$ and $\beta(v)$ for each of the activation or inactivation variables given by the equations

$$\begin{aligned}
\alpha_m(v) &= 0.1(v+25)\left[\exp(\frac{v+25}{10}) - 1\right]^{-1} \\
\beta_m(v) &= 4\exp(\frac{v}{18}) \\
\alpha_n(v) &= 0.01(v+10)\left[\exp(\frac{v+10}{10}) - 1\right]^{-1} \\
\beta_n(v) &= 0.125\exp(\frac{v}{80}) \\
\alpha_h(v) &= 0.07\exp(\frac{v}{20}) \\
\beta_h(v) &= \left[\exp(\frac{v+30}{10}) + 1\right]^{-1}.
\end{aligned} \tag{5}$$

Since m, n, and h depend only on v, the time course of these variables can be approximated with arbitrary precision for a given voltage trace $v(t)$ by numerical integration with a sufficiently small time step, even in the presence of unknown values for the maximal conductance variables. Let $\tilde{m}(t_i)$, $\tilde{n}(t_i)$, and $\tilde{h}(t_i)$ denote the approximate values for the activation and inactivation variables computed by numerical integration for a set of times $t_1, ...t_N$, with $N > 3$.

The Hodgkin-Huxley equation governing the time evolution of the voltage trace $v(t)$ is

$$I = C\frac{dv}{dt} + x_1^* m^3 h(v - E_{Na}) + x_2^* n^4(v - E_K) + x_3^*(v - E_L). \tag{6}$$

Integrating to get $v(t)$ explicitly,

$$\begin{aligned} v(t) = \\ v(0) + \frac{1}{C}\Bigg[\int_0^t I(t')\,dt' - x_1^* \int_0^t m^3(t')h(t')\cdot(v(t') - E_{Na})\,dt' \\ -x_2^* \int_0^t n^4(t')\cdot(v(t') - E_K)\,dt' - x_3^* \int_0^t (v(t') - E_L)\,dt'.\Bigg] \end{aligned} \tag{16}$$

With functions $f_j(t)$, $j = 1, 2, 3$, defined as

$$\begin{aligned} f_1(t) &= -\frac{1}{C}\int_0^t m^3(t')h(t')\cdot(v(t') - E_{Na})\,dt', \\ f_2(t) &= -\frac{1}{C}\int_0^t n^4(t')\cdot(v(t') - E_K)\,dt', \\ f_3(t) &= -\frac{1}{C}\int_0^t (v(t') - E_L)\,dt', \end{aligned} \tag{17}$$

and $b(t)$ defined by

$$b(t) = v(t) - v(0) - \int_0^t I(t')\,dt', \tag{18}$$

we have

$$b(t) = x_1^* f_1(t) + x_2^* f_2(t) + x_3^* f_3(t). \tag{19}$$

Assuming the externally applied current $I(t)$ is chosen so that the integral

$$\int_0^t I(t')\,dt' \tag{20}$$

can be evaluated in closed form, the function $b(t)$ is known exactly for all t from the given voltage trace $v(t)$ and external current $I(t)$.

Given a voltage trace $v(t)$ and external current $I(t)$ each known for all t, and estimates $\tilde{m}(t_i)$, $\tilde{n}(t_i)$, and $\tilde{h}(t_i)$ for the activation and inactivation variables m, n, and h at time t_i, $i = 1, \ldots, N$, the functions $f_j(t_i)$, $j = 1, 2, 3$, are approximated by numerical integration for $i = 1, \ldots, N$ using the estimates $\tilde{m}$, $\tilde{n}$, and $\tilde{h}$ in place of the activation and inactivation variables m, n, and h. Let $\tilde{f}_j(t_i)$ be the numerical approximation to $f_j(t_i)$. From equation (19), then, the inversion problem is to find

maximal conductance values x that solve the linear system

$$b(t_i) = \sum_{j=1}^{3} \tilde{f}_j(t_i) x_j, \quad i = 1, ..., N. \tag{21}$$

This is an overdetermined system, and it is unlikely that an exact solution exists because the values $\tilde{f}_j$ are approximations to the functions f_j in equation (19). The algorithm solves this problem by selecting three times t_{i_1}, t_{i_2}, t_{i_3} at random and solving the resulting linear system

$$b(t_{i_k}) = \sum_{j=1}^{3} \tilde{f}_j(t_{i_k}) x_j, \quad k = 1, 2, 3 \tag{22}$$

of 3 equations in 3 unknown variables. The algorithm returns a solution to equation

(22) as a solution to the Hodgkin-Huxley inverse problem.

Algorithm 1 for inverting the Hodgkin-Huxley equations

Given the functions α_m, α_n, α_h, β_m, β_n, β_h, the parameters E_{Na}, E_K, E_L, and C, the external current $I(t)$, and a voltage trace $v(t)$ defined on $0 \leq t \leq T$ that is the output of the Hodgkin-Huxley equations for these parameters with finite maximal conductance values $x = (x_1, x_2, x_3)$

1. Choose an algorithm time step δ and define $N = \lfloor T/\delta \rfloor$ and $t_i = i\delta$ for $i = 1, \ldots, N$

2. Randomly choose three times $t_{i_1} < t_{i_2} < t_{i_3}$ from $t_1, \ldots, t_N$

3. Compute the values of $\tilde{f}_j(t_i)$, for $j = 1, 2, 3$, and for all $0 \leq t_i \leq t_{i_3}$ by numerical integration of the equations (17)

4. Construct a 3×3 matrix A^δ whose entries are $a^\delta_{k,j} = \tilde{f}_j(t_{i_k})$

5. Construct the vector $b \in \mathbb{R}^3$ by setting $b_k = b(t_{i_k})$ in equation (18), for $k = 1, 2, 3$

6. Solve the 3×3 linear system $A^\delta x^\delta = b$ and output the solution x^δ, if one exists

In the inversion algorithm given above, the approximate values $\tilde{m}(t_i)$, $\tilde{n}(t_i)$, and $\tilde{h}(t_i)$ obtained by numerical integration for the activation and inactivation variables at each time step depend on the step size δ chosen for the numerical integration procedure. As the step size goes to zero, the approximate values obtained for the activation and inactivation variables approach the true values $m(t_i)$, $n(t_i)$, and $h(t_i)$, for any convergent numerical integration method. (And similarly $\tilde{f}_j \to f_j$ as integration step size approaches zero, for $j = 1, \ldots, 3$.)

In the section that follows, we show that if there is a unique set of maximal conductance values that generates the target voltage trace, then the solution found by Algorithm 1 approaches this set of maximal conductance values if small enough numerical integration time steps are used.

2.4.1 Convergence of Algorithm 1

Let $v(t)$ be a voltage trace generated by the Hodgkin-Huxley equations for a known set of parameters, external current specified by a known analytic function $I(t)$, and maximal conductance values $x \in \mathbb{R}^3$. The procedure given in Algorithm 1 with integration step size δ accepts $v(t)$ as an input and produces a set of maximal conductance values $x^\delta \in \mathbb{R}^3$. We prove in this section that if x is the unique set of maximal conductances for which the Hodgkin-Huxley equations generate $v(t)$ under external current $I(t)$, then $x^\delta \to x$ as $\delta \to 0$.

In proving convergence, we make use of a lemma from matrix perturbation theory. In the following, a consistent matrix norm refers to a norm $||\cdot||$ that satisfies $||AB|| \leq ||A||\,||B||$ for all $A \in \mathbb{R}^{m\times k}$ and $B \in \mathbb{R}^{k\times n}$.

The lemma deals with perturbations of a linear system $Ax = b$ for a square, nonsingular matrix A, placing bounds on the solution of the system of equations for small changes in A.

Lemma 1 (Stewart and Sun [28])**.** *Let $A \in \mathbb{R}^{n\times n}$ be nonsingular, and let $\tilde{A} = A + E$ be a perturbation to A. For $b \in \mathbb{R}^n$ let*

$$Ax = b.$$

Let $||\cdot||$ be a consistent matrix norm that is also consistent with the vector norm $||\cdot||$. If there is a vector $\tilde{x}$ such that

$$\tilde{A}\tilde{x} = b, \tag{23}$$

then

$$\frac{||\tilde{x} - x||}{||\tilde{x}||} \leq ||A^{-1}E||. \tag{24}$$

If in addition

$$||A^{-1}E|| < 1, \tag{25}$$

then (23) always has a unique solution, which satisfies

$$\frac{||\tilde{x} - x||}{||x||} \leq \frac{||A^{-1}E||}{1 - ||A^{-1}E||}. \tag{26}$$

If $\kappa(A) = ||A||\,||A^{-1}||$ *is the condition number of* A *and*

$$\kappa(A)\frac{||E||}{||A||} < 1, \tag{27}$$

then

$$\frac{||\tilde{x} - x||}{||x||} \leq \frac{\kappa(A)\frac{||E||}{||A||}}{1 - \kappa(A)\frac{||E||}{||A||}}. \tag{28}$$

Using Lemma 1, we show that as the numerical integration step size δ used in Algorithm 1 approaches zero, the maximal conductances produced by the inversion algorithm approach the maximal conductance values used to generate the voltage trace $v(t)$. This result requires that the matrix A defined below be nonsingular, a requirement that will be addressed in Theorem 3.

Theorem 2. *Let* x^δ *be the solution produced for randomly chosen times* t_{i_1}, t_{i_2}, *and* t_{i_3} *by Algorithm 1. Define* $A \in \mathbb{R}^{3\times 3}$ *to be the matrix whose entries are* $a_{k,j} = f_j(t_{i_k})$, *for* $f_j(t_{i_k})$ *as in equation (17). If* A *is nonsingular then, as* $\delta \to 0$, x^δ *exists and* $x^\delta \to x$.

Proof. Let A^δ and b be defined as in Algorithm 1. Integration of the Hodgkin-Huxley equations (6) gives an expression for $v(t_i)$ for each i.

$$\begin{aligned} v(t_i) = \\ & v(0) + \frac{1}{C}\int_0^{t_i} I(t)\,dt - x_1\,\frac{1}{C}\int_0^{t_i} m(t)^3 h(t)\,(v(t) - E_{Na})\,dt \\ & - x_2\,\frac{1}{C}\int_0^{t_i} n(t)^4\,(v(t) - E_K)\,dt - x_3\,\frac{1}{C}\int_0^{t_i} (v(t) - E_L)\,dt. \end{aligned} \tag{29}$$

The three times t_{i_k} randomly chosen by Algorithm 1 give three linear equations in the unknowns x_j:

$$\sum_{j=1}^{3} a_{k,j}\, x_j = v(t_{i_k}) - v(0) - \frac{1}{C}\int_0^{t_{i_k}} I(t)\, dt = b_k, \qquad k = 1, 2, 3. \tag{30}$$

Expressed in matrix form,

$$Ax = b. \tag{31}$$

The matrix entries $a_{k,j}$ are not known since the integrals (17) cannot be evaluated analytically, but by numerically integrating (17) and the differential equations (4) for m, n, and h using the exact values for $v(t)$ in the numerical integration process we obtain an estimate $a^{\delta}_{k,j}$ for $a_{k,j}$. Using any convergent numerical integration procedure, $a^{\delta}_{k,j} \to a_{k,j}$ as the numerical integration time step $\delta \to 0$. Since A is nonsingular $\det A \neq 0$. The determinant of a matrix is a continuous function of its entries, so $\det A^{\delta} \neq 0$ for small enough $\delta > 0$; for such a δ there is a vector x^{δ} such that $A^{\delta}x^{\delta} = b$.

Defining $E^{\delta} \in \mathbb{R}^{3\times 3}$ by

$$A^{\delta} = A + E^{\delta} \tag{32}$$

to be the error in A introduced by the numerical integration,

$$\lim_{\delta\to 0} a^{\delta}_{k,j} = a_{k,j} \tag{33}$$

implies E^{δ} converges to the zero matrix as $\delta \to 0$:

$$\lim_{\delta\to 0} |E^{\delta}| = 0. \tag{34}$$

Then for any sufficiently small $\delta > 0$

$$||A^{-1}E^{\delta}|| < 1, \tag{35}$$

and so by Lemma 1 $A^{\delta}x^{\delta} = b$ has a unique solution, which satisfies

$$\frac{||x^{\delta} - x||}{||x||} \leq \frac{||A^{-1}E^{\delta}||}{1 - ||A^{-1}E^{\delta}||}. \tag{36}$$

In the limit $\delta \to 0$, then, the relative error in x^δ goes to zero:

$$\lim_{\delta \to 0} \frac{||x^\delta - x||}{||x||} = 0. \tag{37}$$

For finite x, this implies $x^\delta \to x$ as $\delta \to 0$. □

The theorem above requires that the matrix A be nonsingular. Theorem 3 shows that this is true with probability 1 if the times t_{i_k} in Algorithm 1 are randomly chosen independently from a continuous distribution, and if the set of maximal conductance values x that generates $v(t)$ is unique.

Theorem 3. *Let t_{i_1}, t_{i_2}, and t_{i_3} be random values chosen independently from an interval $[0, T]$ according to a continuous probability distribution and let $A \in \mathbb{R}^{3\times 3}$ be defined as in Theorem 2. If x is the unique set of maximal conductance values that generates $v(t)$, then with probability 1 the matrix A is nonsingular.*

Proof. By integration of the Hodgkin-Huxley equations (6),

$$\begin{aligned} v(t) - v(0) - \frac{1}{C}\int_0^t I(t')\,dt' = \\ - x_1 \frac{1}{C}\int_0^t m(t')^3 h(t')\,(v(t') - E_{Na})\,dt' \\ - x_2 \frac{1}{C}\int_0^t n(t')^4\,(v(t') - E_K)\,dt' - x_3 \frac{1}{C}\int_0^t (v(t') - E_L)\,dt'. \end{aligned} \tag{38}$$

Since $x = (x_1, x_2, x_3)$ is the unique set of maximal conductance values that generates the trace $v(t)$ with external current $I(t)$ and initial voltage $v(0)$, the functions

$$\begin{aligned} f_1(t) &= -\frac{1}{C}\int_0^t m^3(t')h(t') \cdot (v(t') - E_{Na})\,dt' \\ f_2(t) &= -\frac{1}{C}\int_0^t n^4(t') \cdot (v(t') - E_K)\,dt' \\ f_3(t) &= -\frac{1}{C}\int_0^t (v(t') - E_L)\,dt' \end{aligned} \tag{39}$$

are linearly independent.

Since the functions $f_j(t)$, $j = 1, \ldots, 3$, are analytic functions of t, if the set of zeros of $f_j(t)$ has an accumulation point on $[0, T]$ then $f_j(t) = 0$ for all t. Therefore,

since none of these functions is identically zero, they must each have a finite number of zeros on $[0, T]$ and for each $j = 1, \ldots, 3$ with probability 1 it is not the case that $f_j(t_{i_1}) = 0$. Then, defining $b \in \mathbb{R}^3$ as in Theorem 2 and

$$X_1 = \{x \in \mathbb{R}^3 : x_1 f_1(t_{i_1}) + x_2 f_2(t_{i_1}) + x_3 f_3(t_{i_1}) = b_1\}, \tag{40}$$

the dimension of X_1 is 2.

Let x' be a vector from X_1 other than x (x' exists by the dimensionality of X_1). The function

$$(x'_1 - x_1) f_1(t) + (x'_2 - x_2) f_2(t) + (x'_3 - x_3) f_3(t) \tag{41}$$

is analytic, and so it either has a finite number of zeros on $[0, T]$ or it is zero everywhere. If it is zero everywhere then $x' = x$ by the linear independence of $f_j(t)$. Since this is not the case, the function above has a finite number of zeros on $[0, T]$ and with probability 1

$$(x'_1 - x_1) f_1(t_{i_2}) + (x'_2 - x_2) f_2(t_{i_2}) + (x'_3 - x_3) f_3(t_{i_2}) \neq 0 \tag{42}$$

and

$$x'_1 f_1(t_{i_2}) + x'_2 f_2(t_{i_2}) + x'_3 f_3(t_{i_2}) \neq x_1 f_1(t_{i_2}) + x_2 f_2(t_{i_2}) + x_3 f_3(t_{i_2}) = b_2. \tag{43}$$

Defining

$$X_2 = X_1 \cap \{x \in \mathbb{R}^3 : x_1 f_1(t_{i_2}) + x_2 f_2(t_{i_2}) + x_3 f_3(t_{i_2}) = b_2\}, \tag{44}$$

$x' \notin X_2$ means the dimension of X_2 is 1.

A similar argument shows that for t_{i_3} chosen randomly from $[0, T]$ according to a continuous distribution, with probability 1 the dimension of

$$X_3 = X_2 \cap \{x \in \mathbb{R}^3 : x_1 f_1(t_{i_3}) + x_2 f_2(t_{i_3}) + x_3 f_3(t_{i_3}) = b_3\} \tag{45}$$

is 0, and so $Ax = b$ has a unique solution and A is nonsingular. □

Theorems 2 and Theorem 3 together imply that if x is the unique set of maximal conductance values that generates the given voltage trace, then the output x^δ from Algorithm 1 approaches x if the integration time step used in the algorithm is sufficiently small.

Corollary 4. *Let the times t_{i_1}, t_{i_2}, and t_{i_3} be selected in Algorithm 1 by choosing three real numbers r_1, r_2, and r_3 independently from a continuous random distribution on $[0, T]$, and rounding to the three nearest values $t_i = i\delta$. If x is the unique set of maximal conductance values that generates $v(t)$ with external current $I(t)$ and initial voltage $v(0)$, then with probability 1, $x^\delta \to x$ as $\delta \to 0$.*

Proof. Define $A^r \in \mathbb{R}^{3\times 3}$ to be the matrix whose entries are $a^r_{k,j} = f_j(r_k)$, for $f_j(r_k)$ as in equation (17) and r_k as in the statement of the corollary. The matrix A^r is nonsingular with probability 1, by Theorem 3. By the continuity of the determinant function, a matrix whose entries are all within a small enough neighborhood of the entries of A^r is also nonsingular. As $\delta \to 0$ the times $t_{i_k} \to r_k$ for $k = 1, 2, 3$, and the matrix A in Theorem 2 converges to A^r. Then for small enough δ the matrix A is nonsingular with probability 1, and Theorem 2 implies $x^\delta \to x$ as $\delta \to 0$. □

2.4.2 Computational results for Algorithm 1

The exact, continuous solution to the Hodgkin-Huxley equations for a known set of input parameters was approximated by numerically integrating the Hodgkin-Huxley equations with a very small time step of 10^{-6} ms, with initial voltage $v(0) = -15$ mV and zero external current $I(t)$. The parameters used in the model are those given in Section 2.1. The voltage trace obtained by this simulation was used as the input to Algorithm 1 for solving the inverse problem.

Algorithm 1 was tested for convergence using time steps δ ranging in size from 0.5 ms to 3×10^{-6} ms. For each value of δ three times were selected at random as in

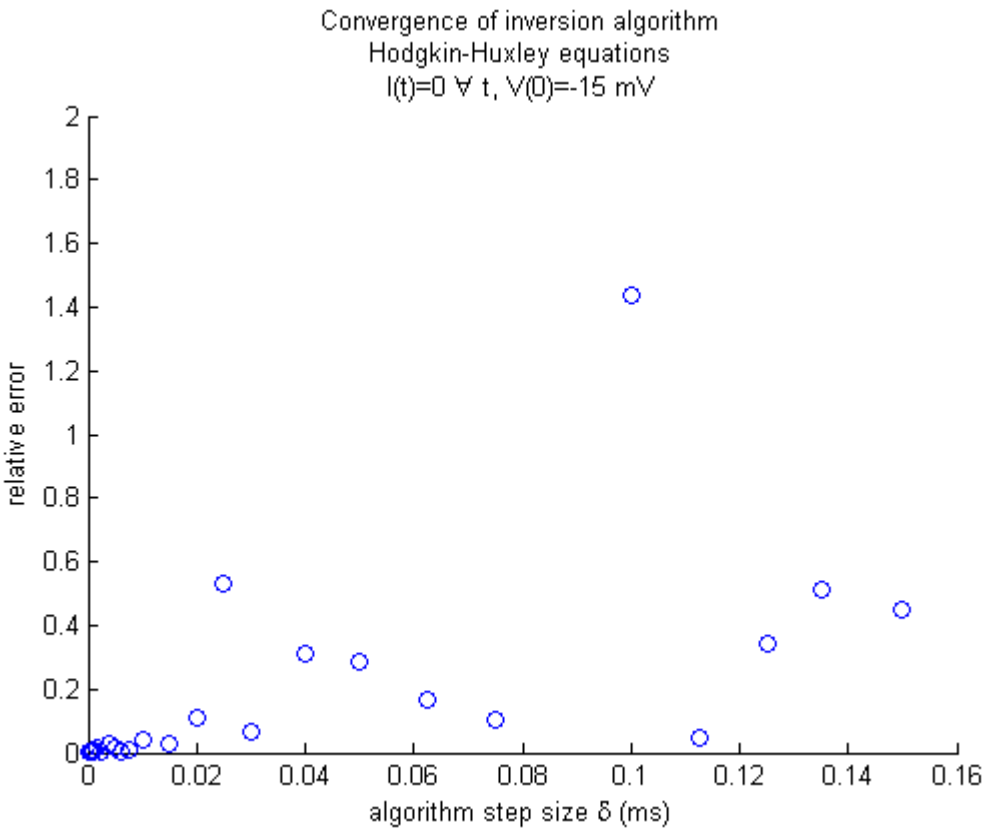

Figure 8: Performance of Algorithm 1

the description of Algorithm 1. Figure 8 plots the relative error

$$\frac{||x^\delta - x^*||}{||x^*||} \tag{46}$$

where $x^* = (120, 36, 0.3)$ mS/cm^2 is the vector of maximal conductance values used to generate $v(t)$, x^δ is the vector of maximal conductances produced by Algorithm 1, and $||\cdot||$ is the Euclidean norm.

Testing shows that x^δ does approach x^* as δ goes to zero, but the convergence is neither monotonic nor particularly rapid. In the next section we introduce an improved algorithm which is also proved to converge, and which performs significantly better in practice.

2.5 An improved inversion algorithm for the Hodgkin-Huxley equations

The second inversion algorithm for the Hodgkin-Huxley equations uses the same overdetermined system of linear equations (21) as the first algorithm, but rather than select three times at random it finds an approximate solution to the system by treating it as a linear least squares problem. By using the full set of data generated during the numerical integration phase of the algorithm, rather than data from only 3 time steps, the algorithm obtains a more accurate estimate for the maximal conductance values.

The procedure is to

1. numerically integrate the Hodgkin-Huxley equations while treating the maximal conductance values as unknown in order to approximate m, n, and h for a finite set of times t_i, and

2. find a set of maximal conductances that gives a best fit to the given voltage trace values $v(t_i)$ in the least squares sense.

When the algorithm arrives at the system of equations (21), rather than using data from only 3 times selected at random it produces a best fit solution in the least squares sense by finding an optimal solution to

$$\min_x \sum_{i=1}^{N} \left(b(t_i) - \sum_{j=1}^{3} \tilde{f}_j(t_i) x_j \right)^2 . \tag{47}$$

Defining $A^\delta \in \mathbb{R}^{N\times 3}$ to be the matrix whose entries are $a^\delta_{i,j} = \tilde{f}_j(t_i)$, $i = 1, \ldots, N$, and $b \in \mathbb{R}^N$ by setting $b_i = b(t_i)$ in equation (18), for $i = 1, \ldots, N$ this can be rewritten in matrix form as

$$\min_x ||A^\delta x - b||_2. \tag{48}$$

Since the equations $A^\delta x = b$ are linear in x, a solution is easily obtained by (for

example) linear regression.

Algorithm 2 for inverting the Hodgkin-Huxley equations

Given the functions α_m, α_n, α_h, β_m, β_n, β_h, the parameters E_{Na}, E_K, E_L, and C, the external current $I(t)$, and a voltage trace $v(t)$ defined on $0 \leq t \leq T$ that is the output of the Hodgkin-Huxley equations for these parameters with finite maximal conductance values $x = (x_1, x_2, x_3)$

1. Choose an algorithm time step δ and define $N = \lfloor T/\delta \rfloor$ and $t_i = i\delta$ for $i = 1, \ldots, N$

2. Compute the values of $\tilde{f}_j(t_i)$, for $j = 1, 2, 3$, and for all $0 \leq t_i \leq T$ by numerical integration of the equations (17)

3. Construct a $N \times 3$ matrix A^δ whose entries are $a^\delta_{i,j} = \tilde{f}_j(t_i)$

4. Construct the vector $b \in \mathbb{R}^N$ by setting $b_i = b(t_i)$ in equation (18), for $i = 1, \ldots, N$

5. Obtain an approximate solution to the overdetermined $N \times 3$ linear system $A^\delta x^\delta = b$ by solving equation(47) and output the solution x^δ

The vast majority of the computational time in these inversion algorithms is consumed by the numerical integration, and the increase in expected computational time for Algorithm 2 relative to Algorithm 1 is a small constant factor associated with carrying out the numerical integration over the full N time steps rather than stopping at t_{i_3}, the largest of the three randomly chosen times.

2.5.1 Convergence of Algorithm 2

As in Section 2.4.1, let $v(t)$ be a voltage trace generated by the Hodgkin-Huxley equations for a known set of parameters, external current specified by a known analytic

function $I(t)$, and maximal conductance values $x \in \mathbb{R}^3$. The procedure of Algorithm 2 with integration step size δ again accepts $v(t)$ as an input and produces a set of maximal conductance values $x^\delta \in \mathbb{R}^3$. We prove in this section that if x is the unique set of maximal conductances for which the Hodgkin-Huxley equations generate $v(t)$ under external current $I(t)$, then $x^\delta \to x$ as $\delta \to 0$.

To prove convergence of Algorithm 2 we use a lemma due to Bauer and Skeel which can be found in [28]. This lemma places bounds on the solution to a linear system of equations $Ax = b$, with A square and nonsingular, when both A and b are perturbed by a small amount. In the following $|A|$ denotes the matrix whose elements are the absolute values of the elements of A, an absolute vector norm is one whose value for an arbitrary vector x does not change when each element of x is replaced by its absolute value, and $||\cdot||_2$ denotes the Euclidean norm.

Lemma 5 (Bauer and Skeel [28])**.** *Let A be nonsingular. Let $Ax = b$, and $(A+E)\tilde{x} = b+e$. Let $||\cdot||$ be an absolute vector norm, and let $||\cdot||$ also denote a consistent vector norm. If for some nonnegative S, s, and ϵ*

$$|E| \leq \epsilon S \quad \textit{and} \quad |e| \leq \epsilon s \tag{49}$$

and in addition

$$\epsilon || \, |A^{-1}| \, S \, || < 1, \tag{50}$$

then

$$||\tilde{x} - x|| \leq \frac{\epsilon || \, |A^{-1}| \, (S \, |x| + s) \, ||}{1 - \epsilon || \, |A^{-1}| \, S \, ||}. \tag{51}$$

The next theorem sets up a convergence proof (with Theorem 3) for Inversion Algorithm 2, which minimizes the least squares error to find an approximate solution for an overdetermined linear system.

Theorem 6. *Let x^δ be the solution produced by Algorithm 2, and define $A \in \mathbb{R}^{N \times 3}$ to be the matrix whose entries are $a_{i,j} = f_j(t_i)$, as in equation (17). Then x^δ exists for all $\delta > 0$, and if A has rank 3 then $x^\delta \to x$ as $\delta \to 0$.*

Proof. The solution x^δ produced by Algorithm 2 is an optimal solution to

$$\min_y ||A^\delta y - b||_2. \tag{52}$$

When the expression $||A^\delta y - b||_2$ reaches a minimum, the gradient of

$$(A^\delta y - b)^T (A^\delta y - b) \tag{53}$$

is equal to zero. Since

$$\nabla \left[(A^\delta y - b)^T (A^\delta y - b) \right] = 2(A^\delta)^T A^\delta y - 2(A^\delta)^T b, \tag{54}$$

x^δ is given by

$$(A^\delta)^T A^\delta x^\delta = (A^\delta)^T b. \tag{55}$$

Defining $E^\delta \in \mathbb{R}^{k \times 3}$ as in the proof of Theorem 2 by

$$A^\delta = A + E^\delta \tag{56}$$

to be the error in A introduced by the numerical integration, from (55) we have

$$\left(A^T A + (E^\delta)^T A + A^T E^\delta + (E^\delta)^T E^\delta \right) x^\delta = A^T b + (E^\delta)^T b. \tag{57}$$

As in the proof of Theorem 2, we know that

$$Ax = b, \tag{58}$$

and so

$$A^T A x = A^T b. \tag{59}$$

Since A has full rank, $A^T A$ is nonsingular. Equation (57) represents a perturbation to the linear system (59), and if the perturbation is small enough we can use Lemma 5 to bound $||x^\delta - x||$. Let $\epsilon_1(\delta)$ be the largest element of the matrix $\left|(E^\delta)^T A + A^T E^\delta + (E^\delta)^T E\right|$ and let $\epsilon_2(\delta)$ be the largest element of the vector $|(E^\delta)^T b|$, and set $\epsilon(\delta) = \max(\epsilon_1(\delta), \epsilon_2(\delta))$.

Then

$$\left|(E^\delta)^T A + A^T E^\delta + (E^\delta)^T E^\delta\right| \leq \epsilon(\delta) S, \tag{60}$$

where S is the 3 by 3 matrix whose entries are each 1, and

$$|(E^\delta)^T b| \leq \epsilon(\delta) s, \tag{61}$$

where $s \in \mathbb{R}^3$ is the vector of ones. Since, as in Theorem 2,

$$\lim_{\delta \to 0} |E^\delta| = 0, \tag{62}$$

we see that

$$\lim_{\delta \to 0} \epsilon(\delta) = 0. \tag{63}$$

For small enough δ, then,

$$\epsilon(\delta) || \ |A^{-1}| \ S \ || < 1 \tag{64}$$

and from Lemma 5

$$||x^\delta - x|| \leq \frac{\epsilon(\delta) || \ |A^{-1}| \ (S|x| + s) \ ||}{1 - \epsilon(\delta) || \ |A^{-1}| \ S \ ||}. \tag{65}$$

In the limit as $\delta \to 0$, $\epsilon(\delta) \to 0$ implies the right hand side goes to 0, and so

$$\lim_{\delta \to 0} ||x^\delta - x|| = 0 \tag{66}$$

and $x^\delta \to x$ as $\delta \to 0$.

□

Theorem 6 states that if the matrix A used by Algorithm 2 has rank 3 then the maximal conductance values x^δ produced by Algorithm 2 converge to the maximal conductance values x that generate the voltage trace $v(t)$ in the limit $\delta \to 0$. Theorem 3 tells us that if the vector x is the unique set of maximal conductance values that generates $v(t)$ with external current $I(t)$ and initial voltage $v(0)$, then the matrix A in Theorem 6 has rank 3 with probability 1 as $\delta \to 0$.

Corollary 7. *If x is the unique set of maximal conductance values that generates $v(t)$ with external current $I(t)$ and initial voltage $v(0)$ and x^δ is the set of maximal conductances produced by Algorithm 2 with time step δ, then with probability 1, $x^\delta \to x$ as $\delta \to 0$.*

Proof. As $\delta \to 0$ the $N \times 3$ matrix defined in Theorem 6 has rank 3, using the reasoning in the proof of Corollary 4. The result follows from Theorem 6. □

Finally, continuity of the Hodgkin-Huxley equations implies the traces generated by the maximal conductances found by the inversion algorithms converge to the target trace in the limit $\delta \to 0$.

Corollary 8. *If $x = (x_1, x_2, x_3)$ is the unique set of maximal conductance values that generates the trace $v(t)$ with external current $I(t)$ and initial voltage $v(0)$, $v_{x^\delta}(t) \to v_x(t)$ as $\delta \to 0$.*

2.5.2 Computational results for Algorithm 2

The exact, continuous solution to the Hodgkin-Huxley equations for a known set of input parameters was approximated by numerically integrating the Hodgkin-Huxley equations with a very small time step of 10^{-6} ms. The voltage trace obtained by this simulation was used as the input to the algorithm for solving the inverse problem.

The Algorithm 2 was tested for convergence by sampling from the target voltage trace described above at intervals ranging in size from $\delta = 0.5$ ms to $\delta = 3 \times 10^{-6}$ ms. In each case the inversion algorithm was run with time step δ using the voltage trace data obtained by sampling at regular time intervals of length δ from the approximately continuous trace. 6 milliseconds of simulated data (roughly the duration of a single action potential) was used in the testing so that the approximately continuous voltage trace consists of 6 million data points, and the inversion algorithm used $N = 12$ data points in the coarsest approximation ($\delta = 0.5$ ms) and $N = 2$ million data points in the finest approximation ($\delta = 3 \times 10^{-6}$ ms). In the results that follow, the maximal

Table 2: Three stimuli used in testing the Hodgkin-Huxley inversion algorithm

Stimulus 1	$v(0) = -15$ mV	$I(t) = 0$ for all t
Stimulus 2	$v(0) = 0$	$I(t) = 5\ \mu\text{A/cm}^2$ for all t
Stimulus 3	$v(0) = 0$	$I(t) = \begin{cases} 20\mu\text{A/cm}^2 & t \in [0.5\text{ms}, 1.0\text{ms}] \\ 0 & \text{otherwise} \end{cases}$

conductance values generated by the inversion algorithm with time step δ are denoted (as before) by x^δ.

The parameters used in generating the target voltage trace were those used by Hodgkin and Huxley (Section 2.1). In particular, the maximal conductance values used to generate the target voltage trace were $x^* = (120, 36, 0.3)$ millisiemens per square centimeter. Several choices for the initial voltage $v(0)$, corresponding to a depolarizing or hyperpolarizing stimulus, were tested. Testing was performed for constant (both zero and nonzero) external current $I(t)$, and for step function external current impulses. Results are shown below for voltage traces generated by the three combinations of $v(0)$ and $I(t)$ in Table 2. In all cases, the activation and inactivation variables were initialized to their steady state values at the membrane resting potential ($v = 0$) at time $t = 0$. Figures 10(a)-12(a) show the relative error

$$\frac{||x^\delta - x^*||}{||x^*||} \tag{67}$$

for the three stimuli described in Table 2 for a range of time steps δ. Here $||\cdot||$ denotes the Euclidean norm. In all cases x^* is set to the value used by Hodgkin and Huxley, $x^* = (120.0, 36.0, 0.3)$ mS/cm^2. For all stimuli tested the maximal conductance values x^δ produced by Algorithm 2 with time step δ were found empirically to approach x^* as δ approaches zero.

Figures 10(b)-12(b) show the voltage traces generated by x^δ for each of the three stimuli given in Table 2. For small δ the traces generated by x^δ are found to converge to the target trace produced by x^* for each stimulus tested.

Algorithm 2 was also tested with similar success on voltage trace data generated

Table 3: Performance of Algorithm 2 for the three test stimuli given in Table 2 (δ in ms and conductances in mS/cm^2).

	Stimulus 1			Stimulus 2			Stimulus 3		
delta	x1	x2	x3	x1	x2	x3	x1	x2	x3
1.50E-01	93.92	26.98	0.22	102.12	29.27	0.46	110.57	31.34	0.57
1.00E-01	107.92	31.27	0.33	112.53	32.57	0.49	117.03	33.71	0.54
5.00E-02	116.76	34.35	0.35	118.50	34.85	0.43	121.16	35.53	0.47
1.00E-02	119.80	35.79	0.32	120.03	35.86	0.33	120.57	36.00	0.34
5.00E-03	119.93	35.90	0.31	120.03	35.93	0.32	120.30	36.00	0.32
1.00E-03	119.99	35.98	0.30	120.01	35.99	0.30	120.06	36.00	0.30
5.00E-04	120.00	35.99	0.30	120.00	35.99	0.30	120.03	36.00	0.30
1.00E-04	120.00	36.00	0.30	120.00	36.00	0.30	120.01	36.00	0.30
5.00E-05	120.00	36.00	0.30	120.00	36.00	0.30	120.00	36.00	0.30
1.00E-05	120.00	36.00	0.30	120.00	36.00	0.30	120.00	36.00	0.30

by maximal conductance values other than those used by Hodgkin and Huxley. Table 4 shows the results of testing using traces generated by values of x^* that differ from those of Hodgkin and Huxley by $\pm 15\%$ in each component. The target trace was generated from x^* using the technique above with Stimulus 1. The results given in Table 4 are for step size $\delta = 0.1$ μs. The convergence of x^δ to x^* holds for the values of x^* presented in Table 4 and for the other physiologically reasonable (i.e. non-negative) values tested. The traces generated by x^δ are nearly identical to the trace generated by x^* for the values of x^δ and x^* given in Table 4.

Table 4: Performance of Algorithm 2 for various values of x^*. Conductances in mS/cm^2.

x^*			x^δ		
x_1^*	x_2^*	x_3^*	x_1^δ	x_2^δ	x_3^δ
138.000	40.400	0.345	137.999	40.398	0.345
138.000	40.400	0.255	137.999	40.398	0.255
138.000	30.600	0.345	138.005	30.599	0.345
138.000	30.600	0.255	138.005	30.599	0.255
102.000	40.400	0.345	101.997	40.398	0.345
102.000	40.400	0.255	101.997	40.398	0.255
102.000	30.600	0.345	101.999	30.599	0.345
102.000	30.600	0.255	101.999	30.599	0.255

In principle it is sufficient as in Algorithm 1 to use data from only three times

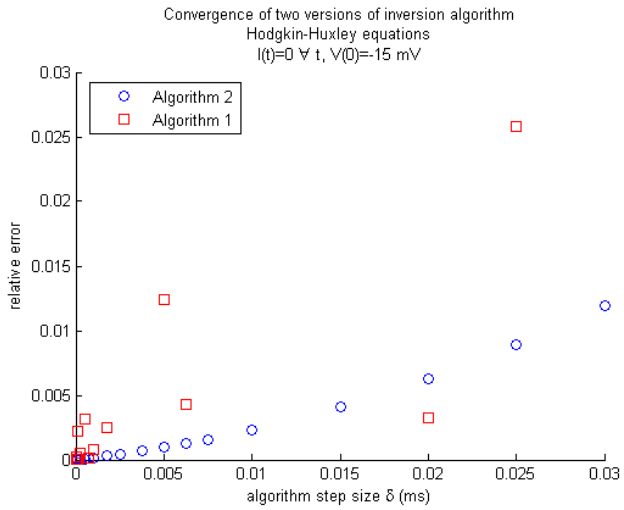

Figure 9: Performance of Algorithm 1 and Algorithm 2

t_i provided the resulting submatrix is nonsingular (which is almost certainly true if the inverse problem has a unique solution by Theorem 3). In practice the algorithm performs better when more data are used and x^δ is an approximate solution to an overdetermined system of linear equations as in Algorithm 2. Figure 9 shows convergence of the algorithm where x^δ is obtained for the same target trace using Algorithm 1 and Algorithm 2. The convergence for Algorithm 2 appears monotonic, and the relative error in the maximal conductance values is almost always smaller for Algorithm 2 for the time steps δ tested.

2.6 Summary

The key feature of the Hodgkin-Huxley equations that enables the inversion algorithms developed in this section is the fact that aside from the linear dependence of the voltage trace on the unknown maximal conductance values, all variables of the model can be computed to arbitrary precision by numerical integration if the voltage trace $v(t)$ is known. The inversion procedures of this section would work similarly for other Hodgkin-Huxley type models involving additional membrane currents provided this condition holds.

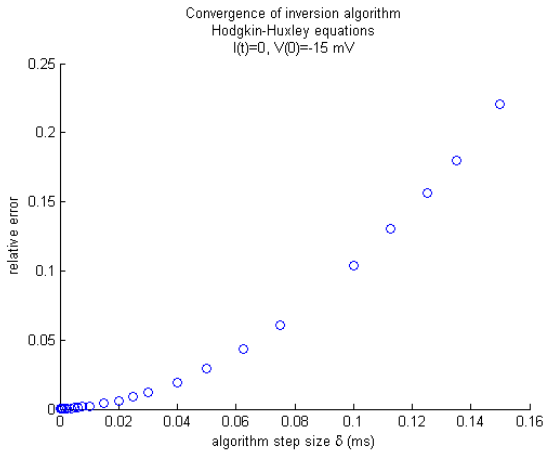

(a) Relative error in maximal conductance values for Stimulus 1 in Table 2

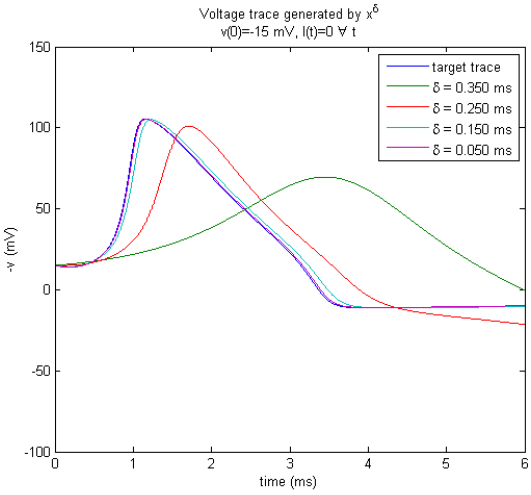

(b) Voltage trace generated by x^{δ}, Stimulus 1

Figure 10: Performance of Algorithm 2 for Stimulus 1 in Table 2

For more complex Hodgkin-Huxley type models where the time course of one or more of the variables cannot be computed directly from the voltage trace, the algorithm needs to be modified. In the next section we explore one such model and develop an iterative algorithm to solve the associated inverse problem of finding a set of maximal conductance parameters to match a voltage trace generated by the model.

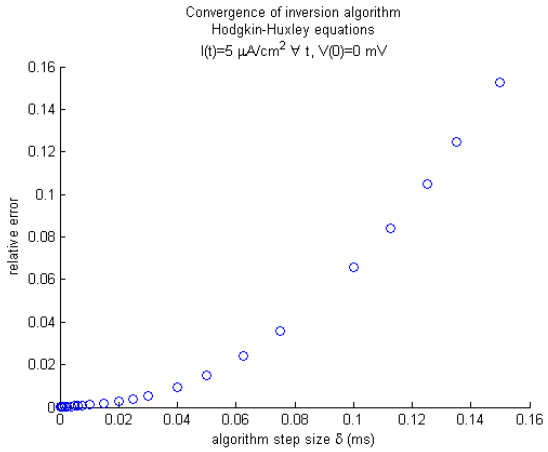

(a) Relative error in maximal conductance values for Stimulus 2 in Table 2

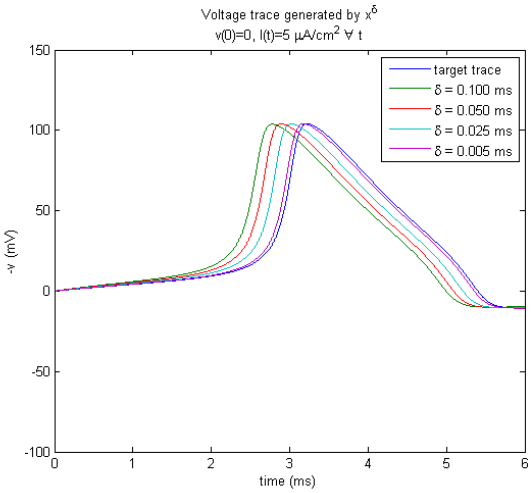

(b) Voltage trace generated by x^{δ}, Stimulus 2

Figure 11: Performance of Algorithm 2 for Stimulus 2 in Table 2

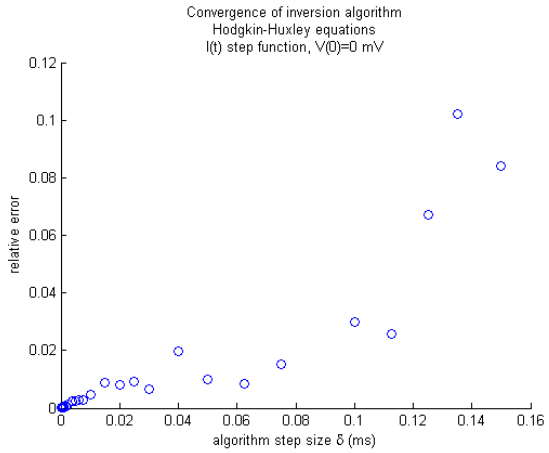

(a) Relative error in maximal conductance values for Stimulus 3 in Table 2

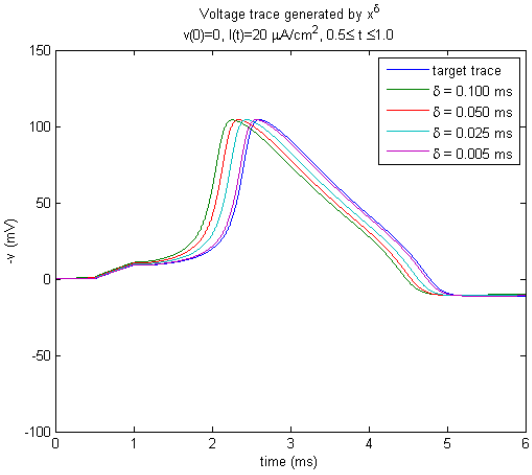

(b) Voltage trace generated by x^{δ}, Stimulus 3

Figure 12: Performance of Algorithm 2 for Stimulus 3 in Table 2

CHAPTER III

AN ALGORITHM FOR INVERTING A HODGKIN-HUXLEY TYPE MODEL FOR A LOBSTER STOMATOGASTRIC NEURON

The lobster stomatogastric (STG) neuron is described by a system of differential equations similar in character to those developed by Hodgkin and Huxley to model the behavior of the squid giant axon. The STG neuron model presented in this section and the code used to numerically integrate the equations of the model were provided by the Prinz Lab at Emory University. The STG neuron model used is closely related to the models presented by Liu et al. [19] and Prinz et al. [24]. The STG model presented in this chapter poses a more challenging inversion problem than the original Hodgkin-Huxley model and allows us to test our procedure on a type of neuronal model currently in use by computational neuroscientists.

The model includes 8 ionic currents, rather than the 3 present in the orginal Hodgkin-Huxley equations. In addition to having a larger number of membrane currents (which would not require a different inversion technique from the one developed for the original Hodgkin-Huxley equations), the inverse problem for the STG neuron model is complicated by the dependence of some of the currents on the (time-varying) intracellular concentration of calcium ions [Ca]. The STG model includes a calcium-dependent potassium current whose activity is influenced by [Ca]. In addition, the model includes two distinct calcium currents whose reversal potential depends on [Ca]. The algorithm developed in Chapter 2 made use of the fact that aside from the linear dependence on the unknown maximal conductance values, all of the variables involved in the ionic currents could be computed directly from the voltage trace by

numerical integration. In the STG neuron model, the intracellular calcium ion concentration depends nonlinearly on the unknown maximal conductance values, and the linear least squares approach used in Chapter 2 needs to be modified to accomodate this.

The algorithm developed for inverting the original Hodgkin-Huxley equations is replaced by an iterative procedure that

1. approximates the membrane currents by numerical integration using the given voltage trace and an estimate for the maximal conductance values

2. uses the newly estimated values for the membrane currents to update the estimate for the maximal conductance values before returning to 1.

The inversion procedure is tested on voltage trace data generated by numerical integration of the equations of the STG neuron model, including data representing a wide range of spontaneous periodic bursting and spiking behavior as well as non-periodic behavior. The inversion procedure is also tested against voltage trace data generated by numerical integration of the STG neuron equations with one or more parameters of the model perturbed by an unknown amount, representing uncertainty in the exact form of the equations describing the voltage trace.

The algorithm is found empirically to be very successful in producing a set of maximal conductance values that closely matches the behavior of a given target trace. In almost all cases the maximal conductance values produced by the inversion algorithm agree extremely closely with the maximal conductance values that were used to generate the trace, suggesting that under certain conditions a set of maximal conductance values is uniquely identifiable from the voltage trace that it generates. Studies have suggested ([9, 10, 24], and [25] showed something similar for a network of 3 neurons) that similar voltage trace behavior can be produced by widely different sets of maximal conductance values, and our findings do not call this into question. While similar

Table 5: The currents of the STG neuron model

I_1	Na	fast sodium
I_2	CaT	fast transient calcium
I_3	CaS	slow calcium
I_4	Kd	delayed rectifier potassium
I_5	KCa	calcium-dependent potassium
I_6	A	fast transient potassium
I_7	H	hyperpolarization-activated inward cation
I_8	L	passive leakage

neuronal behavior may arise as a result of maximal conductance values chosen from different regions of parameter space, it may be the case that an exact match to the function $v(t)$ that is generated by the parameters x^* is only achieved by x^*.

3.1 The STG neuron model

The membrane currents used in the model for the STG neuron are fast sodium, fast transient calcium, slow calcium, delayed rectifier potassium, calcium-dependent potassium, fast transient potassium, hyperpolarization-activated inward cation, and passive leakage (see Table 5). The details of the individual membrane currents are found in Table 6. The model has considerable range in the types of spontaneous activity exhibited. Various spontaneous STG neuron behaviors are plotted in Appendix A.

The equations for the STG neuron (as in the original Hodgkin-Huxley equations) treat the neuron as an electrical circuit, with the membrane potential v determined by the ionic currents I_j flowing through the voltage-gated ion channels:

$$C\frac{dv}{dt} = -\sum_{j=1}^{8} I_j. \tag{68}$$

Equation (68) is the analog of equation (1) of the original Hodgkin-Huxley model. The STG neuron model exhibits spontaneous activity in the absence of external stimuli,

Table 6: Parameters and functions describing the membrane currents of the STG neuron model. Membrane potentials are in mV, time constants are in ms, and [Ca] is the micromolar intracellular Ca^{2+} concentration.

j	Current	p_j, q_j	E_j	m_j^*	h_j^*	τ_{m_j}	τ_{h_j}
1	Na	3,1	50	$\frac{1}{1+\exp\left(\frac{V+25.5}{-5.29}\right)}$	$\frac{1}{1+\exp\left(\frac{V+48.9}{5.18}\right)}$	$132-\frac{1.26}{1+\exp\left(\frac{V+120}{-25}\right)}$	$\frac{0.67}{1+\exp\left(\frac{V+62.9}{-10.0}\right)}\left(1.5+\frac{1}{1+\exp\left(\frac{V+34.9}{3.6}\right)}\right)$
2	CaT	3,1	See eq (70)	$\frac{1}{1+\exp\left(\frac{V+27.7}{-7.2}\right)}$	$\frac{1}{1+\exp(\frac{V+32.1}{5.5})}$	$21.7-\frac{21.3}{1+\exp\left(\frac{V+68.1}{-20.5}\right)}$	$105-\frac{89.8}{1+\exp\left(\frac{V+55}{-16.9}\right)}$
3	CaS	3,1	See eq (70)	$\frac{1}{1+\exp\left(\frac{V+33}{-8.1}\right)}$	$\frac{1}{1+\exp(\frac{V+60}{6.2})}$	$1.4+\frac{7}{\exp\left(\frac{V+27}{10}\right)+\exp\left(\frac{V+70}{-13}\right)}$	$60+\frac{150}{\exp\left(\frac{V+55}{9}\right)+\exp\left(\frac{V+65}{-16}\right)}$
4	A	3,1	-80	$\frac{1}{1+\exp\left(\frac{V+27.2}{-8.7}\right)}$	$\frac{1}{1+\exp\left(\frac{V+56.9}{4.9}\right)}$	$11.6-\frac{10.4}{1+\exp\left(\frac{V+32.9}{-15.2}\right)}$	$38.6-\frac{29.2}{1+\exp\left(\frac{V+38.9}{-26.5}\right)}$
5	KCa	4,0	-80	$\left(\frac{[Ca]}{[Ca]+3}\right)\frac{1}{1+\exp\left(\frac{V+28.3}{-12.6}\right)}$	–	$90.3-\frac{75.1}{1+\exp\left(\frac{V+46}{-22.7}\right)}$	–
6	Kd	4,0	-80	$\frac{1}{1+\exp\left(\frac{V+12.3}{-11.8}\right)}$	–	$7.2-\frac{6.4}{1+\exp\left(\frac{V+28.3}{-19.2}\right)}$	–
7	H	1,0	-20	$\frac{1}{1+\exp\left(\frac{V+75}{5.5}\right)}$	–	$\frac{1}{\exp(-14590-86V)+\exp(-1870+70.1V)}$	–
8	L	0,0	-50	–	–	–	–

and the external current is taken to be zero in this chapter unless otherwise noted. $C = 0.628$ nF is the membrane capacitance, as in [24] and [19].

As in the Hodgkin-Huxley model for the squid giant axon, the richness of the model comes from the fact that the conductances associated with the ionic currents are variable and dependent on voltage. The form of this dependence is:

$$I_j = x_j m_j^{p_j} h_j^{q_j} (v - E_j), \quad j = 1, \ldots, 8, \tag{69}$$

where the variables x_j are the maximal conductance values and m_j and h_j are activation and inactivation functions, respectively. The exponents p_j and q_j and the reversal potentials E_j are constants as defined in Table 6, with the exception of E_2 and E_3 which depend on intracellular calcium concentration [Ca] and are given by the Nernst equation:

$$E_2 = E_3 = c_N \ln\left(\frac{3.0 \text{ mM}}{[\text{Ca}]}\right). \tag{70}$$

where c_N is the Nernst constant and 3.0 mM represents the extracellular calcium concentration. For Ca^{2+}, $c_N \approx 12.2$ mV at 283K, the simulation temperature used in our work. The dependence of E_2 and E_3 on the intracellular calcium ion concentration means the reversal potential for these currents varies with time. All other reversal potentials E_j, $j \neq 2, 3$, are fixed parameters as given in Table 6.

For each ionic current, the behavior of the activation and inactivation variables m_j and h_j is determined by

$$\begin{aligned} \tau_{m_j} \frac{dm_j}{dt} &= m_j^*(v) - m_j \\ \tau_{h_j} \frac{dh_j}{dt} &= h_j^*(v) - h_j. \end{aligned} \tag{71}$$

Here $m_j^*(v)$ and $h_j^*(v)$, with the exception of $m_5^*(v, [Ca])$ which depends also on intracellular calcium ion concentration [Ca], are functions only of the membrane potential and are given in Table 6. They play the roles of the functions $m_\infty(v)$, $n_\infty(v)$, and $h_\infty(v)$ in the original Hodgkin-Huxley model and, as can be seen in equation (71), give the steady state values of the variables m_j and h_j at constant voltage v. These

Intracellular calcium ion concentration [Ca] is determined by integrating the equation

$$\tau_{Ca}\frac{d[\text{Ca}]}{dt} = -\kappa(I_2 + I_3) - [\text{Ca}] + 0.05\ \mu\text{M}, \tag{72}$$

with

$$\kappa = \frac{(0.94\ \mu\text{M}\cdot\text{nF/nA})}{C} = 14.96\ \mu\text{M/nA} \tag{73}$$

and

$$\tau_{Ca} = 200\ \text{ms}. \tag{74}$$

This equation (see [19]) reflects the fact that the calcium membrane current $I_2 + I_3$ determines the rate at which calcium ions enter the neurons and assumes that calcium ions are buffered at a rate that depends linearly on [Ca]. The constant 0.05 μM is the steady state intracellular calcium ion concentration if no calcium ions traverse the cell membrane, τ_{Ca} is a time constant, and κ determines the amount by which a unit of calcium ionic current changes the intracellular calcium ion concentration.

The additional difficulty in inverting the equations of the STG model relative to the original Hodgkin-Huxley model arises due to

1. the dependence of the reversal potential for the fast transient and slow calcium membrane currents on the intracellular concentration of calcium ions (E_2 and E_3 depend on [Ca] as in equation (70)), and

2. the [Ca]-dependence in the calcium-dependent potassium membrane current I_5 ($m_5^*(v)$ depends on [Ca] as in Table 6).

Since [Ca] is found for time t by integrating equation (72), which requires the currents I_2 and I_3 and hence from equation (69) the maximal conductance values x_2 and x_3, the membrane currents I_2, I_3, and I_5 have a nonlinear dependence on x that was not present in the original Hodgkin-Huxley model of Chapter 2, rendering the single-stage algorithm of Chapter 2 inapplicable for inverting the equations of the

STG model. An iterative procedure for inverting the equations of the STG model is developed in Section 3.4.

3.2 The problem

The problem is to consider a voltage trace generated by the equations of the STG neuron model with an unknown set of maximal conductance values, and to produce a set of maximal conductance values that generates a voltage trace that is a good behavioral match to the given voltage trace.

As was the case with the original Hodgkin-Huxley equations, the output of the equations of the STG model in Section 3.1 is a voltage trace $v(t)$ describing the electrical activity of a model neuron on the domain $t \in [0, \infty)$, giving the voltage across the neuron cell membrane as a function of time. The equations of the STG model are a mapping from an 8 dimensional parameter space to a space $\mathcal{F}$ of real analytic functions (voltage traces) taking $\mathbb{R}_+$ to $\mathbb{R}$. For a set of maximal conductance values $x \in \mathbb{R}^8$, the equations of the STG model send x to a voltage trace $v_x(t) \in \mathcal{F}$. The inverse problem is, as in Chapter 2, to consider a given voltage trace $v_{x^*}(t)$ that is generated by the equations of the STG neuron model for an unknown set of maximal conductance parameters $x^* \in \mathbb{R}^8$ and to produce a set of maximal conductance parameter values $x \in \mathbb{R}^8$ so that $v_x(t) = v_{x^*}(t)$.

Unlike the procedure developed in Chapter 2 for inverting the Hodgkin-Huxley equations for the squid giant axon, we do not assume that the initial values of the activation and inactivation variables m_j and h_j are known for time $t = 0$. In the inversion procedure for the original Hodgkin-Huxley equations of Chapter 2, the activation and inactivation variables m, n, and h are set to their steady state values $m_\infty(v = 0)$, $n_\infty(v = 0)$, and $h_\infty(v = 0)$ for the membrane resting potential at $t = 0$. This is reasonable for a model of a neuron at rest before the application of the stimulus that triggers the action potential. (The stimulus can be either nonzero external current

$I(t)$, or an initial value $v(0) \neq 0$ that differs from the membrane resting potential.) Since the STG neuron exhibits periodic spontaneous behavior, it is not assumed that the values of these variables are known at the time selected to be $t = 0$. In the case of the STG model, the fact that the model neuron fires repetitively in the absence of external stimulus means the activation and inactivation variables do not all approach their steady state values at any instant in time, and the values of all of the activation and inactivation variables are not known at any instant by inspection of the voltage trace.

In the original Hodgkin-Huxley model the inversion algorithm makes use of the fact that the differential equations governing the activation and inactivation variables m, n, and h can each be solved independently by numerical integration using only the given voltage trace data. In the case of the STG neuron model, the differential equations for the activation and inactivation variables cannot be solved independently due to the unknown initial conditions and the dependence on [Ca], and hence on the unknown maximal conductance values.

3.3 Solving the equations of the STG neuron model

The voltage trace generated by the STG neuron is obtained by integrating the equations (68), (71), and (72). As was the case with the original Hodgkin-Huxley equations, it is not possible to obtain a closed form solution, and the integration must be done numerically. This numerical integration is carried out using simulation software used by the Prinz Lab at Emory University. The output for a given set of maximal conductances $x \in \mathbb{R}^8$ is a discrete approximation V_i to the values taken by the true voltage trace $v_x(t_i)$ for a finite set of times t_i, $i = 1, \ldots, N$, with fixed time step $\Delta t = t_{i+1} - t_i$. In what follows the subscripts i will denote the numerical integration time step t_i, and the subscripts j will denote the membrane current so that (for example) $h_{i,j}$ refers to the value computed by the numerical integration procedure for

the inactivation variable of membrane current j at time t_i.

The simulation procedure uses the Euler method to compute the time course of the activation and inactivation variables m_j and h_j, $j = 1, \ldots, 8$, from equation (71) and the exponential Euler method described below to compute the time course of the membrane potential v and the intracellular calcium ion concentration [Ca] from equations (68) and (72).

In the exponential Euler method [3, 27], proposed by Moore and Ramon as a hybrid analytic-numerical integration procedure [22], an equation of the form

$$\frac{dy}{dt} = \alpha - \beta y \tag{75}$$

is integrated numerically according to the rule

$$y_{i+1} = y_i e^{-\beta \Delta t} + \frac{\alpha}{\beta}\left(1 - e^{-\beta \Delta t}\right), \tag{76}$$

derived by treating α and β as constant over the course of each numerical integration time step (the assumption being that these quantities are varying slowly in comparison to y). Rearranging terms and using the expression for $\frac{dy}{dt}$ given in equation (75), the exponential Euler integration rule is

$$y_{i+1} = y_i + \left.\frac{dy}{dt}\right|_i \frac{1}{\beta}\left(1 - e^{-\beta \Delta t}\right). \tag{77}$$

In using the exponential Euler method to compute V_i by numerically integrating equation (68), the activation and inactivation variables m_j and h_j are treated as constant over the course of each integration time step, and the numerical solution at V_{i+1} at time t_{i+1} is

$$V_{i+1} = V_i + \left.\frac{dV}{dt}\right|_i \cdot \tau_i(x)\left(1 - \exp\left(\frac{-\Delta t}{\tau_i(x)}\right)\right), \tag{78}$$

where

$$\tau_i(x) = \frac{1}{\frac{1}{C}\sum_{j=1}^{8} x_j m_{ij}^{p_j} h_{ij}^{q_j}}. \tag{79}$$

and $\frac{dV}{dt}\big|_i$ is

$$\left.\frac{dV}{dt}\right|_i = -\frac{1}{C}\sum_{j=1}^{8} x_j m_{i,j}^{p_j} h_{i,j}^{q_j}(V_i - E_{i,j}), \tag{80}$$

from equations (68) and (69), so that the change in the membrane potential between steps i and $i+1$ is

$$V_{i+1} - V_i = -\frac{1}{C}\left(\sum_{j=1}^{8} x_j m_{i,j}^{p_j} h_{i,j}^{q_j}(V_i - E_{i,j})\right)\tau_i(x)\left(1 - \exp\left(\frac{-\Delta t}{\tau_i(x)}\right)\right). \tag{81}$$

The exponential Euler method is also used to numerically integrate equation (72) to find $[\mathrm{Ca}]_{i+1}$, the intracellular calcium ion concentration at time t_{i+1}, giving

$$[\mathrm{Ca}]_{i+1} = [\mathrm{Ca}]_i - (\kappa\,(I_{i,2} + I_{i,3}) - [\mathrm{Ca}]_i + 0.05\ \mu\mathrm{M})\left(1 - \exp\left(\frac{-\Delta t}{\tau_{Ca}}\right)\right). \tag{82}$$

The exponential Euler method is sometimes used (as described in [3]) to solve for the activation and inactivation variables m_j and h_j by numerically integrating equation (71) so that

$$m_{i+1,j} = m^*(V_i) + (m_{i,j} - m^*(V_i))\exp\left(-\frac{\Delta t}{\tau_{m_j}(V_i)}\right) \tag{83}$$

or, rearranging terms as above,

$$m_{i+1,j} = m_{i,j} + \left.\frac{dm_j}{dt}\right|_i \tau_{m_j}(V_i)\cdot\left(1 - \exp\left(-\frac{\Delta t}{\tau_{m_j}(V_i)}\right)\right), \tag{84}$$

and equivalently for h_j. In our implementation, however, we do not use the exponential Euler method to compute the time course for the variables m_j and h_j. Using the procedure of the Prinz Lab, we perform the numerical integration for the activation and inactivation variables according to the Euler method. The time evolution of the activation and inactivation variables is computed according to

$$\begin{aligned} m_{i+1,j} &= m_{i,j} + \left.\frac{dm_j}{dt}\right|_i \cdot \Delta t, \\ h_{i+1,j} &= h_{i,j} + \left.\frac{dh_j}{dt}\right|_i \cdot \Delta t, \end{aligned} \tag{85}$$

where the derivatives of the activation and inactivation variables are, from equation (71),

$$\left.\frac{dm_j}{dt}\right|_i = \frac{m_j^*(V_i) - m_{i,j}}{\tau_{m_j}(V_i)}, \quad \forall j \neq 5,$$
$$\left.\frac{dh_j}{dt}\right|_i = \frac{h_j^*(V_i) - h_{i,j}}{\tau_{h_j}(V_i)}, \quad \forall j = 1, ..., 8. \tag{86}$$

For $j = 5$ (the calcium-dependent potassium current), the function m_j^* depends on the intracellular calcium ion concentration in addition to membrane potential as in Table 6:

$$\left.\frac{dm_5}{dt}\right|_i = \frac{m_5^*(V_i, [\mathrm{Ca}]_i) - m_{i,5}}{\tau_{m_5}(V_i)}, \quad j = 5. \tag{87}$$

At each time step t_i the reversal potentials $E_{i,j}$ are given for $j \neq 2, 3$ by the constants in Table 6. Only the calcium reversal potential has time-dependence. The calcium reversal potential $E_{i,2} = E_{i,3}$ at time t_i is computed by solving the Nernst equation (70) using the intracellular calcium ion concentration at time t_i

$$E_{i,2} = E_{i,3} = 12.2 \text{ mV} \ln\left(\frac{3.0 \text{ mM}}{[\mathrm{Ca}]_i}\right). \tag{88}$$

The initial conditions used in the numerical integration procedure are (unless otherwise noted in the text) $V_1 = -70$ mV, $[\mathrm{Ca}]_1$=0.05 μM, $m_{1,j} = m_j^*(V_1)$, and $h_{1,j} = h^*(V_1)$, for $j = 1, \ldots, 8$ (i.e. the activation and inactivation variables are set to their steady state values for the initial membrane potential of 70 mV).

3.4 Inversion procedure for the STG neuron model

Let $V \in \mathbb{R}^N$ denote a given voltage trace that has been generated by numerical integration of the STG equations of Section 3.1 with maximal conductance values x^*, so that V_i denotes the calculated membrane potential at time t_i, for $i = 1, \ldots, N$. The time steps t_i are equally spaced, with interval $\Delta t = t_{i+1} - t_i$.

The iterative procedure will repeatedly estimate values for the unknown maximal conductance values; let $x^k \in \mathbb{R}^8$ be the estimated maximal conductance values

produced in the kth iteration. The time course of the activation and inactivation variables m_j and h_j will be estimated at every step of the iterative procedure by numerical integration using the most recent estimates x^k. Let $m_{i,j}^k$ denote the estimated value for the variable m_j at time t_i produced in the kth iteration, and similarly for $h_{i,j}^k$, $I_{i,j}^k$, and $E_{i,j}^k$, for $j = 1, \ldots, 8$ and $i = 1, \ldots, N$. Note that the reversal potentials for all of the membrane currents except for the two calcium currents I_2 and I_3 are constants specified in Table 6 and do not vary with time or depend on the choice of maximal conductance values. The time course of the intracellular ionic calcium concentration [Ca] will also be estimated by the algorithm in each iteration. Let $[\mathrm{Ca}]_i^k$ be the estimated intracellular ionic calcium concentration at time t_i produced in iteration k.

An outline of the iterative inversion algorithm for the STG neuron model follows:

1. Set $k = 0$ and arbitrarily assign maximal conductance values x^0.

2. Numerically integrate the equations of the STG model using the given voltage trace data V and the current maximal conductance estimates x^k to produce $m_{i,j}^k$, $h_{i,j}^k$, and $E_{i,j}$ for each $i = 1, \ldots, N$ and $j = 1, \ldots, 8$.

3. Find a set of maximal conductance values x^{k+1} that gives a best fit to the given voltage trace values V in the least squares sense for the computed values $m_{i,j}^k$, $h_{i,j}^k$, and $E_{i,j}$.

4. Replace x_j^{k+1} by 0 for any negative maximal conductance values x_j^{k+1}.

5. Increment k and repeat from 2.

Prior to the first iteration, we assign arbitrary values to the variables $x^0 \in \mathbb{R}^8$. The algorithm is not sensitive to the choice of values for x^0, provided these values are in a physiologically reasonable range (Section 3.5). The initial choice of the maximal conductance values x_2^0 and x_3^0 associated with the calcium currents play a role by

determining the time evolution of the intracellular calcium ion concentration [Ca] in the first iteration of the algorithm. The initial choices for the remaining maximal conductance values x_j^0, for $j \neq 2, 3$, have no influence on the progress of the algorithm.

At the beginning of each iteration k of the algorithm, the values for the variables $[\text{Ca}]^k$, m_j^k, and h_j^k, $j = 1, \ldots, 8$ whose time course will be computed by numerical integration must be fixed for time t_1. These values are also chosen somewhat arbitrarily. $[\text{Ca}]_1^k$ is set to 0.05 μM, m_{1j}^k is set to the steady state value corresponding to the membrane potential at time t_1 ($m_{1j}^k = m_j^*(V_1)$), and similarly h_{1j}^k is initialized to $h_j^*(V_1)$.

Unlike the original Hodgkin-Huxley model, which was assumed to be quiescent at its resting potential prior to the application of an external stimulus, the STG neuron exhibits ongoing spontaneous activity and there is no reason to suppose that the activation and inactivation variables are at their respective steady state values $m_j^*(V_1)$ and $h_j^*(V_1)$ at time t_1 since in general variations in voltage in the times leading up to t_1 will have prevented the activation and inactivation variables from settling at their steady state values. The initial values m_{1j}^k, h_{1j}^k, $[\text{Ca}]_1^k$ chosen for these variables will generally be incorrect (in the sense that they do not correspond to the values of these variables at time t_1 during the process of solving the equations of the STG neuron to generate the given voltage trace V), but testing shows (Section 3.5) the performance of the inversion algorithm to be similar for any physiologically reasonable values assigned to these variables.

With the exception of m_5^*, the function giving the steady state value for the activation variable for calcium-dependent potassium current, the functions m_j^*, h_j^*, τ_{m_j}, and τ_{h_j} (Table 6) are all explicit functions of voltage whose values are known for each time t_i from the given membrane potential V_i for time t_i.

Step 2 of the inversion algorithm for the STG neuron involves numerically integrating the equations (71) and (72) to obtain estimates for the time course of the

intracellular calcium ion concentration [Ca] and the activation and inactivation variables $m_{i,j}^k$ and $h_{i,j}^k$ for each of the 8 membrane currents for each time step $t_1, \ldots, t_N$. From the intracellular calcium ion concentration [Ca] the time course of the reversal potentials $E_{i,j}^k$ are computed using equation (70) (for $j = 2, 3$) or the constants in Table 6 (for $j \neq 2, 3$).

The numerical integration procedure used during the kth iteration of the inversion algorithm is the procedure described in Section 3.3, with the most recent set of maximal conductance values x^k.

Having used x^k to compute the time course of the variables by numerical integration, the algorithm uses these results in Step 3 to obtain x^{k+1}, the updated estimate for the maximal conductance values. Defining $b \in \mathbb{R}^{N-1}$ by

$$b_i = V_{i+1} - V_i, \quad i = 1, \ldots, N-1 \tag{89}$$

we have from equation (81)

$$b_i = -\tau_i \left[1 - \exp\left(\frac{-\Delta t}{\tau_i}\right)\right] \frac{1}{C} \sum_{j=1}^{8} x_j m_{i,j}^{p_j} h_{i,j}^{q_j} \left(V_i - E_{i,j}\right), \quad i = 1, \ldots, N, \tag{90}$$

with

$$\tau_i = \frac{1}{\frac{1}{C}\sum_{j=1}^{8} x_j m_{i,j}^{p_j} h_{i,j}^{q_j}}. \tag{91}$$

Using the values of the variables computed for each time step by numerical integration in iteration k, we approximate (90) by

$$b_i = -\tau_i^k \left[1 - \exp\left(\frac{-\Delta t}{\tau_i^k}\right)\right] \frac{1}{C} \sum_{j=1}^{8} x_j (m_{i,j}^k)^{p_j} (h_{i,j}^k)^{q_j} \left(V_i - E_{i,j}^k\right), \quad i = 1, \ldots, N, \tag{92}$$

with

$$\tau_i^k = \frac{1}{\frac{1}{C}\sum_{j=1}^{8} x_j (m_{i,j}^k)^{p_j} (h_{i,j}^k)^{q_j}} \tag{93}$$

to obtain an overdetermined linear system in the unknowns $x \in \mathbb{R}^8$. Excepting the unknown maximal conductance values x, all of the quantities in the equation above are known from the numerical integration in Step 2.

Defining $A^k \in \mathbb{R}^{(N-1)\times 8}$ to be the matrix whose entries are

$$a_{ij}^k = -\tau_i^k \left[1 - \exp\left(\frac{-\Delta t}{\tau_i^k}\right)\right] \frac{1}{C} (m_{i,j}^k)^{p_j} (h_{i,j}^k)^{q_j} \left(V_i - E_{i,j}^k\right), \tag{94}$$

for $i = 1, \ldots, N-1$ and $j = 1, \ldots, 8$, we rewrite equation (90) as

$$A^k x = b. \tag{95}$$

The algorithm completes Step 3 by finding a best solution to this overdetermined system of linear equations in the least squares sense. This solution is the updated estimate x^{k+1} for the unknown maximal conductance values. That is, x^{k+1} is an optimal solution to the optimization problem

$$\min_x ||A^k x - b||_2, \tag{96}$$

where $||\cdot||_2$ denotes the Euclidean norm.

3.5 Computational results

The inversion procedure for the STG neuron model was tested on voltage traces representing a range of spontaneous behavior exhibited by the model.

3.5.1 Performance for twenty representative voltage traces

The inversion algorithm was tested on 20 voltage traces selected to represent a range of behaviors exhibited by the STG neuron model. These voltage traces were generated from the STG neuron model by numerically integrating the differential equations of the model according to the procedure given in Section 3.3. The maximal conductance values used to generate each of the 20 voltage traces are given in Table 8.

For each of the sets of maximal conductance values in Table 8 the resulting voltage trace was used as an input into the inversion algorithm for the STG neuron model. The numerical integration to generate the voltage traces was performed with time step 0.05 ms and the simulation period used was 133.5 seconds. Voltage trace data

Table 7: Performance of the inversion algorithm for the 20 target traces described in Table 8. Values given are $\frac{||x^k - x^*||}{||x^*||}$ for each iteration k.

	Inversion algorithm iteration						
Trace	1	2	3	4	5	10	15
1	5.230204	0.255646	0.013582	0.005522	0.001201	1.47E-05	8.34E-08
2	0.116378	0.035027	0.002869	5.85E-05	2.88E-05	1.65E-05	1.65E-05
3	0.077714	0.024526	0.009684	0.004371	0.002062	5.26E-05	3.97E-07
4	0.054206	0.007001	0.00096	0.000127	1.59E-05	1.02E-06	1.02E-06
5	0.255502	0.022682	0.009131	0.000958	0.000327	2.13E-06	2.19E-06
6	0.152972	0.045493	0.013422	0.003951	0.001162	2.34E-06	3.30E-07
7	0.20854	0.071781	0.025134	0.008817	0.003096	2.01E-05	1.26E-05
8	0.041626	0.007841	0.000964	0.000112	1.45E-05	2.00E-06	2.00E-06
9	0.199794	0.068042	0.023487	0.00815	0.002833	1.44E-05	5.62E-08
10	0.098439	0.023735	0.006109	0.001601	0.000419	6.68E-07	6.57E-07
11	0.050055	0.015964	0.002293	0.000681	0.000529	0.000513	0.000513
12	0.22984	0.0822	0.029861	0.010905	0.003991	2.64E-05	1.83E-07
13	0.109223	0.025673	0.006226	0.001521	0.000374	2.55E-05	2.55E-05
14	0.042457	0.003708	0.00041	4.56E-05	6.35E-06	3.08E-06	3.08E-06
15	9.24115	0.739671	0.00199	0.000396	0.000347	2.85E-06	2.70E-06
16	0.38775	0.212347	0.120018	0.068662	0.039533	0.002579	0.00017
17	0.298682	0.134794	0.062493	0.029266	0.013764	0.000321	7.24E-06
18	0.191674	0.064273	0.021943	0.007518	0.002579	1.23E-05	1.03E-07
19	1.045964	664271.9	1.028662	1.0218	664271.2	1.0218	1.028664
20	1	1	1	1	1	1	1

Table 8: Maximal conductance parameters for the target voltage traces used in testing the STG model. All conductances in mS/cm^2.

		Maximal conductance values							
Trace	behavior	Na	CaT	CaS	A	KCa	Kd	H	L
1	spiker	100	0	10	40	0	75	0.02	0.03
2	slow spiker	100	0	4	10	10	75	0.01	0.03
3	spiker with broad spike	200	0	2	0	15	0	0.03	0.04
4	spike triplets	100	0	10	50	10	50	0.03	0.05
5	one-spike-burster	0	12.5	10	20	5	75	0.04	0.03
6	burster with plateau	400	2.5	10	20	5	25	0.04	0.03
7	burster (small duty cycle)	400	2.5	4	50	25	75	0	0.04
8	burster (med. duty cycle)	100	0	4	0	15	50	0.02	0.03
9	burster (large duty cycle)	300	7.5	8	0	10	125	0.01	0.03
10	burster	100	0	8	0	25	100	0.05	0.01
11	burster	100	0	2	10	5	25	0	0
12	burster	500	10	0	40	0	100	0.01	0.04
13	burster	200	5	4	40	5	125	0.01	0
14	parabolic burster	100	0	6	10	10	50	0.03	0.05
15	elliptic burster	100	12.5	0	30	0	50	0.04	0.02
16	alternating burster	500	2.5	8	0	15	75	0.05	0
17	irregular burster	400	0	8	50	20	50	0.04	0
18	non-periodic	300	0	10	20	20	125	0.05	0.01
19	low-amplitude oscillations	0	0	6	20	25	0	0.02	0.05
20	silent	500	0	0	40	0	75	0.01	0

Table 9: Maximal conductance values produced by the inversion algorithm after 15 iterations. All conductances in mS/cm^2. Compare to Table 8.

	Maximal conductance values							
Trace	Na	CaT	CaS	A	KCa	Kd	H	L
1	100.000	0.000	10.000	40.000	0.000	75.000	0.020	0.030
2	100.000	0.000	4.000	10.000	9.998	75.000	0.010	0.030
3	200.000	0.000	2.000	0.000	15.000	0.000	0.030	0.040
4	100.000	0.000	10.000	50.000	10.000	50.000	0.030	0.050
5	0.000	12.500	10.000	20.000	5.000	75.000	0.040	0.030
6	400.000	2.500	10.000	20.000	5.000	25.000	0.040	0.030
7	400.000	2.500	4.000	50.000	24.995	75.000	0.000	0.040
8	100.000	0.000	4.000	0.000	15.000	50.000	0.020	0.030
9	300.000	7.500	8.000	0.000	10.000	125.000	0.010	0.030
10	100.000	0.000	8.000	0.000	25.000	100.000	0.050	0.010
11	100.000	0.000	1.998	10.001	4.947	25.000	0.000	0.000
12	500.000	10.000	0.000	40.000	0.000	100.000	0.010	0.040
13	200.000	5.000	3.999	39.994	5.002	125.001	0.010	0.000
14	100.000	0.000	6.000	10.000	10.000	50.000	0.030	0.050
15	100.000	12.500	0.000	30.000	0.000	50.000	0.040	0.020
16	499.915	2.499	7.998	0.001	14.998	74.987	0.050	0.000
17	399.997	0.000	8.000	49.999	20.000	50.000	0.040	0.000
18	300.000	0.000	10.000	20.000	20.000	125.000	0.050	0.010
19	2.200	0.009	0.000	0.000	0.000	7.540	0.000	0.000
20	0.000	0.000	0.000	0.000	0.000	0.000	0.000	0.000

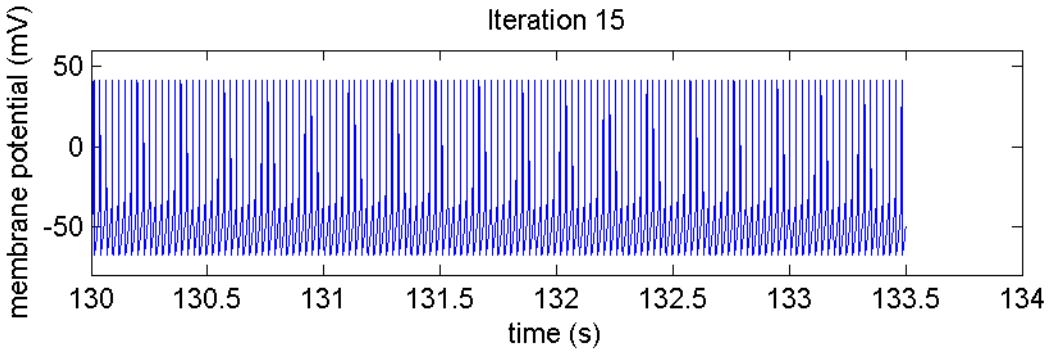

(a) Trace generated by the maximal conductances produced by the inversion algorithm (see Table 9).

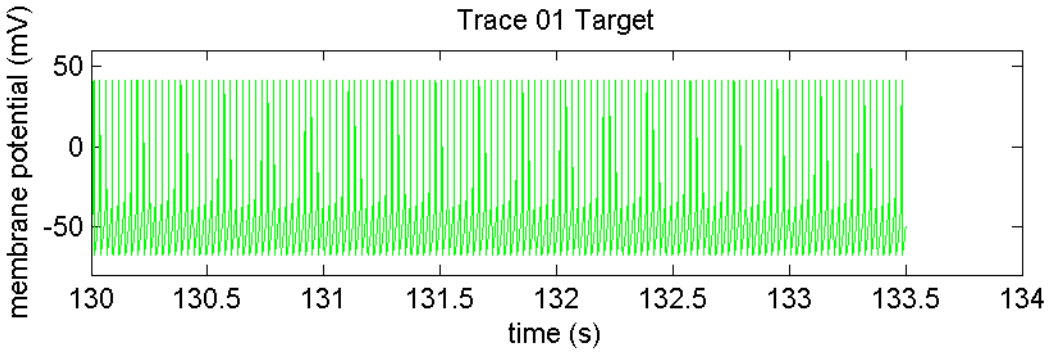

(b) Target Trace 1, specified in Table 8.

Figure 13: Target Trace 1 and the trace generated by the maximal conductances produced by the inversion algorithm.

were recorded for each numerical integration time step during the final 3.5 seconds of the simulation. The 70,000 voltage trace data points obtained in this way were used as the input to the inversion algorithm. The initial 130 seconds of simulation for which data were not recorded was to allow the system to reach equilibrium (130 seconds is significantly more time than is necessary).

In the numerical integration process involved in generating voltage trace data the membrane potential was initialized to -70 mV, the activation and inactivation variables were set to their steady state values for $v = -70$ mV, and the intracellular calcium ion concentration [Ca] was set to 0.05 μM.

The inversion algorithm begins its first iteration with an arbitrary estimate of $x_j = 5$ mS/cm^2 for each of the 8 maximal conductance values. In the numerical integration procedure of the inversion algorithm the activation and inactivation variables are

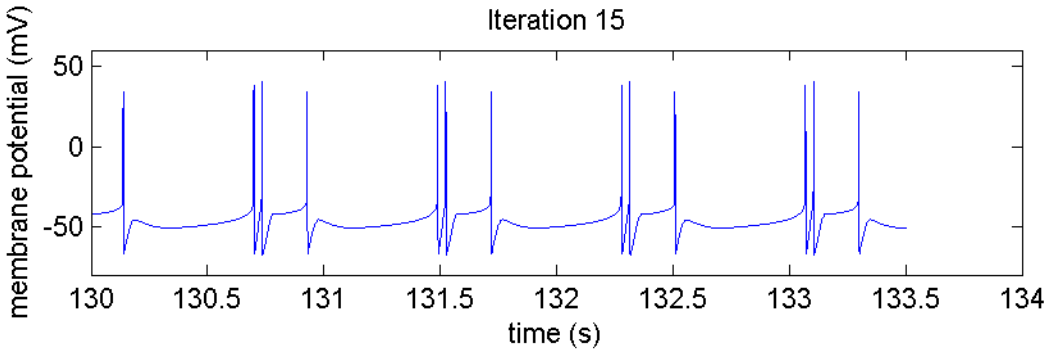

(a) Trace generated by the maximal conductances produced by the inversion algorithm (see Table 9).

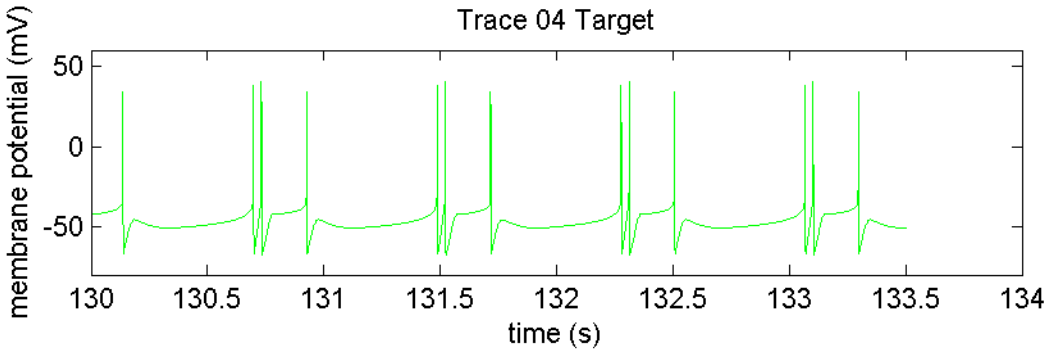

(b) Target Trace 4, specified in Table 8.

Figure 14: Target Trace 4 and the trace generated by the maximal conductances produced by the inversion algorithm.

initialized to their steady state values for the membrane potential of the target trace at $t = 130$ s, and the intracellular calcium ion concentration is initialized to 0.05 μM. These initial values chosen for the first time step of the numerical integration process for the inversion procedure do not generally coincide with the values found for the corresponding variables at the same time in the numerical integration process used to generate the target voltage trace. Despite this initial inaccuracy in the values used by the inversion algorithm for these variables, the procedure is found after 15 iterations to produce maximal conductance values that generate a voltage trace that closely approximates the behavior of the target trace for all but one (Trace 19) of the 20 target traces in Table 8.

In Table 7 we report the results of 15 iterations of the inversion procedure for the STG neuron model, using the 20 target behaviors given in Table 8 as input. The

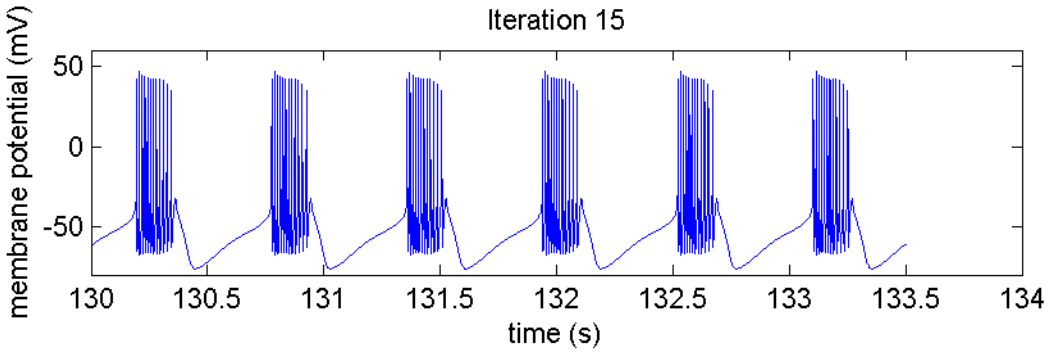

(a) Trace generated by the maximal conductances produced by the inversion algorithm (see Table 9).

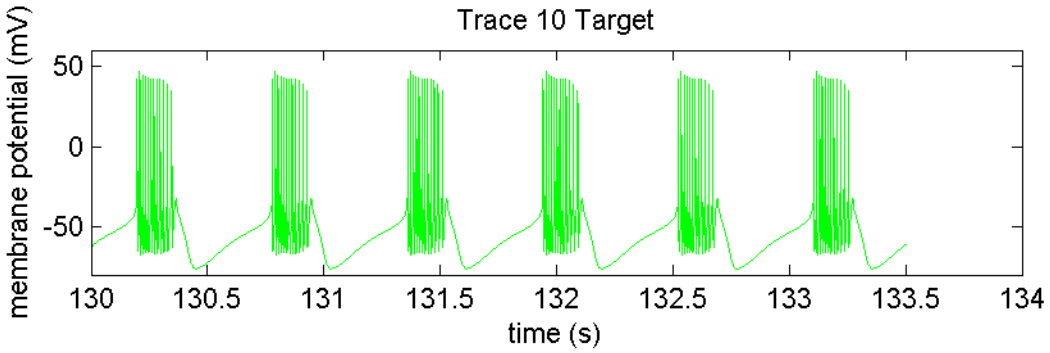

(b) Target Trace 10, specified in Table 8.

Figure 15: Target Trace 10 and the trace generated by the maximal conductances produced by the inversion algorithm.

values given in Table 7 are the normalized difference between the target vector and the vector produced in the 15th iteration of the inversion algorithm:

$$\frac{||x^k - x^*||}{||x^*||} = \sqrt{\frac{\sum_{j=1}^{8} \left(x_j^k - x_j^*\right)^2}{\sum_{j=1}^{8} (x_j^*)^2}}, \tag{97}$$

where $x^* \in \mathbb{R}^8$ is the vector of maximal conductance values that generated the target trace, and $x^k \in \mathbb{R}^8$ is the vector of maximal conductance values produced by the inversion algorithm in iteration k.

For all but two of the 20 target voltage traces, this normalized difference is less than 0.001, indicating that the inversion algorithm produced a set of maximal conductance values very nearly identical to the maximal conductance values used to generate the target voltage trace. The fact that the inversion algorithm converges in 18 of the 20 test cases to the maximal conductance values used to generate the

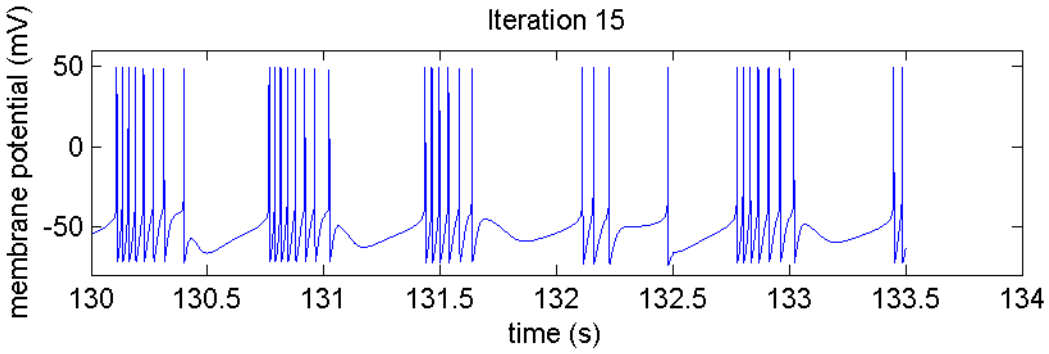

(a) Trace generated by the maximal conductances produced by the inversion algorithm (see Table 9).

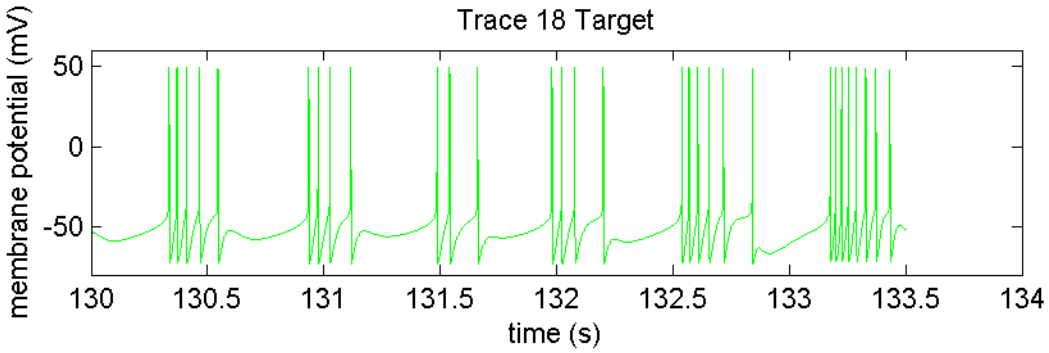

(b) Target Trace 18, specified in Table 8.

Figure 16: Target Trace 18 and the trace generated by the maximal conductances produced by the inversion algorithm.

target trace suggests that in many cases a voltage trace produced by the STG neuron model is generated by a unique set of maximal conductance parameters. This may appear surprising in light of the considerable evidence (see, for example, [20]) that similar neuron behavior can arise in very different regions of parameter space, but these results are not contradictory since the algorithm we have developed searches for parameters that give exact pointwise matches to the target behavior on some interval, rather than behavior that is qualitatively or quantitatively similar but not necessarily identical.

Figures 13-18 show the target trace (green) and the trace generated by the maximal conductances given by the inversion algorithm after 15 iterations (blue). In each case the voltage trace is generated from the maximal conductance values produced by the inversion algorithm using a numerical integration procedure identical to that

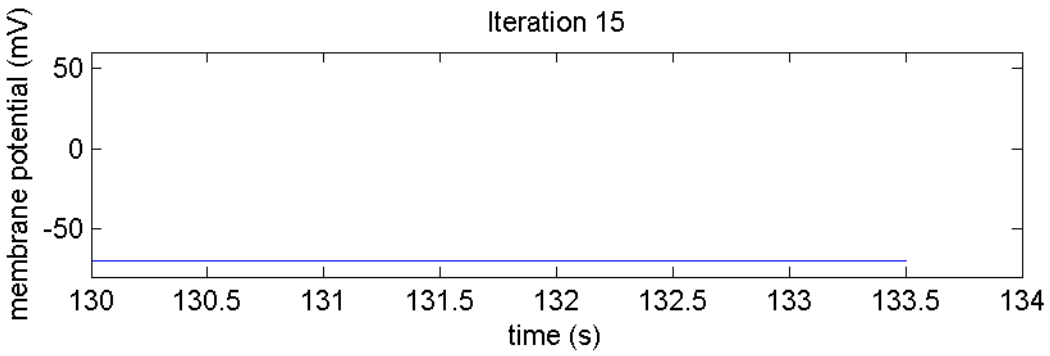

(a) Trace generated by the maximal conductances produced by the inversion algorithm (see Table 9).

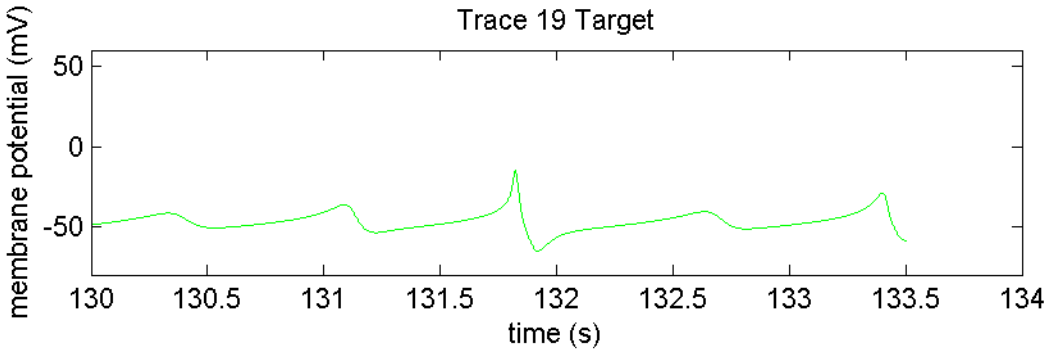

(b) Target Trace 19, specified in Table 8.

Figure 17: Target Trace 19 and the trace generated by the maximal conductances produced by the inversion algorithm.

given above to generate the target voltage trace from the maximal conductance values x^* given in Table 8.

Figures 13-16 show 4 of the 18 cases for which the algorithm produced maximal conductance values nearly identical to the maximal conductance values that generated the target trace. In each of these 18 cases, the trace generated by the maximal conductance values given by the algorithm is a very good match to the target trace. Note that in some cases (for example the nonperiodic Trace 18 for which results are shown in Figure 16) the voltage trace generated by the maximal conductances given by the inversion algorithm is a good behavioral match to the target trace despite not matching the target trace pointwise on the interval 130 s$\leq t \leq$133.5 s. The local sensitivity of the equations of the STG neuron model to changes in the maximal conductance parameters (small deviations from x^* lead to significant changes in $v_{x^*}(t)$)

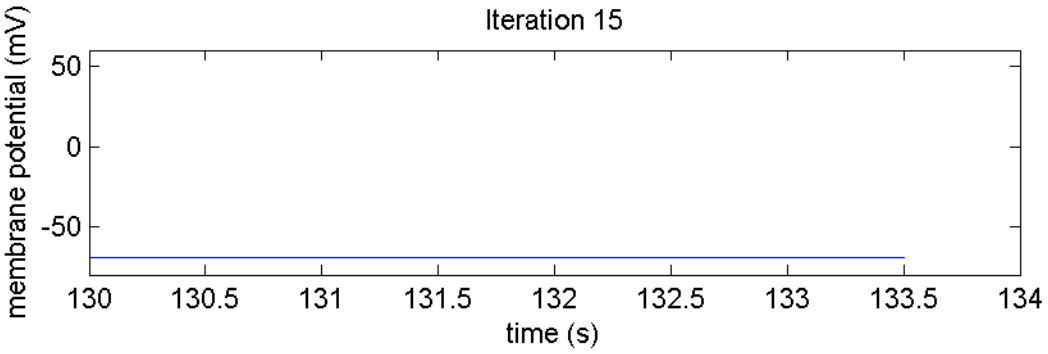

(a) Trace generated by the maximal conductances produced by the inversion algorithm (see Table 9).

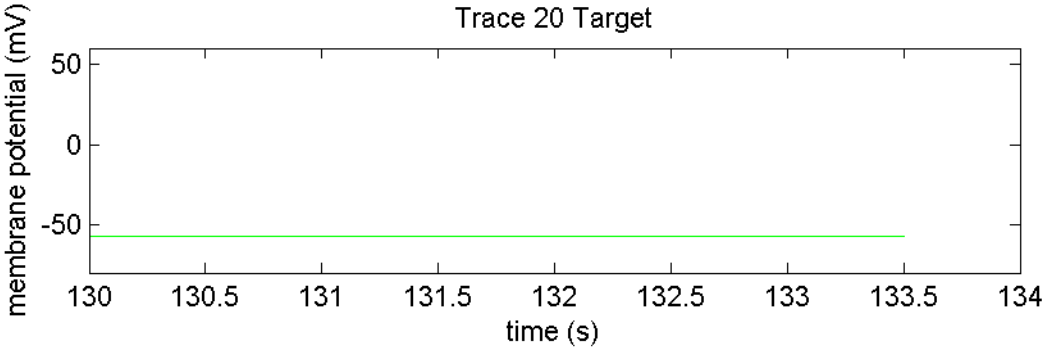

(b) Target Trace 20, specified in Table 8.

Figure 18: Target Trace 20 and the trace generated by the maximal conductances produced by the inversion algorithm.

mean the function $v_x(t)$ may not match $v_{x^*}(t)$ pointwise for all t, even for x in the neighborhood of x^*. From a biological perspective, the qualitative similarity between the target trace in Figure 16(b) and the trace generated by the maximal conductance values given by the algorithm in Figure 16(a) make this a successful reproduction of the target behavior.

Figures 17 and 18 show the two cases for which the algorithm did not converge to maximal conductance values similar to those used to generate the target trace. Figures detailing the performance of the algorithm more fully for each of the 20 target traces are given in Appendix A.

In one of the two cases for which the inversion algorithm does not produce maximal conductance values similar to those used to generate the target trace (Trace 20, silent), the maximal conductance values produced by the inversion algorithm ($x_j = 0$ mS/cm^2

for all $j = 1, \ldots, 8$) nevertheless are a good fit in the sense that they generate a trace with similar behavior ($\frac{dv}{dt} = 0$ for all t, i.e. a silent trace). Figure 18 shows the target trace and the trace generated by the maximal conductance values produced by the inversion algorithm for Trace 20.

Figure 17 shows the single case for which the behavior generated by the maximal conductances given by the algorithm is a poor match to the target behavior (Trace 19, low amplitude oscillations). For the maximal conductance parameters x^* used to generate Trace 19 the inversion algorithm is sensitive to the initial choice of maximal conductance parameters x^0. If x^0 is chosen to be equal to x^* the inversion algorithm returns maximal conductance values in the neighborhood of x^* for several iterations before drifting from this solution, suggesting that the algorithm either does not converge for this choice of x^* or the radius of convergence is much smaller for Trace 19 than for the other cases.

3.5.2 Sensitivity to initial values

The inversion algorithm developed in Section 3.4 requires an initial choice $x^0 \in \mathbb{R}^8$ of maximal conductance values prior to the first iteration. In computing the results presented above, the 8 maximal conductance values were each arbitrarily set to 5 mS/cm^2. In this section we present results showing that in most cases (for the majority of target behaviors) the performance of the algorithm is not sensitive to the choice of x^0.

In addition to setting the initial maximal conductances prior to the first iteration, the numerical integration step of the inversion algorithm requires that initial (time $t = 130$ s) values for the internal calcium ion concentration [Ca] and for each of the activation and inactivation variables be fixed at each iteration. These values are not available by inspection of the given voltage trace data and must also be fixed arbitrarily. In computing the results reported above, the activation and inactivation

variables at time $t = 130$ s were each set to their steady state value for the membrane potential at $t = 130$ s for the target trace, and [Ca] at $t = 130$ s was initialized to 0.05 μM.

To test the sensitivity of the inversion algorithm to the initial values, the algorithm was run for 15 iterations on the 20 target traces generated by the maximal conductance parameters in Table 8 with the initial values fixed randomly. For each of these tests, the maximal conductance for the Na current was chosen randomly between 0 and 500 mS/cm^2, the maximal conductances for the currents CaT and CaS were each chosen randomly between 0 and 10 mS/cm^2, the maximal conductances for the currents A, KCa, and Kd were each chosen randomly between 0 and 100 mS/cm^2, and the maximal conductances for the currents H and L were each chosen randomly between 0 and 0.1 mS/cm^2. In addition, the initial values for the activation and inactivation variables at $t = 130$ s were each chosen randomly between 0 and 1, and the initial value for the intracellular calcium ion concentration at $t = 130$ s was chosen at random between 0 and 0.1 μM during the numerical integration portion of each iteration.

Table 10 reports the value of

$$\frac{||x^{15} - x^*||}{||x^*||} \tag{98}$$

for each of 8 trials with initial values chosen randomly as described above, where x^{15} denotes the maximal conductance values produced by the inversion algorithm after 15 iterations and the norm is the Euclidean norm. In each of the trials, the results were almost indistinguishable from those reported in the previous section; for 18 of the 20 target traces the maximal conductance values produced by the inversion algorithm were nearly identical to those used to generate the target trace, Trace 19 yielded a consistently poor fit, and in each case the algorithm produced the solution $x_j = 0$ for all j for Trace 20.

The fact that the performance of the algorithm is not dependent on the initial

values for the activation and inactivation variables is due to the fact that, as seen in equation 71, the values of the activation and inactivation variables always tend toward the steady state value $m^*(v)$ or $h^*(v)$ for the corresponding variable. As $v(t)$ is known, the activation and inactivation variables eventually equilibrate to the correct values over the course of the numerical integration process that occurs at each iteration of the inversion algorithm.

Table 10: Performance of the inversion algorithm with randomly chosen initial values. Quantities given are $\frac{||x^{15}-x^*||}{||x^*||}$.

	Random initial value, trial number							
Trace	1	2	3	4	5	6	7	8
1	0.00000	0.00001	0.00001	0.00001	0.00000	0.00001	0.00001	0.00000
2	0.00011	0.00001	0.00003	0.00002	0.00015	0.00004	0.00005	0.00004
3	0.00002	0.00001	0.00001	0.00002	0.00000	0.00000	0.00001	0.00002
4	0.00000	0.00000	0.00000	0.00000	0.00000	0.00000	0.00000	0.00000
5	0.00001	0.00001	0.00000	0.00000	0.00002	0.00003	0.00003	0.00001
6	0.00000	0.00000	0.00000	0.00000	0.00000	0.00000	0.00000	0.00000
7	0.00002	0.00002	0.00011	0.00009	0.00002	0.00002	0.00006	0.00011
8	0.00002	0.00000	0.00001	0.00002	0.00005	0.00002	0.00001	0.00006
9	0.00000	0.00000	0.00000	0.00000	0.00000	0.00000	0.00000	0.00000
10	0.00000	0.00000	0.00000	0.00000	0.00000	0.00000	0.00000	0.00000
11	0.00057	0.00036	0.00006	0.00004	0.00065	0.00048	0.00068	0.00046
12	0.00000	0.00000	0.00000	0.00000	0.00000	0.00000	0.00000	0.00000
13	0.00001	0.00001	0.00001	0.00001	0.00001	0.00000	0.00001	0.00002
14	0.00001	0.00001	0.00001	0.00001	0.00001	0.00000	0.00003	0.00001
15	0.00000	0.00000	0.00002	0.00000	0.00001	0.00003	0.00003	0.00000
16	0.00012	0.00014	0.00012	0.00012	0.00003	0.00011	0.00012	0.00014
17	0.00000	0.00001	0.00001	0.00001	0.00000	0.00001	0.00001	0.00001
18	0.00000	0.00000	0.00000	0.00000	0.00000	0.00000	0.00000	0.00000
19	1.03158	1.03164	1.02865	1.03047	1.02865	1.03120	1.03032	1.03169
20	0.99762	0.99762	0.99762	0.99762	0.99762	0.99762	0.99762	0.99762

3.6 Summary

The iterative algorithm developed in this chapter was tested against 20 target voltage traces provided by the Prinz Lab at Emory University that are representative of the range of behaviors displayed by the STG neuron model. The algorithm was successful

in producing a set of maximal conductance values that generates a voltage trace similar to the target trace in 19 of the 20 cases. In 18 of the 20 cases, the maximal conductance values produced by the inversion algorithm were nearly identical to those used to generate the target trace, and the voltage trace generated by the maximal conductance valued found by the algorithm was an excellent behavioral fit to the target voltage trace in each of these cases (Figures 23-40 in Appendix A).

In practice, in solving the problem of selecting parameters that will generate a good match for a given voltage trace, it is more important to produce a good behavioral match than to find a set of parameters that produces a voltage trace that is identical at all time steps to the target trace. For a neuron like the STG that exhibits spontaneous, periodic behavior, a set of parameters that produces a phase-shifted voltage trace that is otherwise a good fit to the target constitutes a good solution to the parameter-fitting problem. In our testing we found that the sets of parameters produced by the iterative algorithm to solve the inverse problem sometimes generated excellent qualitative fits to the target behavior (Figures 33, 35, and 40 in Appendix A) while failing to reproduce the function $v(t)$ exactly.

The increased difficulty of the inverse problem for the STG neuron model relative to the inverse problem for the original Hodgkin-Huxley equations comes from the fact that, unlike the equations of the Hodgkin-Huxley model, the differential equations of the STG neuron model cannot be solved accurately without prior knowledge of the maximal conductance values. This difficulty is compounded by the fact that the initial values of the variables of the STG neuron model cannot be deduced from the voltage trace. However, testing indicates that the performance of the inversion algorithm for the STG neuron model is not sensitive to these initial values.

CHAPTER IV

EXTENSIONS TO THE ALGORITHM FOR INVERTING THE STG NEURON MODEL

In this chapter we test extensions to the STG inversion algorithm on a set of target traces provided by the Prinz Lab at Emory University as modifications to the STG neuron model. These voltage traces are generated using the equations of the STG neuron model with some of the parameters of the model modified by a random amount from the values given in Table 6, or by applying a constant random voltage shift to the membrane potential data of the target voltage trace. These modifications to the STG neuron model are meant to test the limits of the inversion procedure in cases where the exact form of the equations used to generate the target voltage trace data is not known in its entirety to the inversion algorithm. This is the case, for example, when voltage trace data is biological in origin, rather than computationally generated from a model.

In each test case, 3.5 seconds of simulated voltage trace data recorded every 0.05 ms after the model neuron had reached steady state behavior were used as input to the inversion algorithm, so that the inversion algorithm accepted 70,000 membrane potential data points as its only input. The figures in the sections below show the performance of the modified inversion algorithm for representative traces of each type. For the maximal conductance values produced by the algorithm and a complete set of figures showing the performance of the modified algorithm for the extension traces of types 1, 2, and 3 provided by the Prinz Lab, see Appendix B.

The challenge traces provided by the Prinz Lab fall into four categories (see Table 11).

1. Voltage traces chosen at random from the database of 1.7 million model STG neurons constructed by Prinz et al. [24]. These database neurons were generated using a model very similar to that in Chapter 3.

2. Voltage traces generated using sets of maximal conductance values selected at random from the STG database, but the activation and inactivation time constants of all currents were scaled by a random factor.

3. Voltage traces selected at random from the STG database, but each voltage trace was shifted up or down by a random amount.

4. Voltage traces chosen at random from the STG database, but with the activation and inactivation thresholds for each of the membrane currents shifted up or down by a random amount.

Table 11: Traces tested for extensions of the STG neuron model

Trace type	Description	Trace numbers
1	Directly from STG database	101, 106, 107, 111, 114, 121, 123, 125, 134, 138, 142
2	Random time constant scaling	115, 110, 126, 128, 132, 133, 139, 146, 147
3	Random voltage shift	12, 13, 15, 16, 29, 35, 43, 44
4	Random (in)activation threshold shift	2, 3, 4, 8, 19, 20, 22, 27, 31, 37, 40, 41

The STG database developed by Prinz et al. [24] consists of 1.7 million model STG neurons, i.e. sets of maximal conductance parameters. Each set of voltage trace data provided by the Prinz Lab was obtained by selecting one of these model neurons (sets of maximal conductance values) and numerically integrating the equations of the STG neuron model with the modifications to the model specified above.

The modifications to the STG model used to produce the challenge traces provided by the Prinz Lab are meant to approximate experimental uncertainty and variability among neurons. Voltage shifts (traces of type 3) can arise experimentally

from electrochemical potentials at the electrode itself or voltage drift in the recording equipment. Traces of type 2 and 4 represent the variability of activation thresholds and time constants between neurons, and distortions of voltage data due to the fact that real neurons are not single electrical compartments but have spatial extent.

The extended inversion algorithm used in this section first attempts to find maximal conductance values using the procedure of the original algorithm developed in the previous chapter, then (if a satisfactory set of maximal conductance values has not yet been found) searches for maximal conductance values with the activation and inactivation constants scaled by random factors, and finally (if satisfactory maximal conductance values still have not been found) searches for maximal conductance values that match the target trace with some constant voltage shift applied.

This extended version of the inversion algorithm succeeds for each of the traces of types 1, 2, and 3 that were provided by the Prinz Lab for testing (Table 11). This algorithm is not designed to handle the fourth type of challenge trace (where the activation and inactivation thresholds were each shifted by a random amount), and is inapplicable for traces of this kind. Further work is necessary to develop a technique to solve the inversion problem for traces of type 4.

4.1 Extension traces, type 1

The first type of extension traces were each chosen at random from the STG neuron database of Prinz et al. [24]. The model used in generating the neurons in the database is identical to the STG neuron presented in the previous chapter, with the exception of the parametrization for the H current (Table 6). The original algorithm developed in Chapter 3 performs well for traces of type 1. In each of these cases, the maximal conductances given by the algorithm generate a trace that is a very good fit to the target trace.

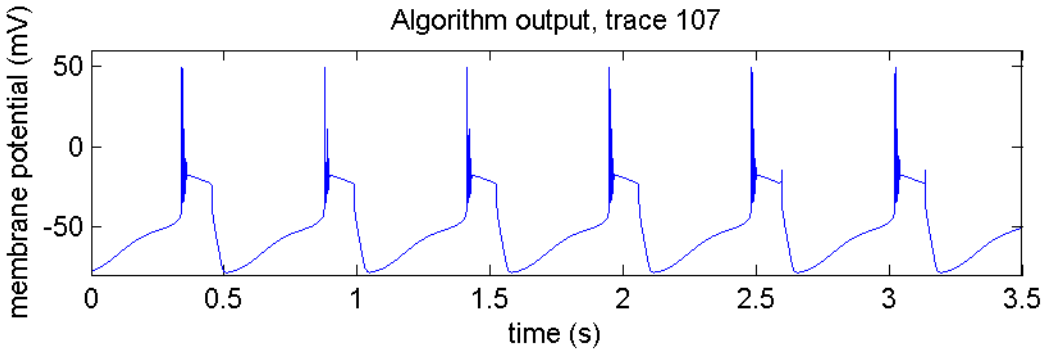

(a) Trace generated by parameters found by inversion algorithm

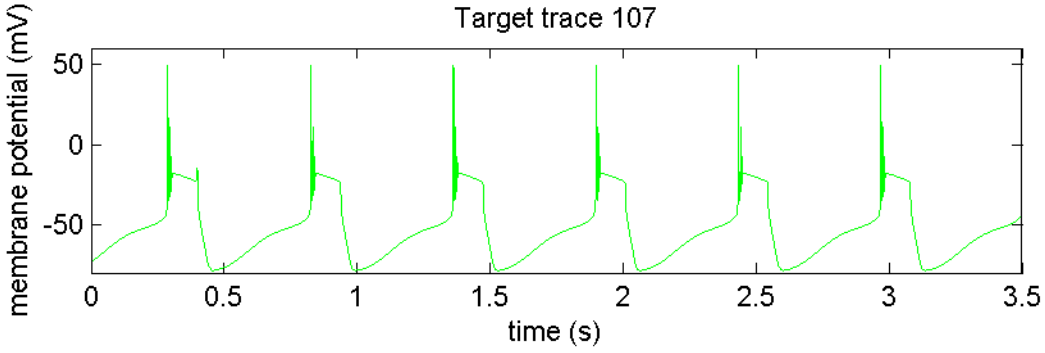

(b) Target trace

Figure 19: Performance of modified inversion algorithm. Trace 107, type 1.

The results for one type 1 trace, Trace 107, are shown in Figure 19. The performance of the algorithm on all traces of this type is given in Appendix B.1. These traces are generated by numerically integrating the equations of the STG model as described in Chapter 3 using the maximal conductance values produced by the algorithm.

4.2 Extension traces, type 2

The second type of extension traces was obtained from model neurons selected at random from the STG database of Prinz et al. by multiplying the activation and inactivation time constants by a random factor. In a biological neuron, these time constants scale with the temperature at which measurements are taken and this random factor is meant to reproduce one type of inaccuracy that could occur in the STG model.

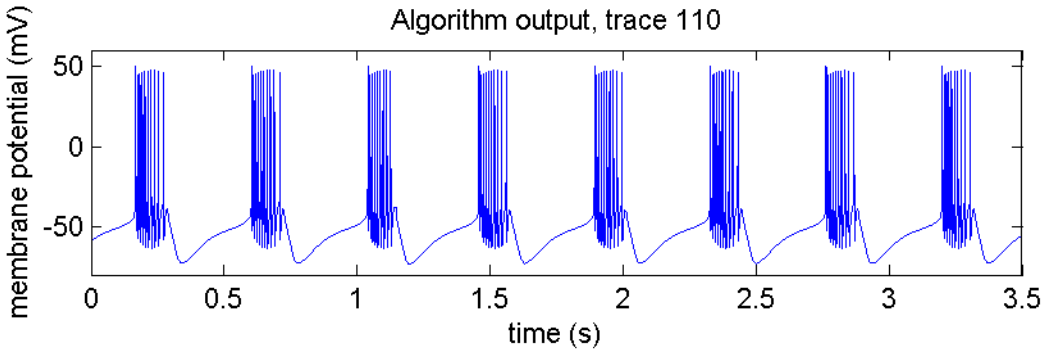

(a) Trace generated by parameters found by inversion algorithm

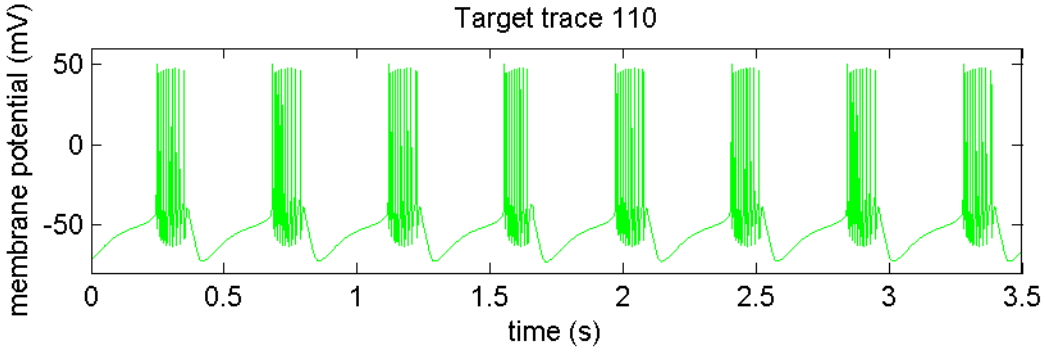

(b) Target trace

Figure 20: Performance of modified inversion algorithm. Trace 110, type 2.

The algorithm was extended to handle traces of this kind by performing a two-dimensional grid search over possible scaling factors for the activation and inactivation time constants. The results reported are the result of performing a grid search over scaling factors between 0.7 and 1.3 with grid increment 0.05. At each grid point the algorithm of Chapter 3 is run for 5 iterations with the appropriate time constants. After the grid search is complete, the algorithm is run for a full 15 iterations with the time constants fixed to the values from the grid point that gave the best least squares objective value at the end of the 5th iteration. The resulting maximal conductance values generated voltage traces that closely approximate the target voltage trace for extension traces of type 2.

The results for one type 2 trace, Trace 110, are shown in Figure 20. The performance of the algorithm for all extension traces of type 2 is shown in Appendix B.2. These traces are generated by numerically integrating the equations of the STG

model as described in Chapter 3 using the maximal conductance values produced by the algorithm, with the time constants scaled by the factor from the best scoring grid point.

4.3 Extension traces, type 3

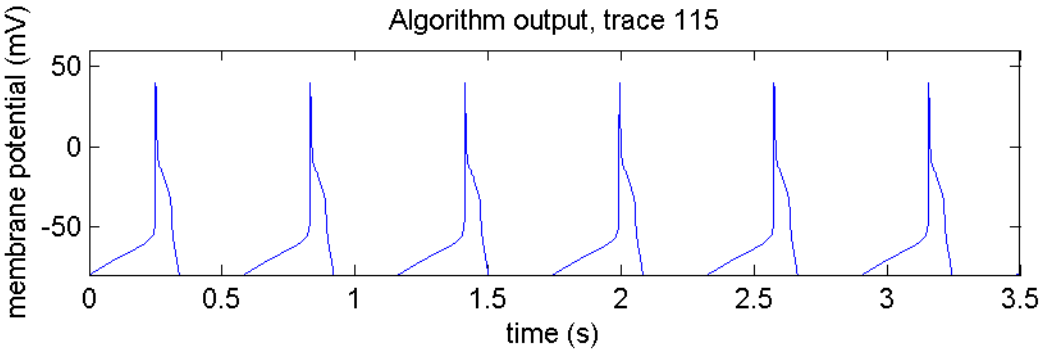

(a) Trace generated by parameters found by inversion algorithm

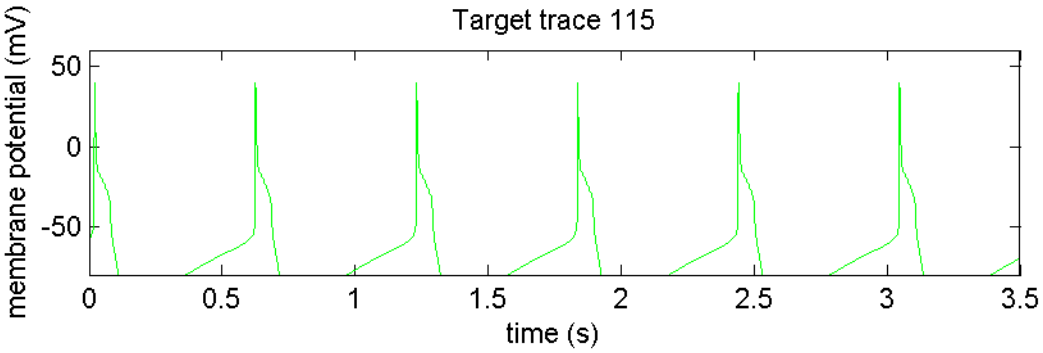

(b) Target trace

Figure 21: Performance of modified inversion algorithm. Trace 115, type 3.

The extension traces of type 3 were the result of randomly choosing model neurons from the STG database and shifting the voltage trace for this neuron up or down by a random constant. The algorithm of the previous chapter was extended to solve the inversion problem for these traces by performing a line search over possible voltage offsets.

The results reported are the result of a line search algorithm that applies voltage offsets of 0, ± 5, and ± 10 mV to the target trace and calls the STG neuron inversion algorithm from the previous chapter using 6 iterations for each applied offset. The

search is centered at the offset that produced the best least squares objective value, and the process is repeated using voltage offsets of half the size previously used (i.e. in the second round of the search voltage offsets of ± 2.5 and ± 5 mV are applied to the best previous offset). The process is repeated until the offset size drops below 0.01 mV, at which point the inversion algorithm from the previous chapter is run for a full 15 iterations using the voltage offset that was found by the line search to give the best objective value. The maximal conductance values obtained in this way were found to generate voltage traces that closely match the extension traces of type 3.

The results for one type 3 trace, Trace 115, are shown in Figure 21. The performance of the algorithm on all type 3 traces is given in Appendix B.3. These traces are generated by numerically integrating the equations of the STG model as described in Chapter 3 using the maximal conductance values produced by the algorithm, with all reversal potentials and voltage thresholds shifted by the voltage offset found by the inversion procedure above.

4.4 Extension traces, type 4

These traces were generated by the Prinz Lab from model neurons selected at random from the STG database by randomly varying each of the 11 activation and inactivation thresholds of the model neuron. The methods employed to handle the extensions of type 2 and 3 were not adaptable to type 4 traces because the parameter space to be searched is eleven-dimensional, much too large for the search techniques employed for traces of types 1 and 2 to be effective. Three of the target traces of type 4 are given for reference in Figure 22. We were not able to obtain maximal conductance values to match any traces of this type.

4.5 Summary

Because the exact form of the equations describing the behavior of biological (as opposed to model) neurons is rarely, if ever, known, it is desirable to have an inversion algorithm with the flexibility to produce sets of parameters that approximately match given voltage trace data even when the equations of the model do not perfectly describe the voltage trace data. Working with voltage trace data from perturbed versions of the STG neuron model is a way of testing the ability of the inversion algorithm to accomodate certain types of discrepancies between the model used by the inversion procedure and the model used to generate the target voltage trace.

When the discrepancy between the model used by the inversion procedure and the model used to generate the target trace is comparatively small (type 1), or when the discrepancy involves a small number of parameters (types 2 and 3), the inversion algorithm can be used alone or in conjunction with simple search techniques to find a set of parameters that generates a trace that is a very good match to the target trace. For a discrepancy involving many parameters (type 4), further work is needed to develop an inversion algorithm capable of matching the target trace.

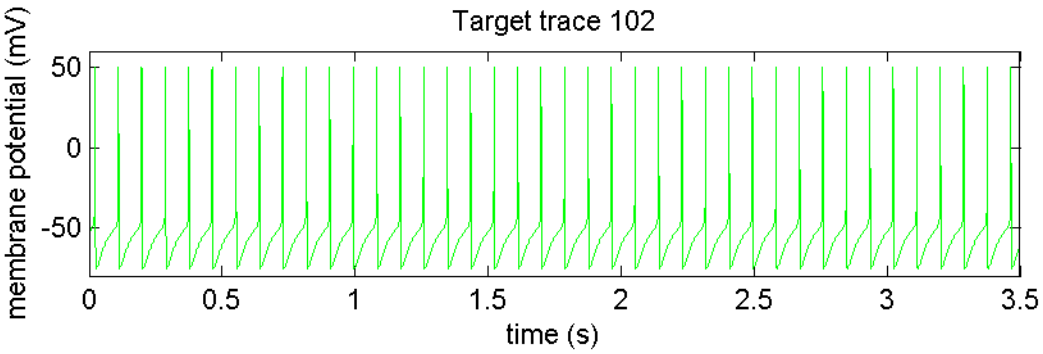

(a) Target trace 102, type 4

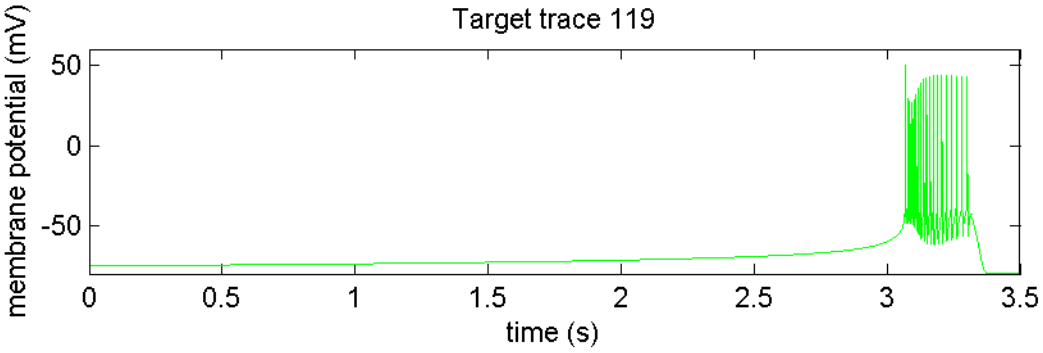

(b) Target trace 119, type 4

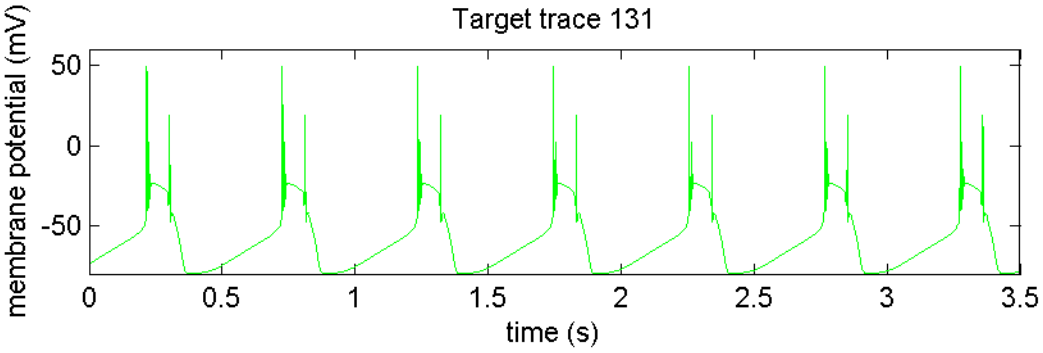

(c) Target trace 131, type 4

Figure 22: Some target traces of type 4.

CHAPTER V

CONCLUSIONS AND FUTURE RESEARCH

The Hodgkin-Huxley equations helped spawn the field of computational neurobiology, and neuron models based on these equations continue to see widespread use by neuroscientists more than half a century later. Hodgkin-Huxley type models accept a set of parameters as input and generate voltage trace data describing the behavior of the neuron. We develop inversion algorithms designed to predict a set of input parameter values from the voltage trace data generated by the model.

Given a target voltage trace generated using the equations of a neuron model with some unknown set of maximal conductance values x^*, the goal of the inversion algorithm is to produce a set of maximal conductance values x that generates the target trace. For a range of maximal conductance values x^*, the inversion algorithms presented for both the original Hodgkin-Huxley equations and the equations of the STG neuron model show evidence of finding maximal conductance values that reproduce the behavior seen in a target voltage trace generated by x^*.

The inversion algorithms for the Hodgkin-Huxley model are proven to converge to x^* with probability 1, provided x^* is the unique set of maximal conductance values that generates the target trace. To our knowledge, this is the first convergence guarantee on a parameter optimization algorithm for Hodgkin-Huxley type neuron models.

Our testing on the original Hodgkin-Huxley equations and on the equations of the STG neuron model suggests that the requirement that x^* be the unique set of maximal conductance values that generates the target trace is not very restrictive; in all of the test cases for the original Hodgkin-Huxley equations and in 18 of the 20

test cases for the more complex STG neuron model the inversion algorithm returned a solution approaching x^*, the maximal conductances used to generate the target trace. In one of the remaining two cases (the silent trace, Trace 20), the algorithm finds an alternative set of maximal conductance values to match the target behavior, in the other (low-amplitude oscillations, Trace 19) the algorithm fails to converge to a solution.

The inversion algorithm for the STG neuron model was extended to handle modifications to the STG neuron model where the parameters of the model were perturbed or the voltage trace generated by the model was shifted by a constant amount. The modified algorithm performed well for small perturbations to the model and when the voltage trace was shifted by a constant amount, but we were not able to modify the algorithm to accomodate perturbations to many model parameters simultaneously.

One direction for future research is extending the inversion algorithm to handle voltage trace data that does not come directly from the model. In solving the inverse problem associated with the equations of a neuron model, we have developed techniques for finding sets of parameters that generate a given voltage trace. Because the voltage trace comes from the equations of the model, the existence of at least one solution to the inverse problem is guaranteed. Adapting the algorithm to find parameter values that give good matches to voltage trace data for which a perfect match does not exist (e.g. noisy data, data from related neuron models, biological neuron data) would enhance its utility and potentially make it a very powerful tool. The work in Chapter 4 is a step in this direction.

As in previous studies ([8, 9, 10, 19, 24]) we focus primarily on the maximal conductances parameters and their relationship to the voltage trace behavior of a model neuron. Another avenue for future research is adapting the algorithms developed to treat more model parameters as unknown variables in the inversion problem. This would give the model increased flexibility to match behavior, at the cost of a higher

dimensional search space. Because the inversion algorithms make use of the equations of the model being inverted, adapting the algorithms to efficiently search over model parameters other than the maximal conductance values is not trivial and requires additional research.

Finally, further research is required to establish theoretical convergence results for the inversion algorithm presented for the STG neuron model. The convergence is complicated relative to that of the inversion algorithm for the original Hodgkin-Huxley model by the iterative nature of the STG inversion algorithm, but the results of our testing suggest that the iterative algorithm does converge to an optimal solution for most target traces.

APPENDIX A

VOLTAGE TRACES TESTED FOR THE STG NEURON MODEL

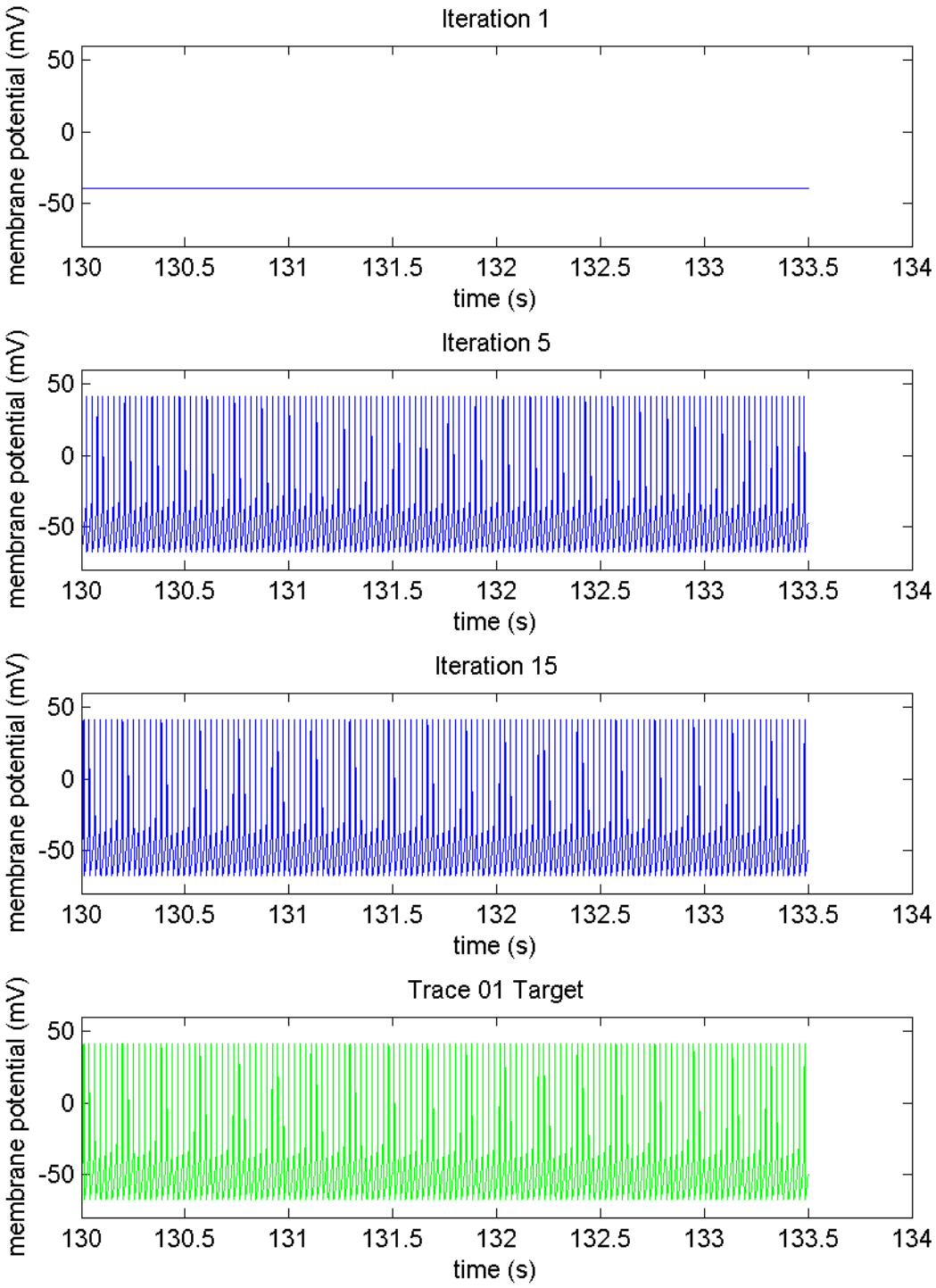

Figure 23: Voltage traces generated by the maximal conductance values produced by the iterative inversion algorithm for the STG neuron model. Target is Trace 1, the spiker specified in Table 8.

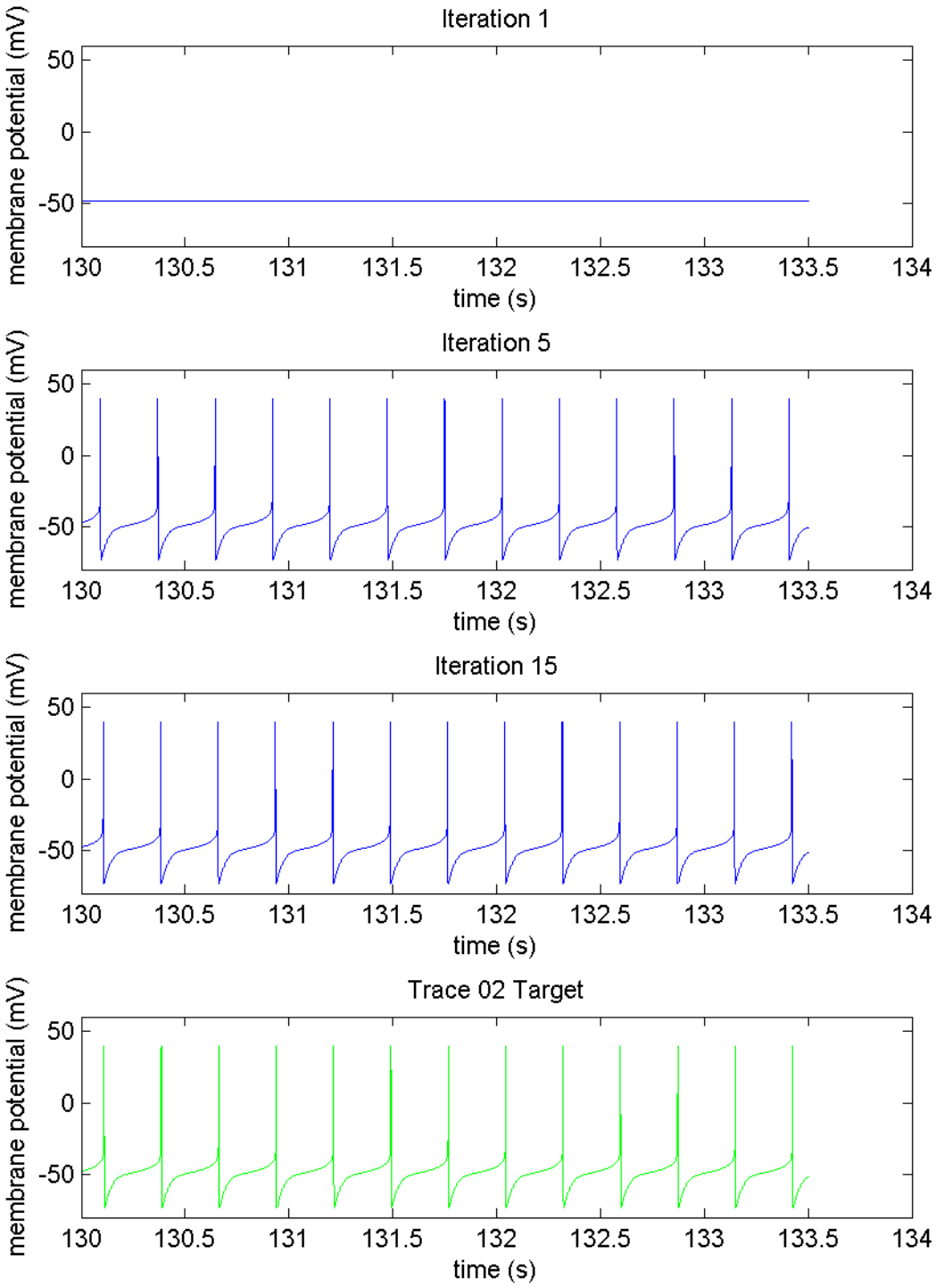

Figure 24: Voltage traces generated by the maximal conductance values produced by the iterative inversion algorithm for the STG neuron model. Target is Trace 2, the slow spiker specified in Table 8.

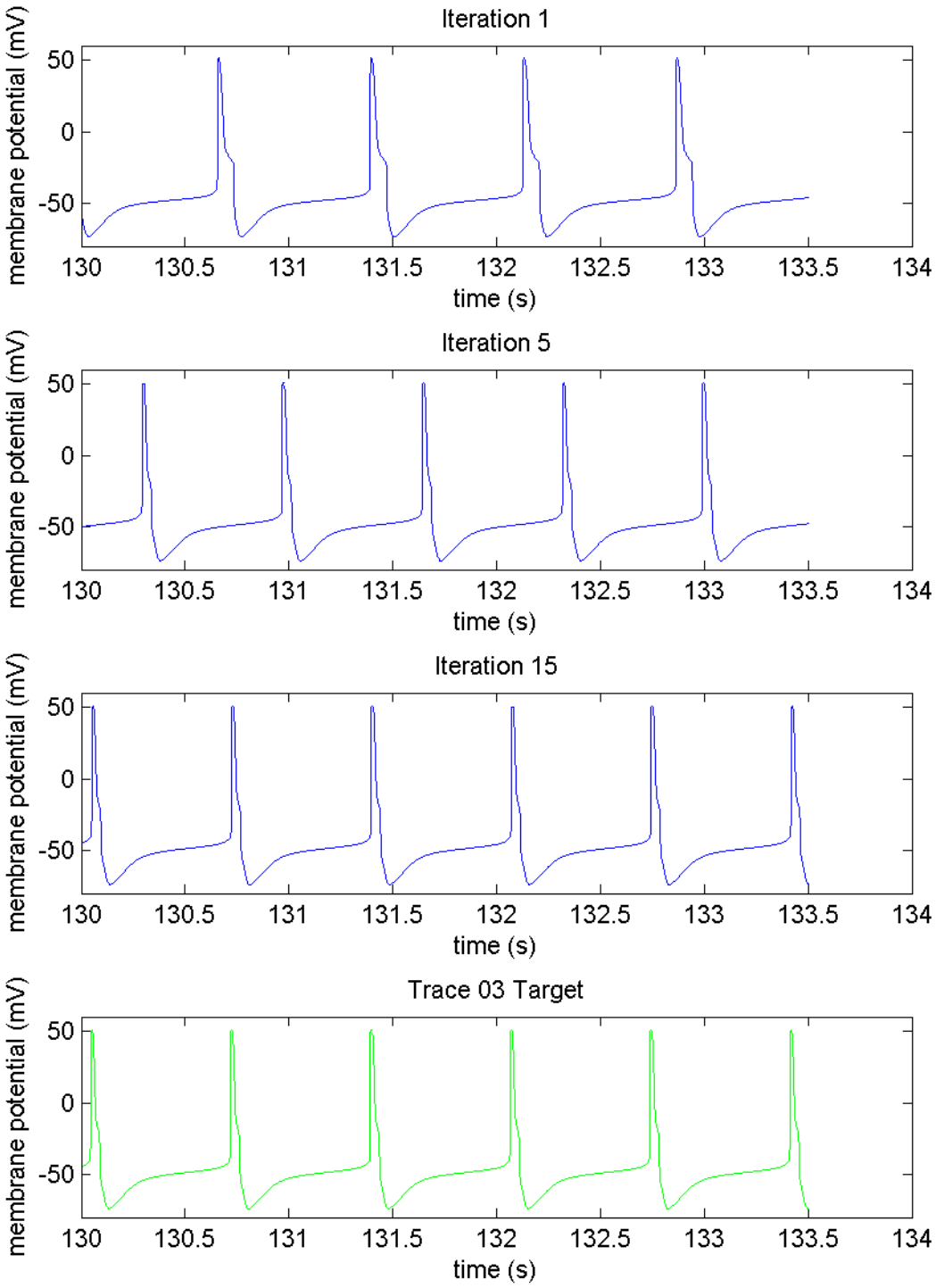

Figure 25: Voltage traces generated by the maximal conductance values produced by the iterative inversion algorithm for the STG neuron model. Target is Trace 3, the spiker with broad spike specified in Table 8.

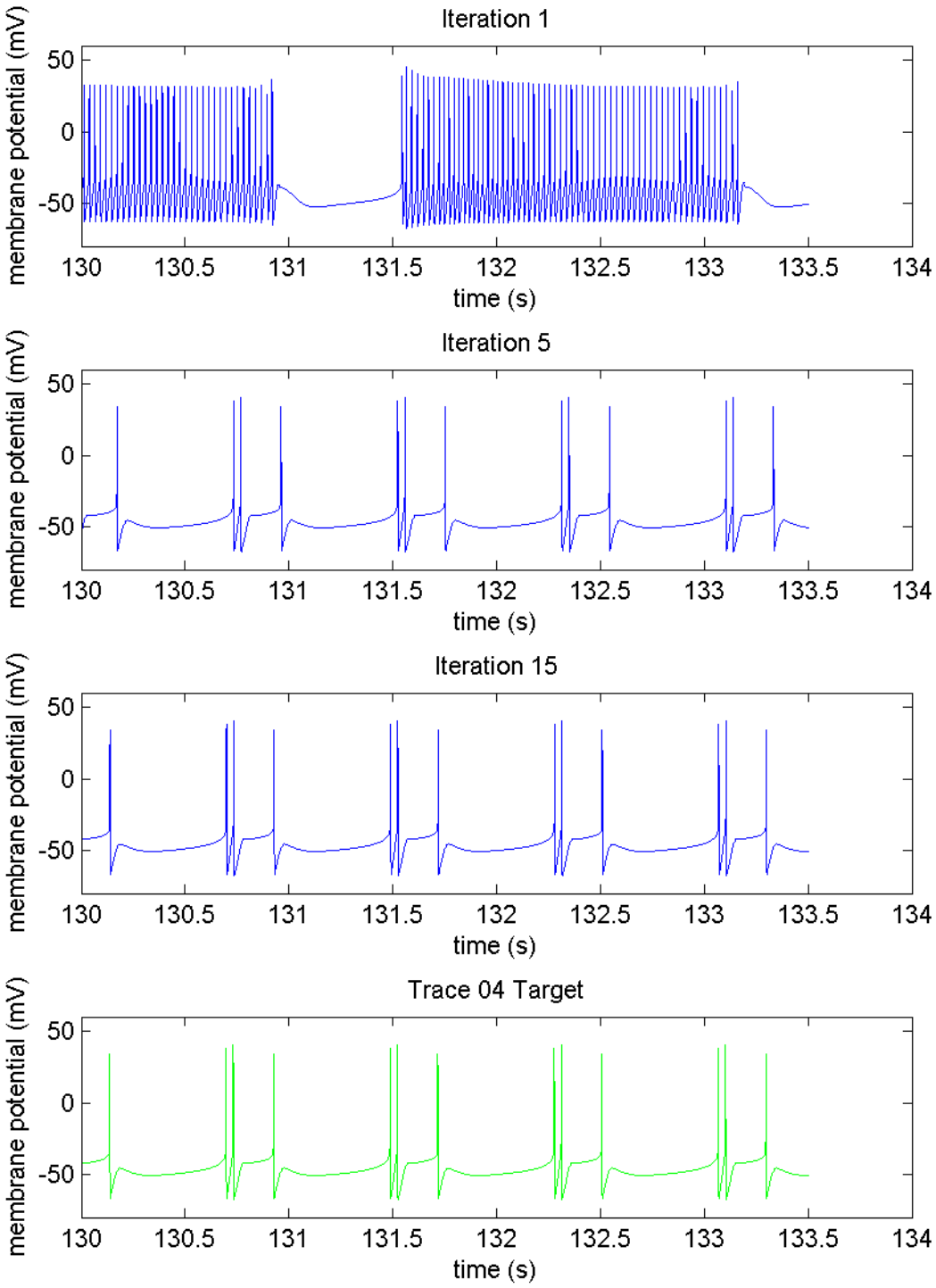

Figure 26: Voltage traces generated by the maximal conductance values produced by the iterative inversion algorithm for the STG neuron model. Target is Trace 4, the spike triplets specified in Table 8.

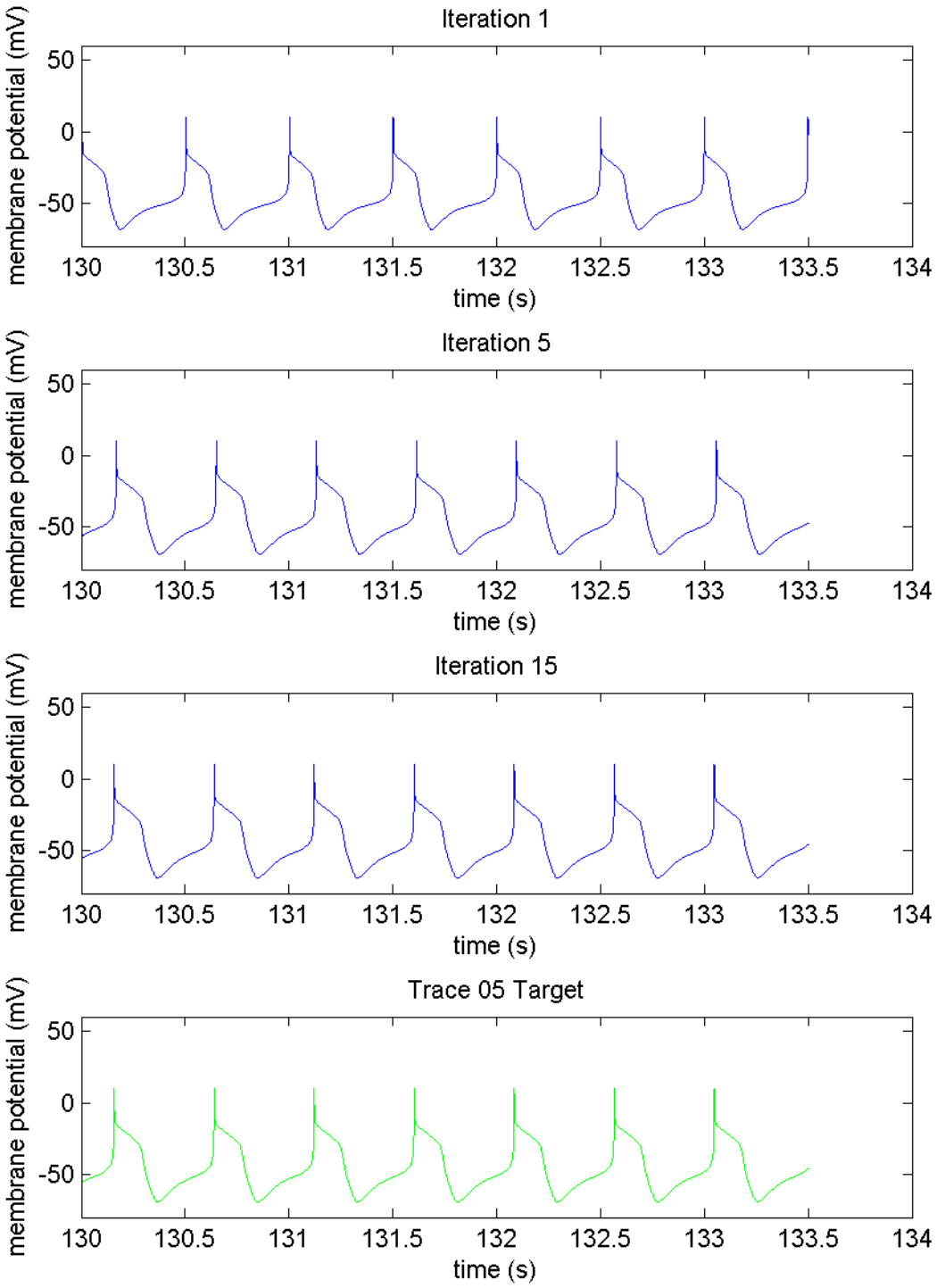

Figure 27: Voltage traces generated by the maximal conductance values produced by the iterative inversion algorithm for the STG neuron model. Target is Trace 5, the one-spike-burster specified in Table 8.

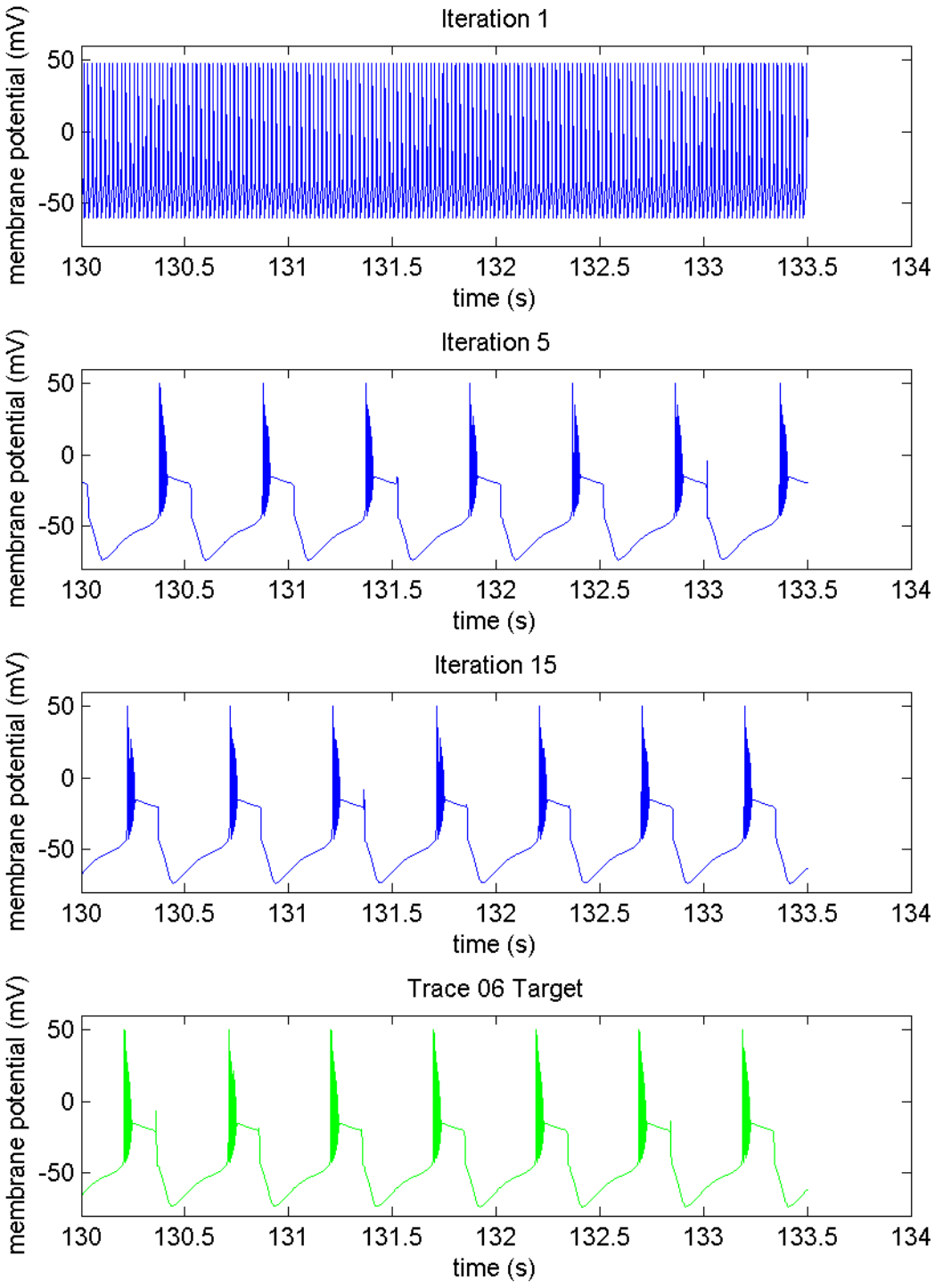

Figure 28: Voltage traces generated by the maximal conductance values produced by the iterative inversion algorithm for the STG neuron model. Target is Trace 6, the burster with plateau specified in Table 8.

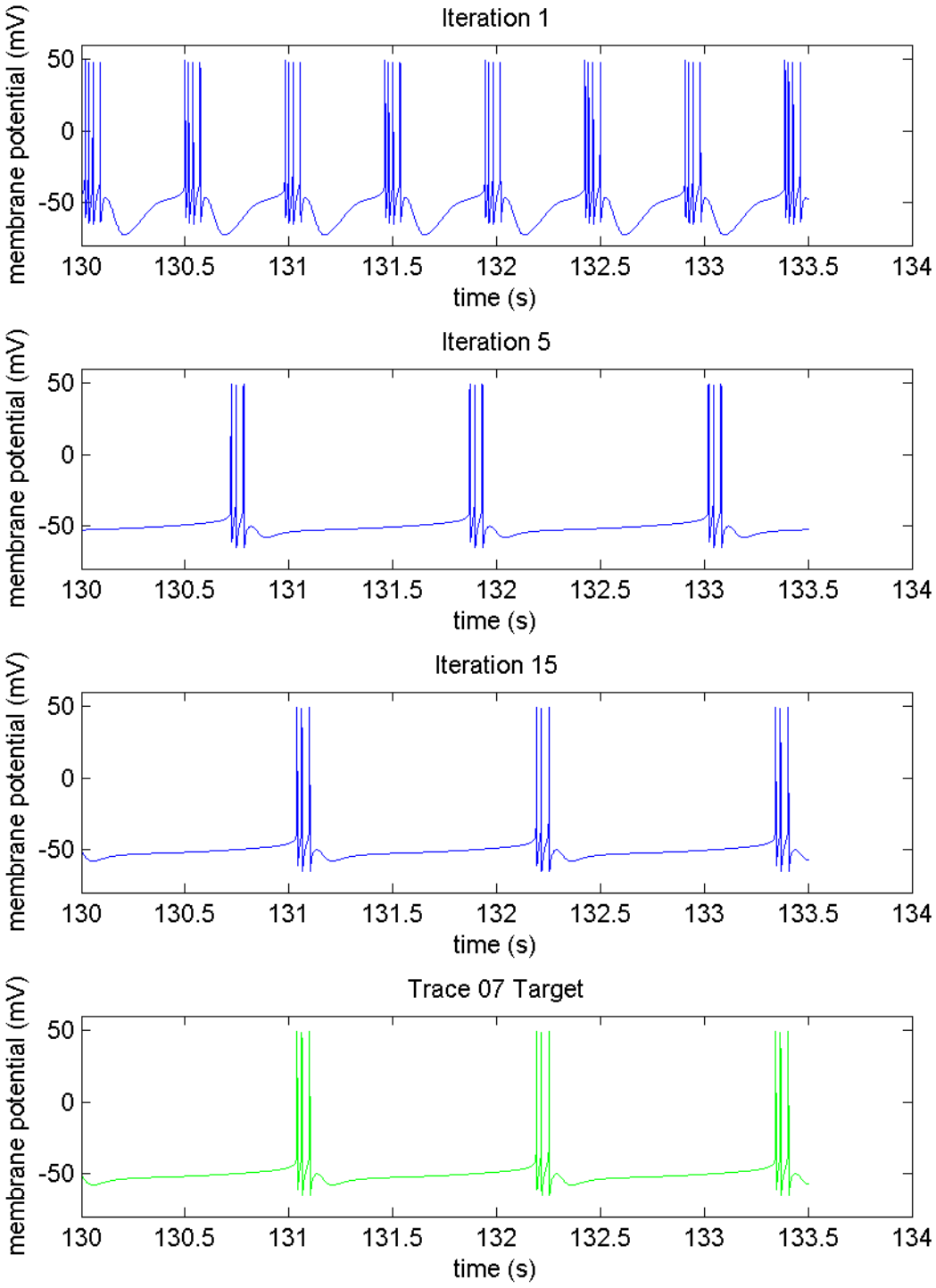

Figure 29: Voltage traces generated by the maximal conductance values produced by the iterative inversion algorithm for the STG neuron model. Target is Trace 7, the burster (small duty cycle) specified in Table 8.

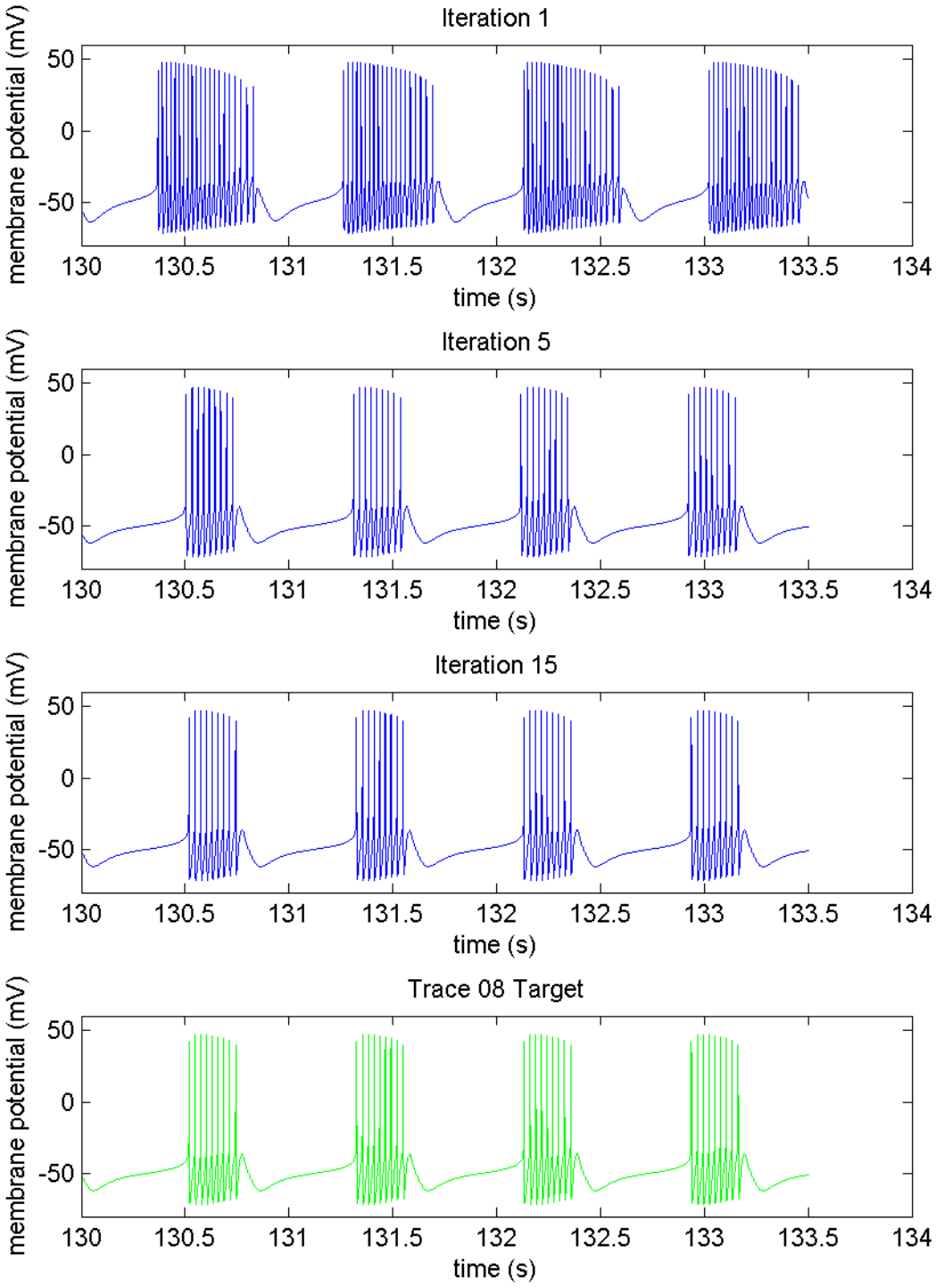

Figure 30: Voltage traces generated by the maximal conductance values produced by the iterative inversion algorithm for the STG neuron model. Target is Trace 8, the burster (medium duty cycle) specified in Table 8.

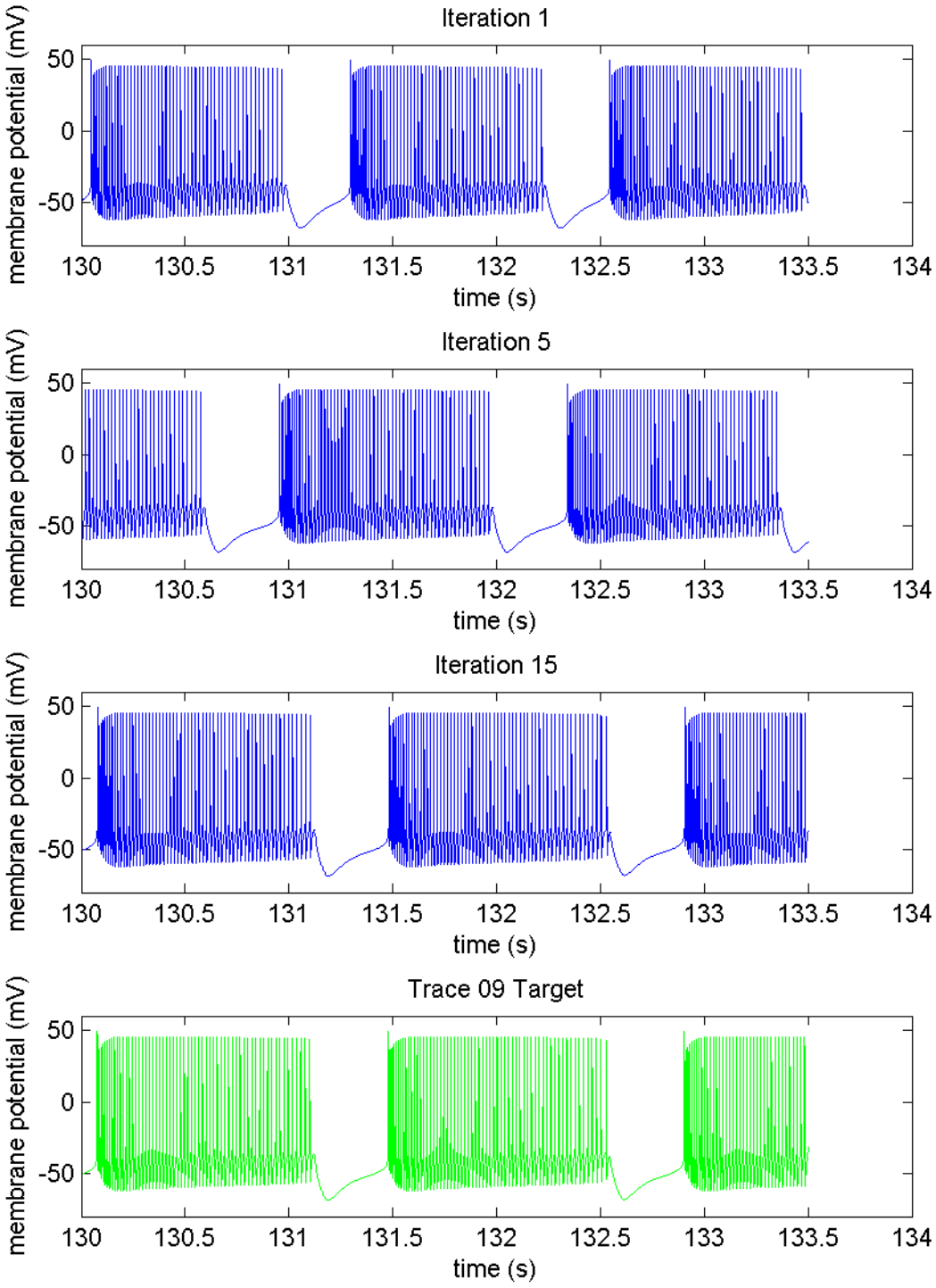

Figure 31: Voltage traces generated by the maximal conductance values produced by the iterative inversion algorithm for the STG neuron model. Target is Trace 9, the burster (large duty cycle) specified in Table 8.

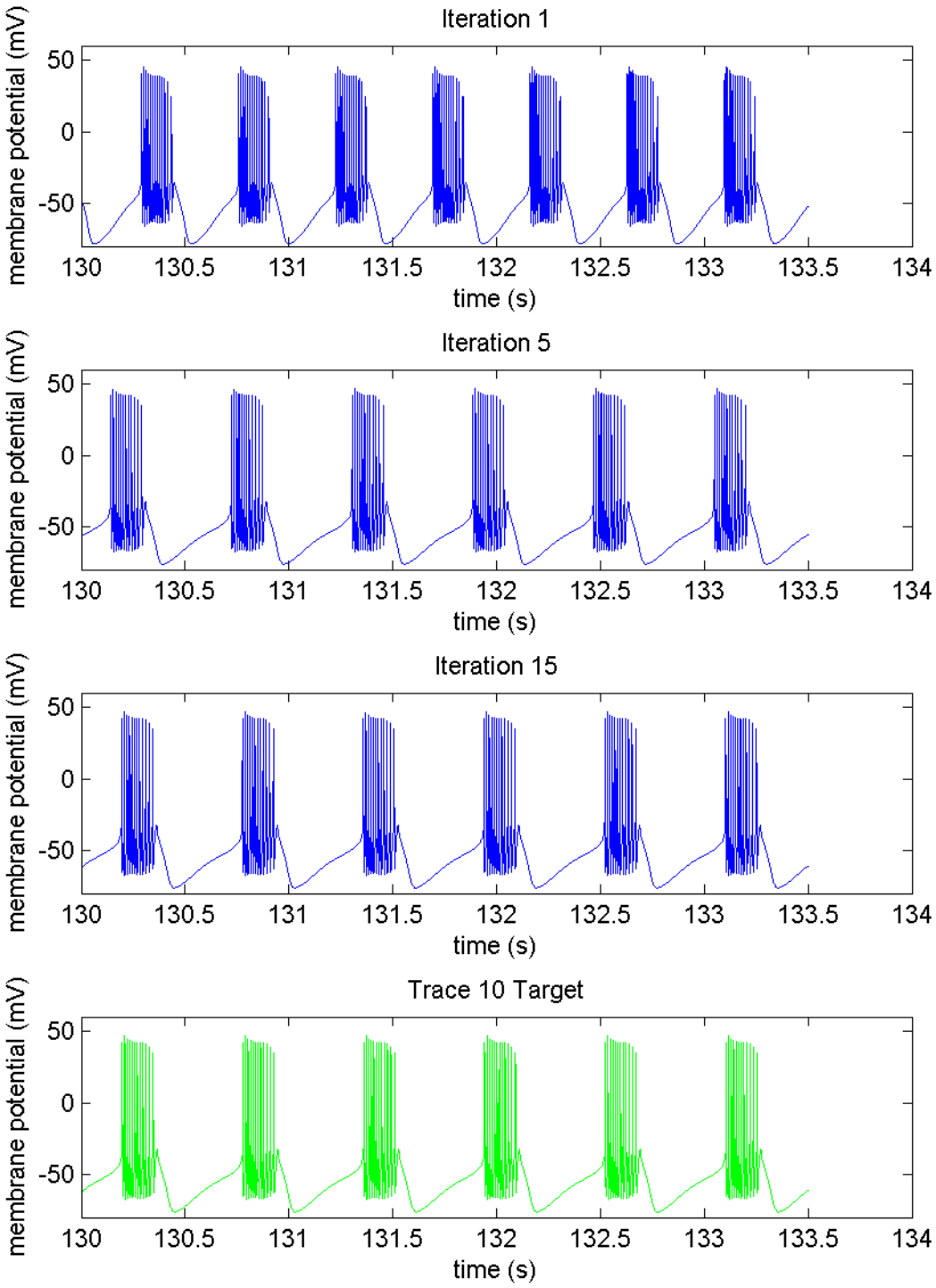

Figure 32: Voltage traces generated by the maximal conductance values produced by the iterative inversion algorithm for the STG neuron model. Target is Trace 10, the burster specified in Table 8.

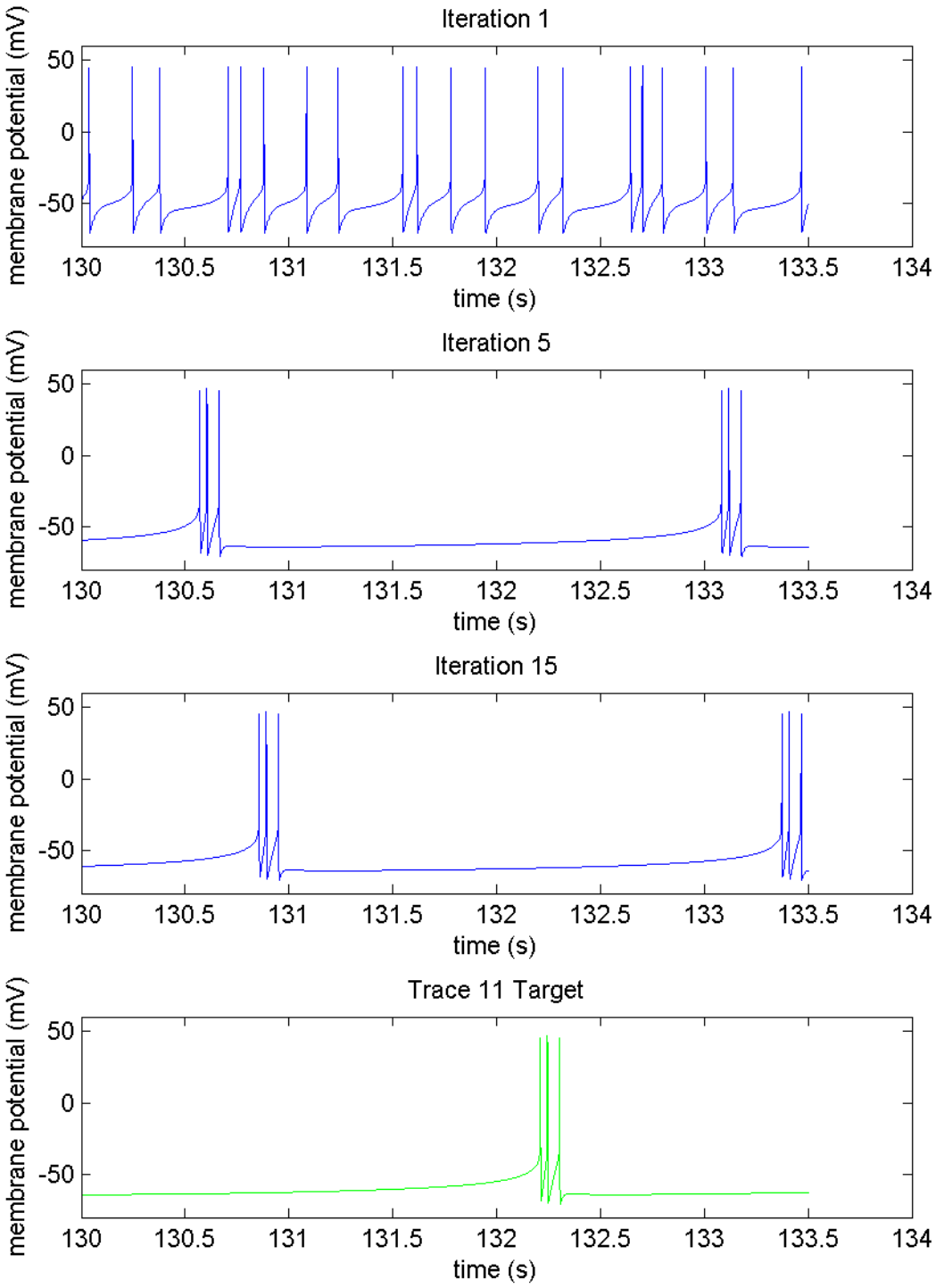

Figure 33: Voltage traces generated by the maximal conductance values produced by the iterative inversion algorithm for the STG neuron model. Target is Trace 11, the burster specified in Table 8.

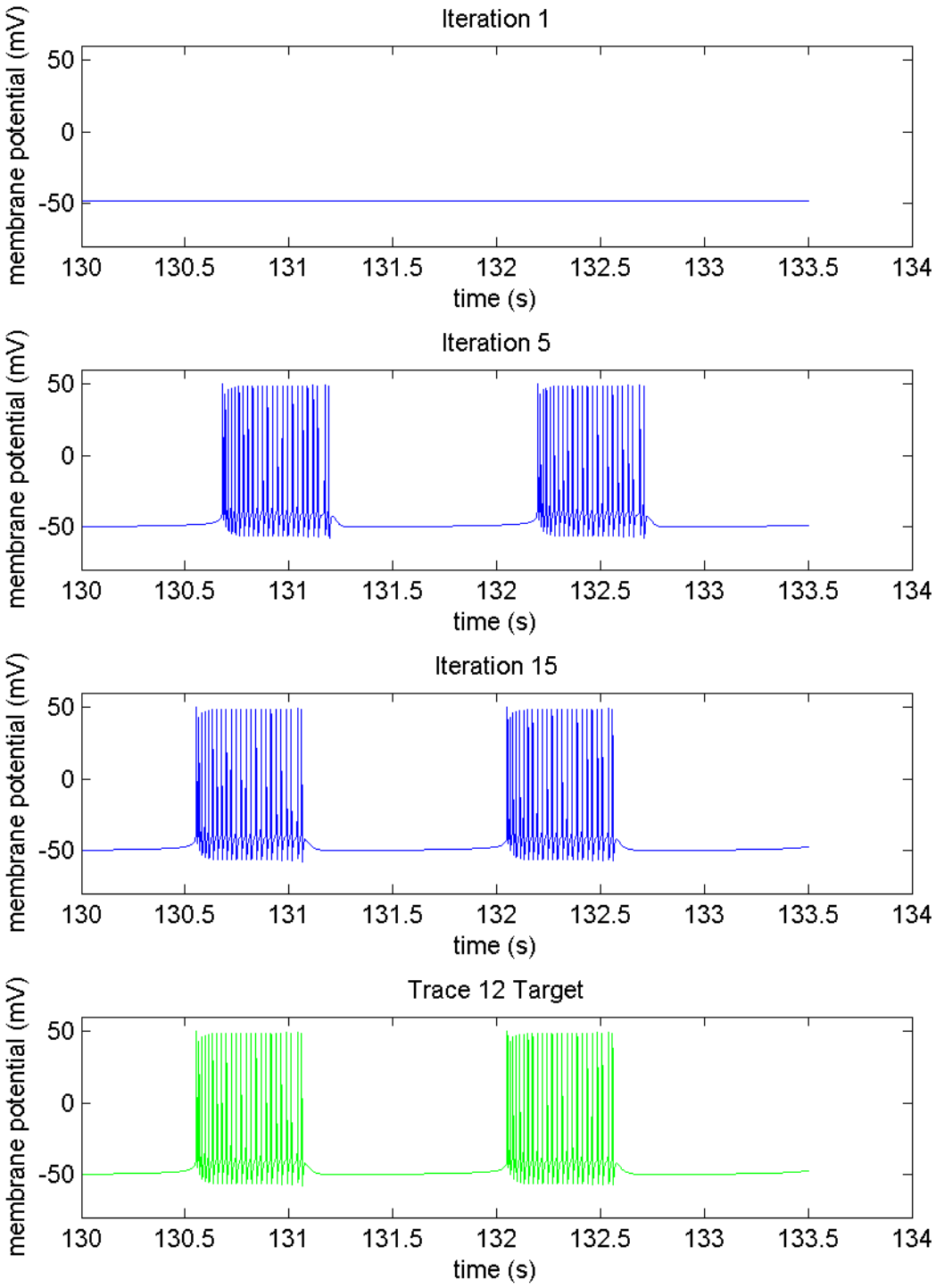

Figure 34: Voltage traces generated by the maximal conductance values produced by the iterative inversion algorithm for the STG neuron model. Target is Trace 12, the burster specified in Table 8.

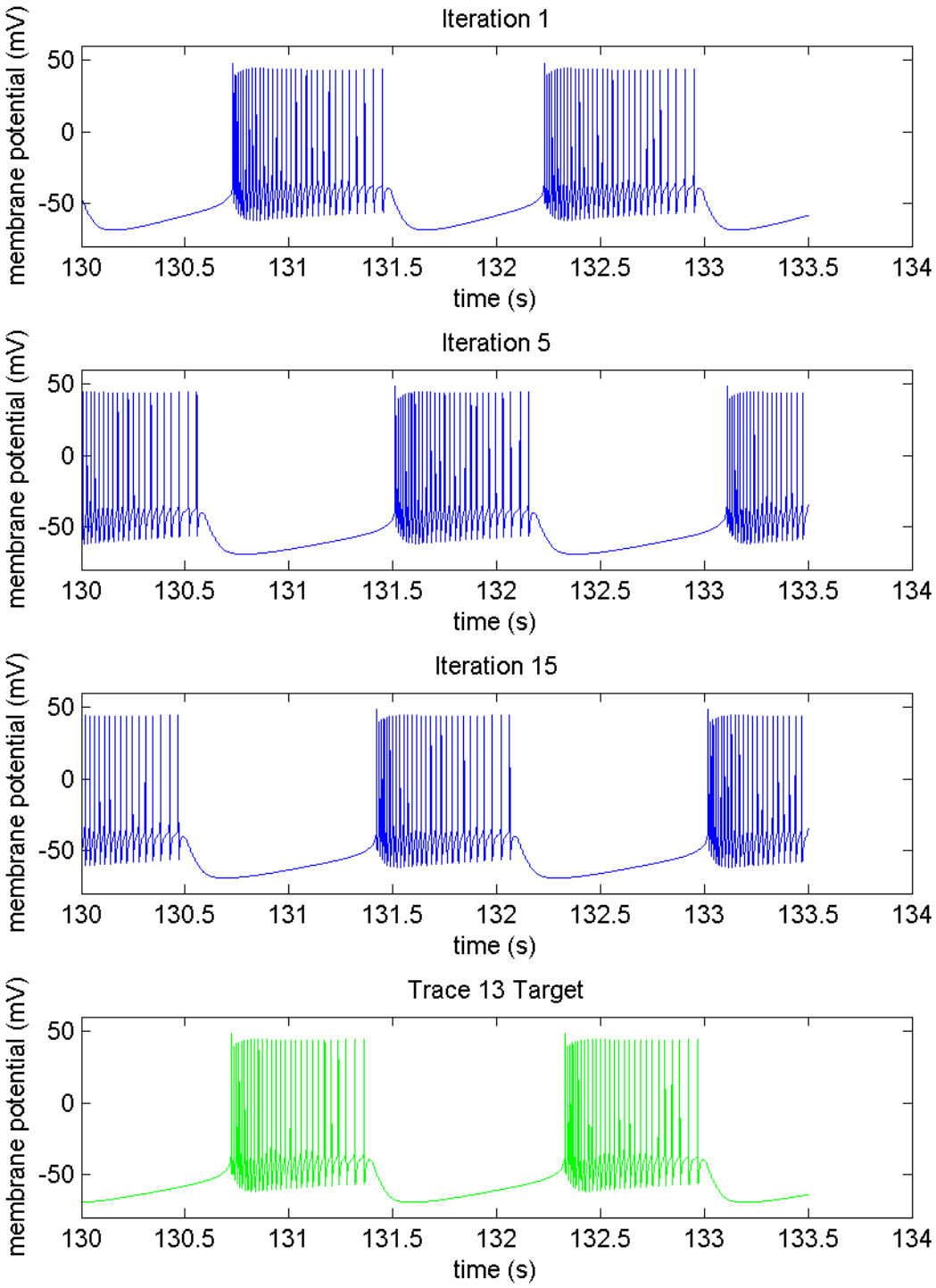

Figure 35: Voltage traces generated by the maximal conductance values produced by the iterative inversion algorithm for the STG neuron model. Target is Trace 13, the burster specified in Table 8.

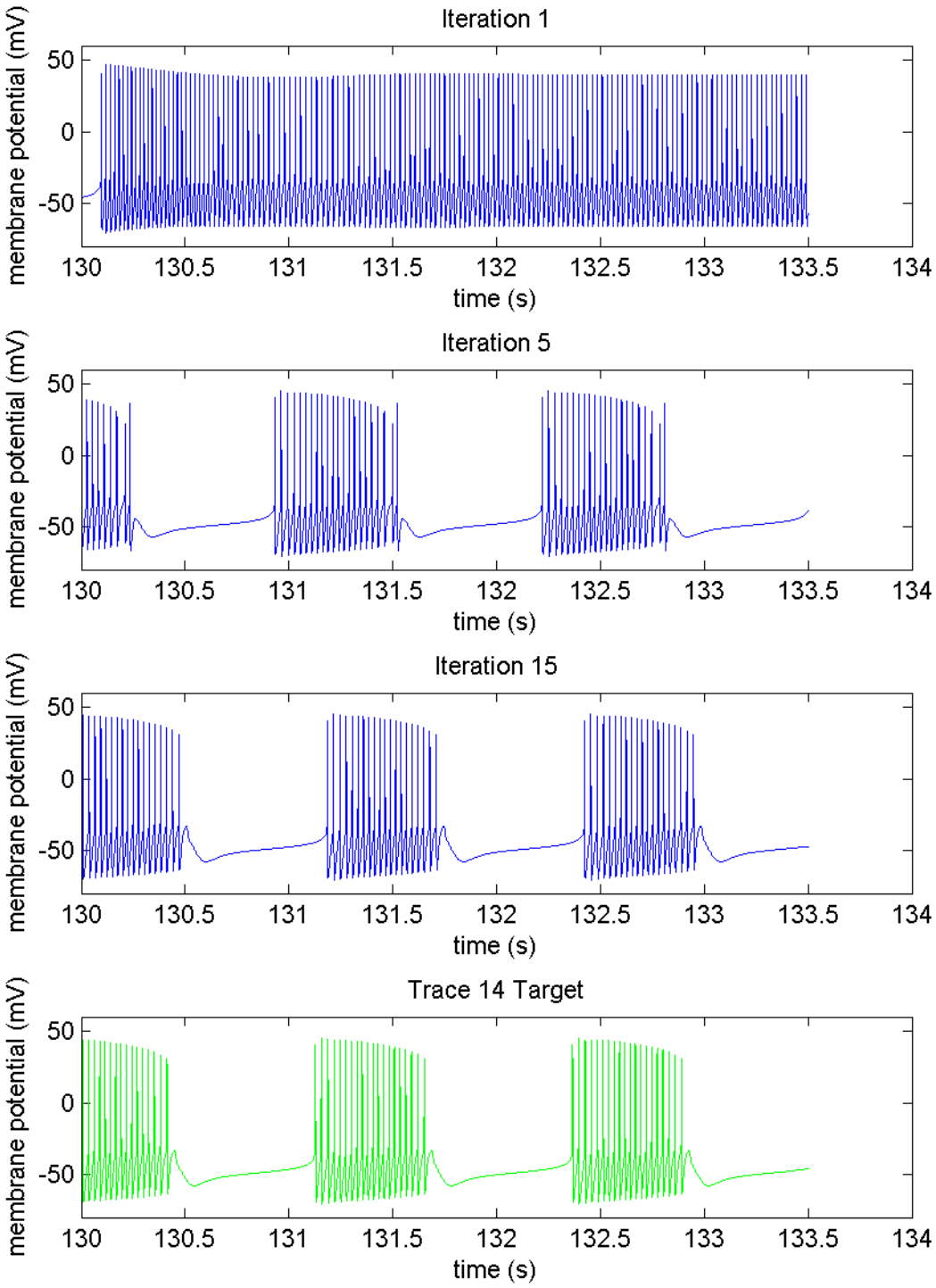

Figure 36: Voltage traces generated by the maximal conductance values produced by the iterative inversion algorithm for the STG neuron model. Target is Trace 14, the parabolic burster specified in Table 8.

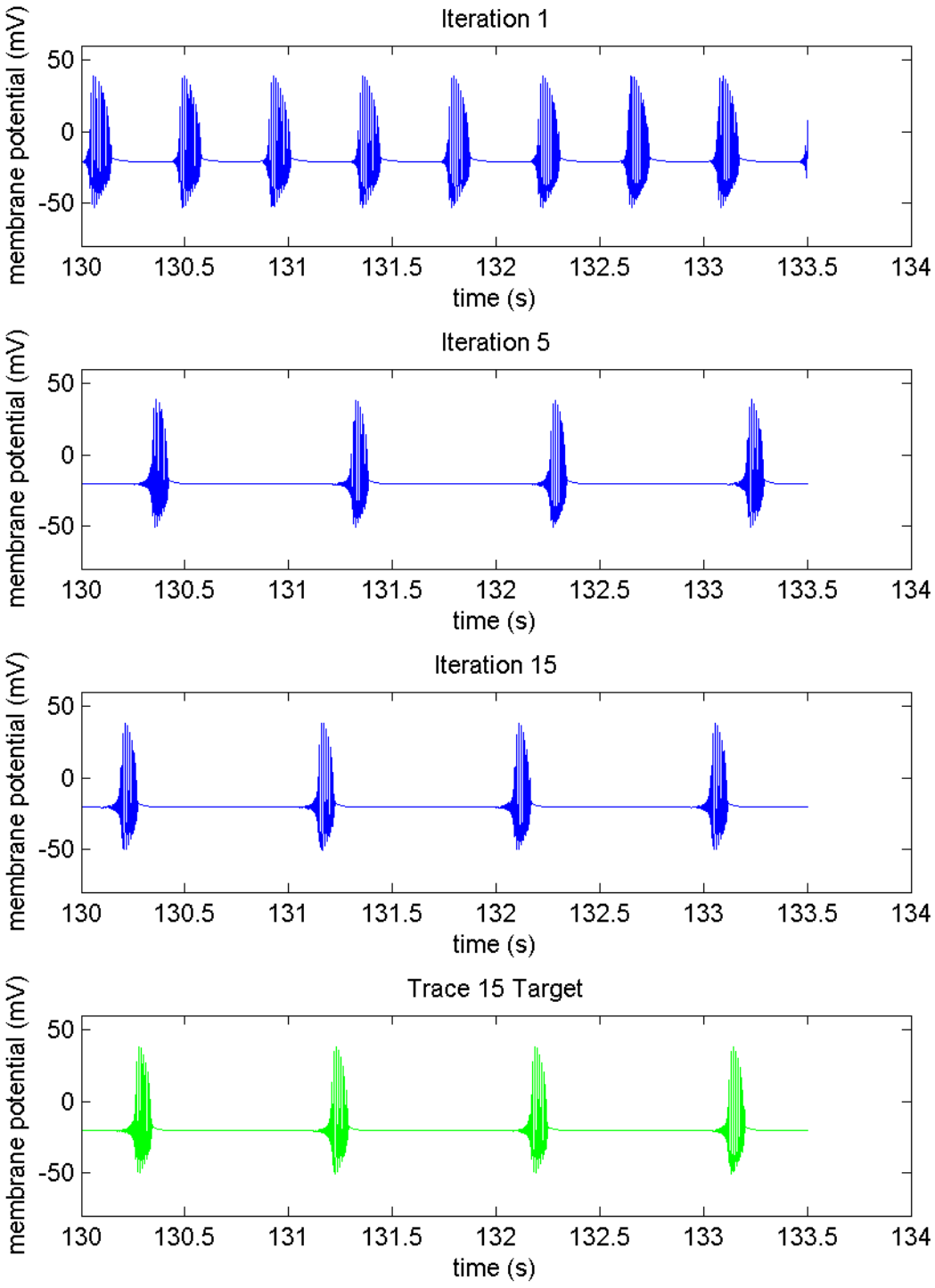

Figure 37: Voltage traces generated by the maximal conductance values produced by the iterative inversion algorithm for the STG neuron model. Target is Trace 15, the elliptic burster specified in Table 8.

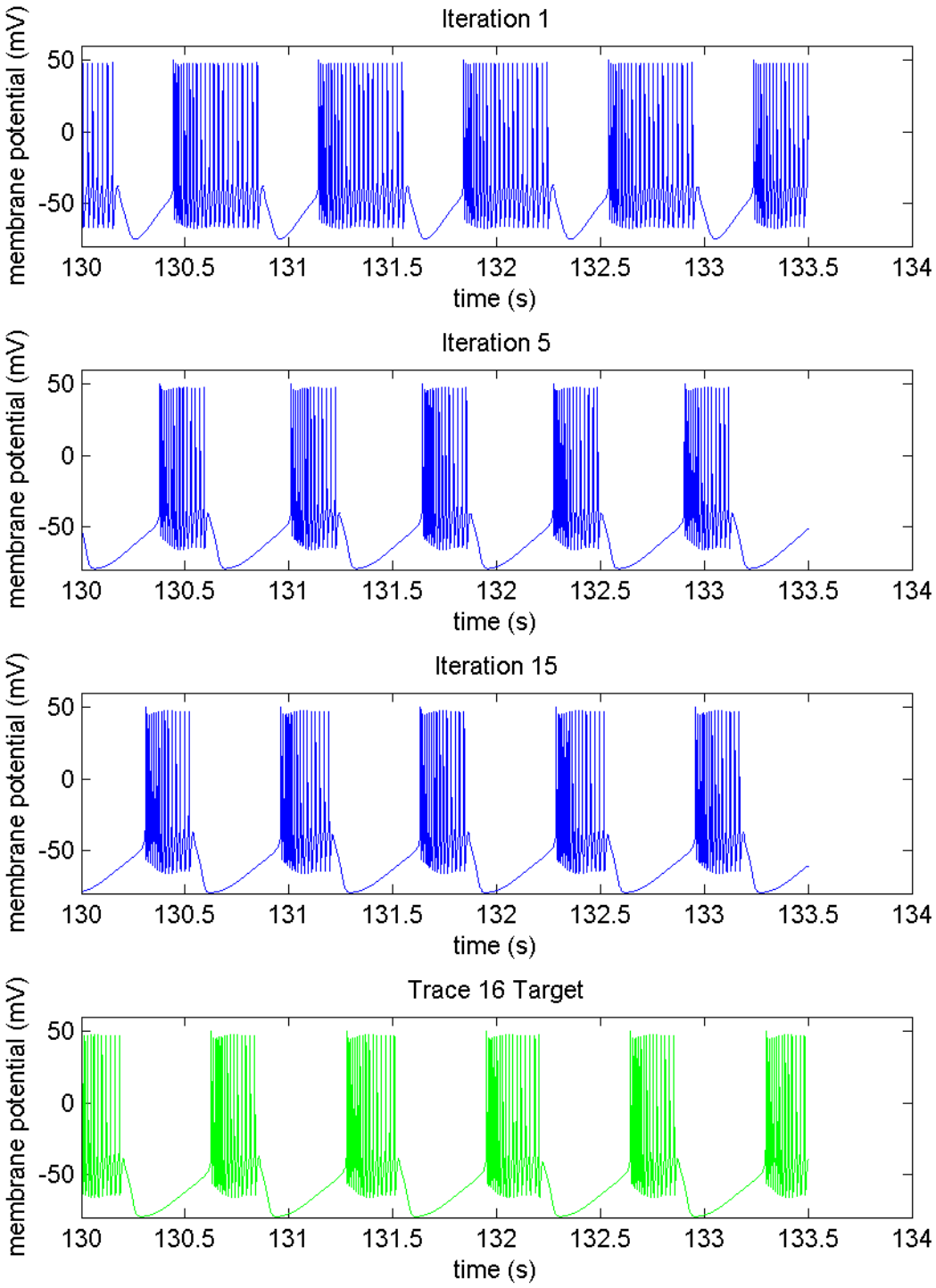

Figure 38: Voltage traces generated by the maximal conductance values produced by the iterative inversion algorithm for the STG neuron model. Target is Trace 16, the alternating burster specified in Table 8.

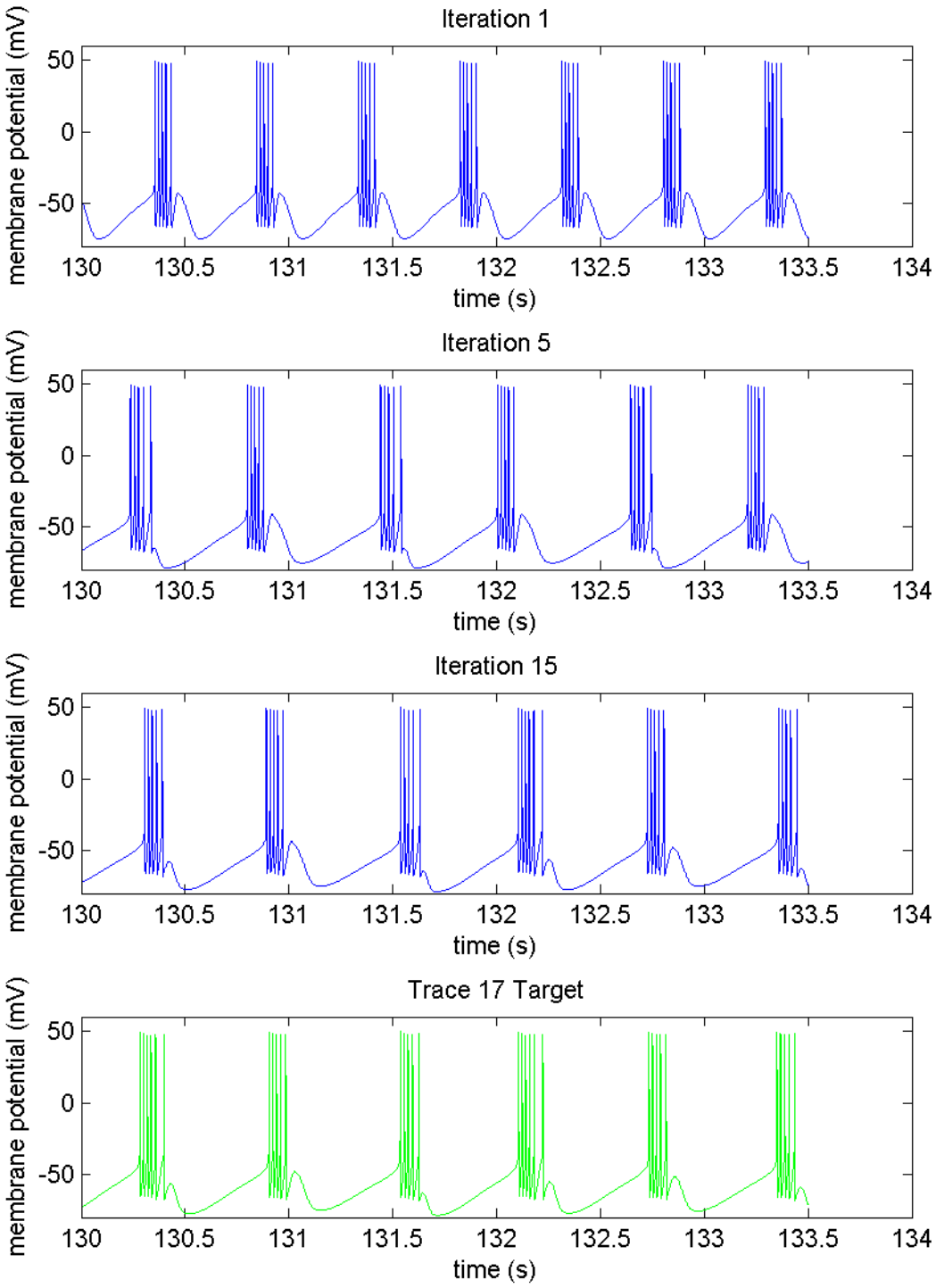

Figure 39: Voltage traces generated by the maximal conductance values produced by the iterative inversion algorithm for the STG neuron model. Target is Trace 17, the irregular burster specified in Table 8.

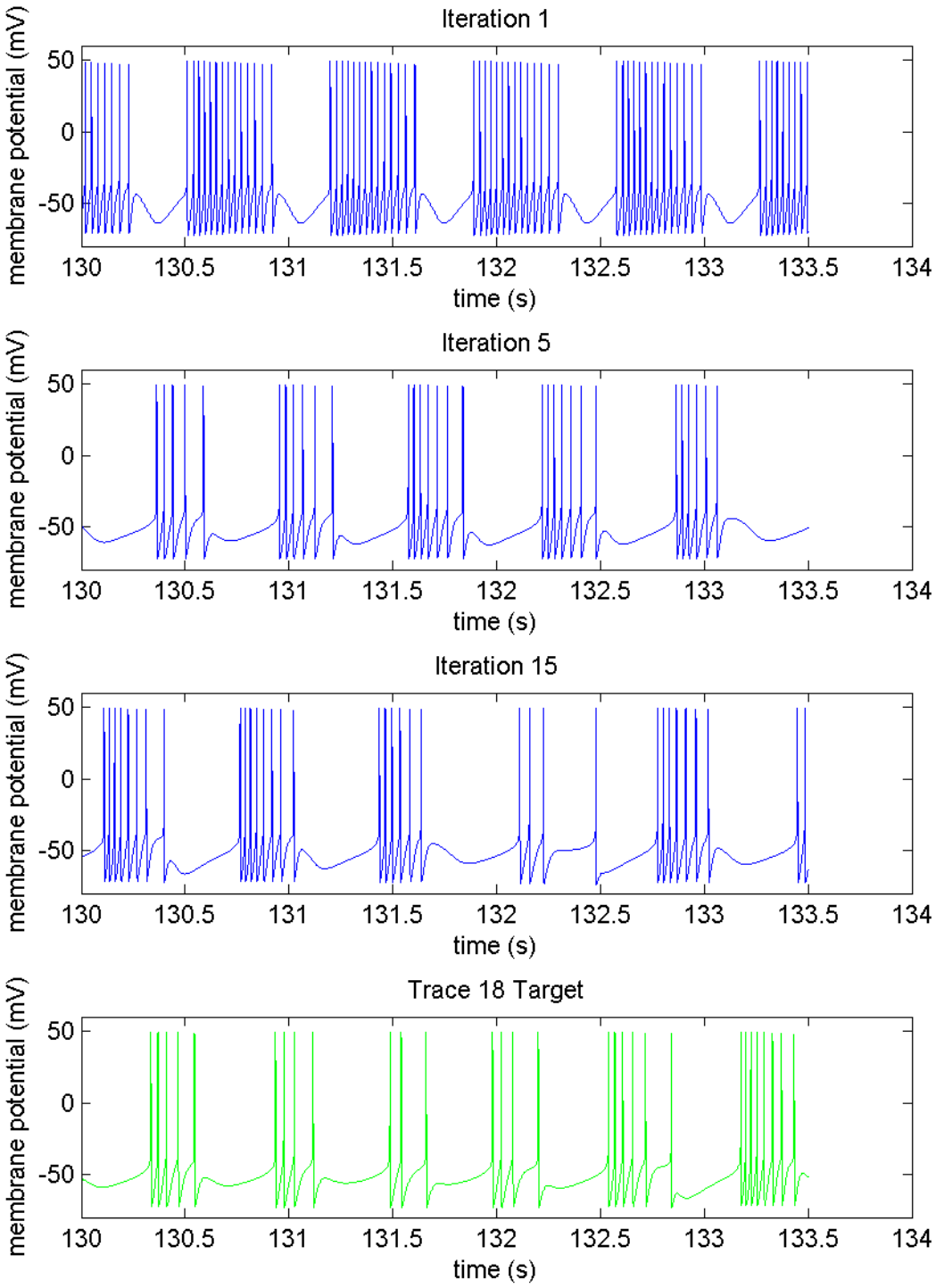

Figure 40: Voltage traces generated by the maximal conductance values produced by the iterative inversion algorithm for the STG neuron model. Target is Trace 18, the nonperiodic behavior specified in Table 8.

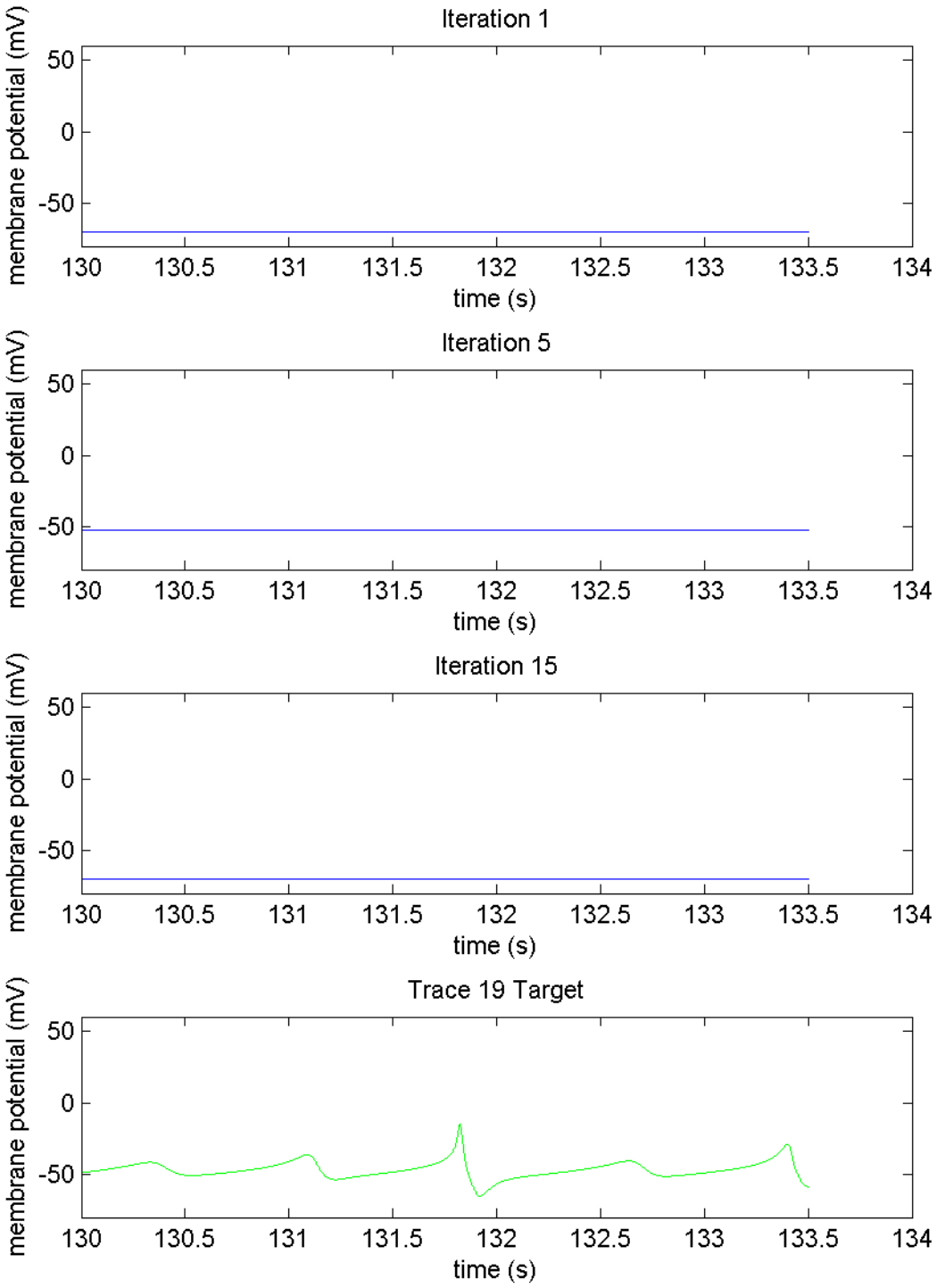

Figure 41: Voltage traces generated by the maximal conductance values produced by the iterative inversion algorithm for the STG neuron model. Target is Trace 19, the low-amplitude oscillations specified in Table 8.

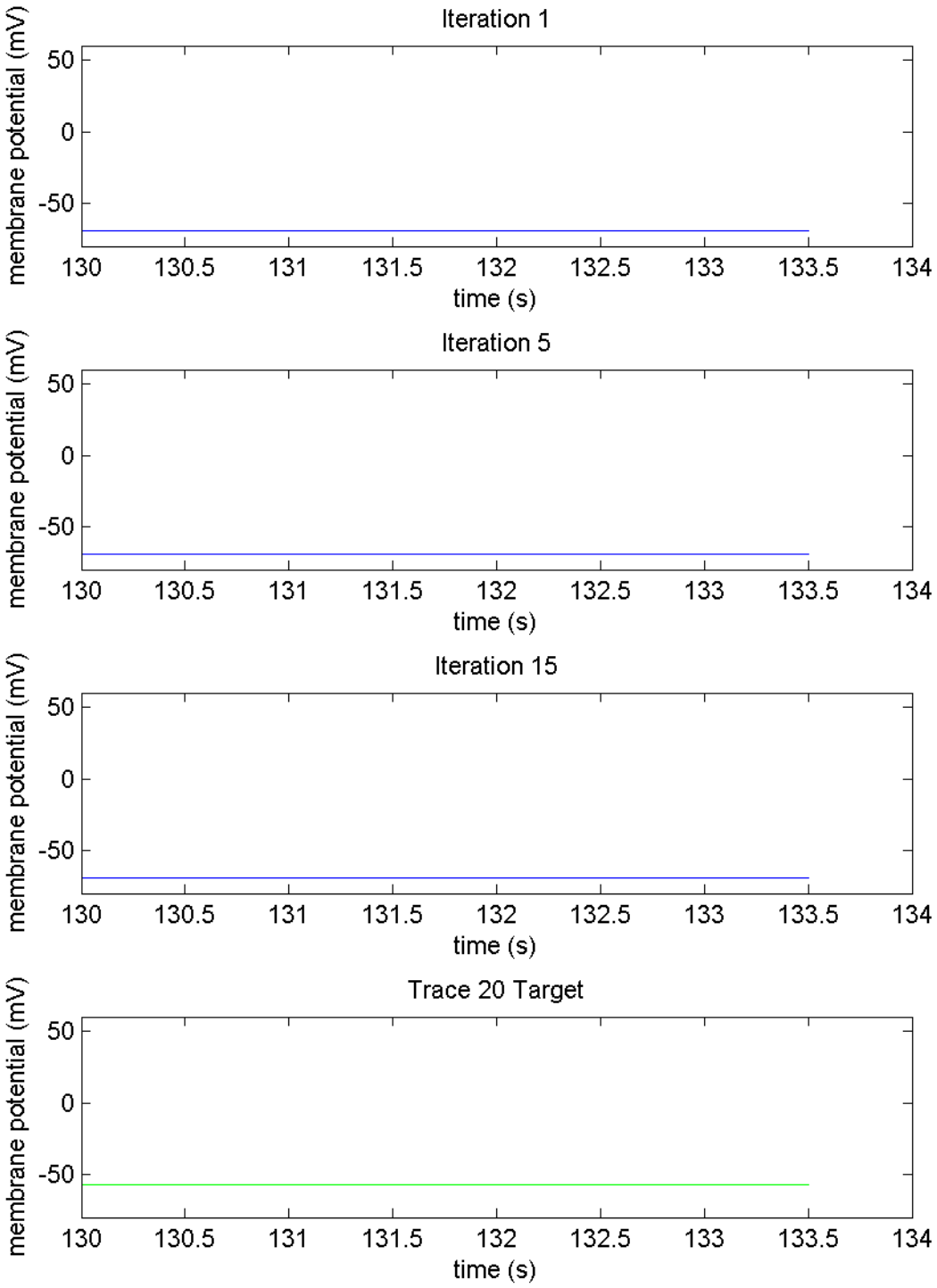

Figure 42: Voltage traces generated by the maximal conductance values produced by the iterative inversion algorithm for the STG neuron model. Target is Trace 20, the silent neuron specified in Table 8.

APPENDIX B

VOLTAGE TRACES TESTED AS EXTENSIONS TO THE STG NEURON MODEL

B.1 Challenge traces of type 1: directly from the STG model database

Table 12: Maximal conductance parameters found by algorithm. Extension traces of type 1, directly from STG database [24]. Conductances in mS/cm^2.

Trace	Na	CaT	CaS	A	KCa	Kd	H	Leak
101	498.77	2.49	9.97	9.97	24.99	124.69	0.01	0.05
106	399.59	4.99	7.99	10.00	14.99	74.92	0.01	0.02
107	399.99	12.50	6.00	50.00	10.00	75.00	0.05	0.01
111	499.84	5.00	2.00	29.99	15.01	74.98	0.01	0.02
114	499.97	10.00	5.99	50.01	0.00	99.99	0.45	0.05
121	0.00	2.50	10.00	10.00	10.00	75.00	0.05	0.01
123	300.00	12.50	0.00	50.00	5.00	0.00	0.02	0.04
125	200.00	0.00	10.00	50.00	10.01	125.00	0.03	0.01
134	499.95	5.00	4.00	20.00	10.00	0.00	0.01	0.05
138	300.00	5.00	8.00	40.00	5.00	50.00	0.01	0.03
142	0.00	0.00	10.00	29.99	5.00	50.00	0.01	0.03

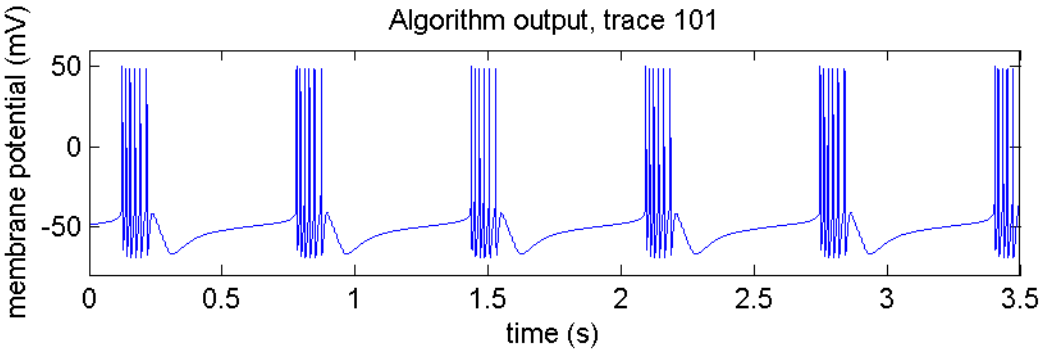

(a) Trace generated by parameters found by inversion algorithm

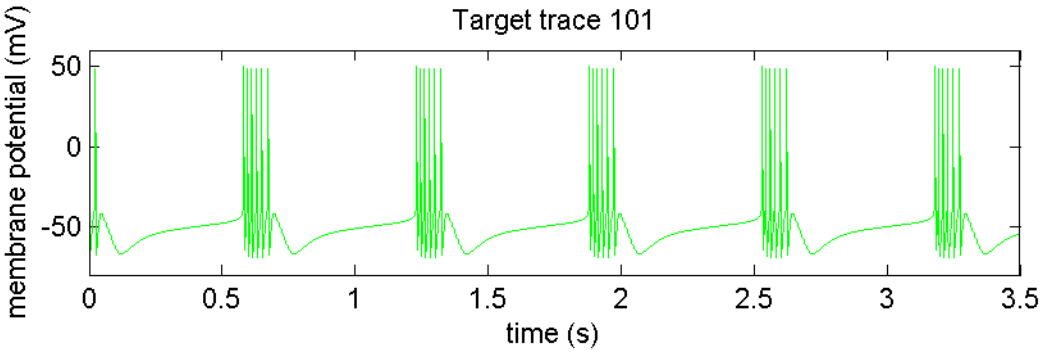

(b) Target trace

Figure 43: Performance of modified inversion algorithm, trace 101

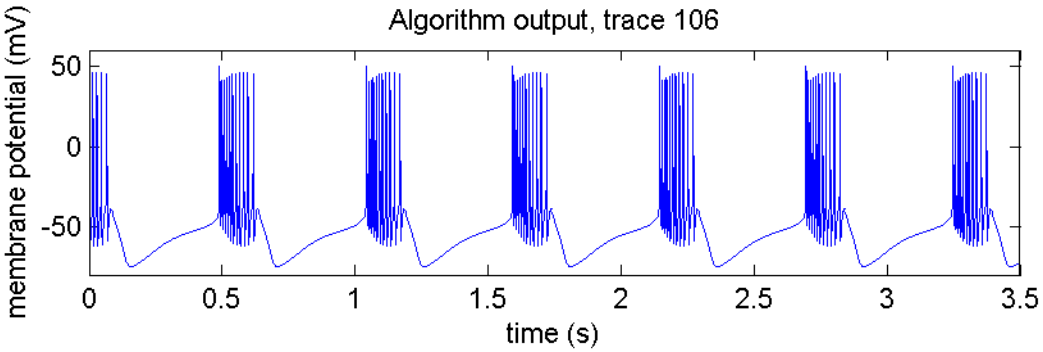

(a) Trace generated by parameters found by inversion algorithm

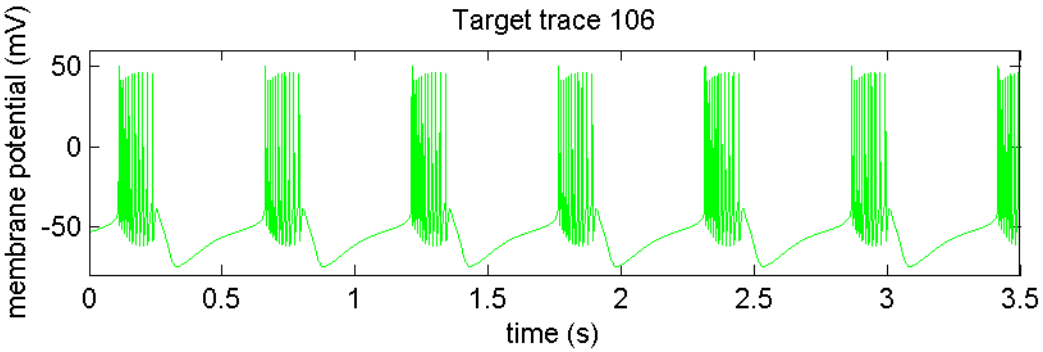

(b) Target trace

Figure 44: Performance of modified inversion algorithm, trace 106

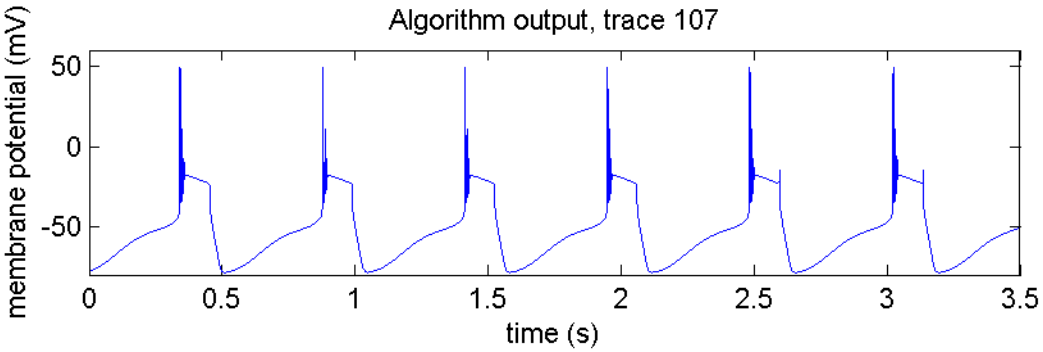

(a) Trace generated by parameters found by inversion algorithm

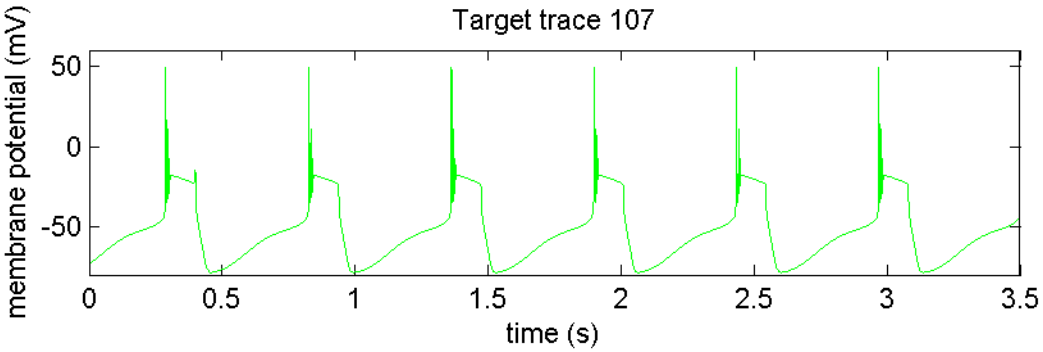

(b) Target trace

Figure 45: Performance of modified inversion algorithm, trace 107

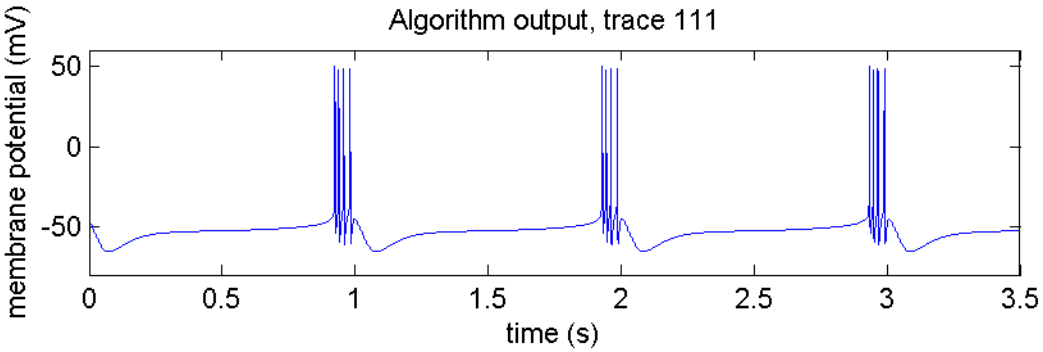

(a) Trace generated by parameters found by inversion algorithm

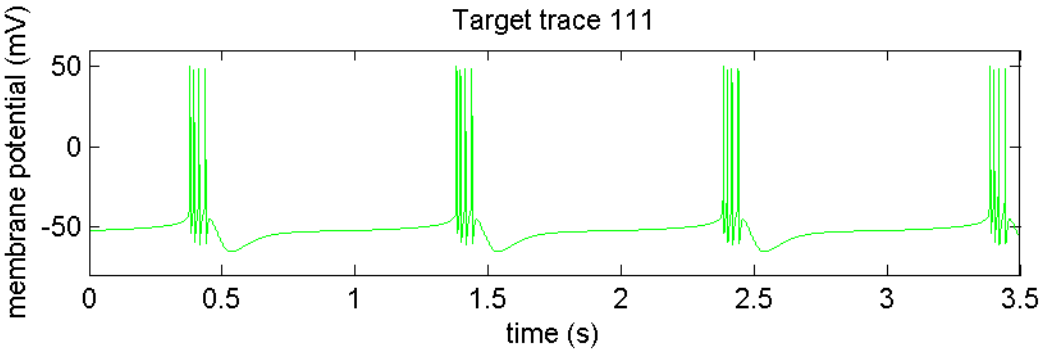

(b) Target trace

Figure 46: Performance of modified inversion algorithm, trace 111

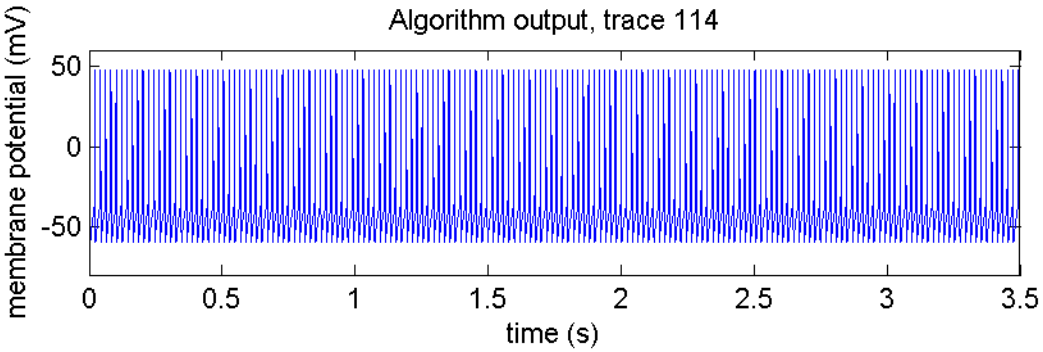

(a) Trace generated by parameters found by inversion algorithm

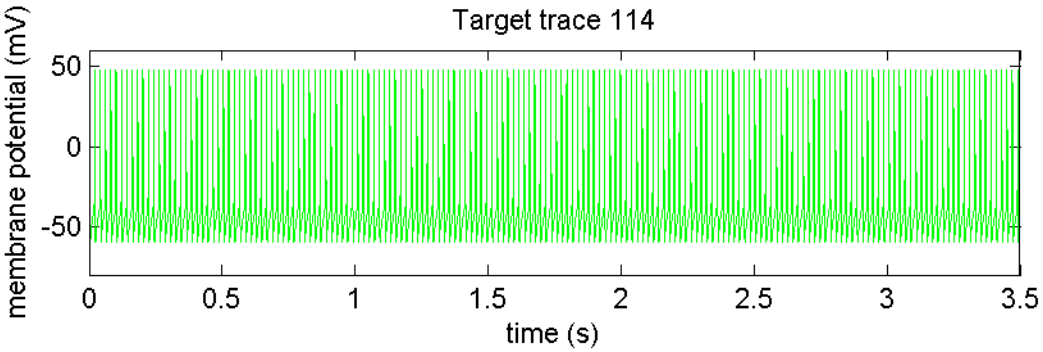

(b) Target trace

Figure 47: Performance of modified inversion algorithm, trace 114

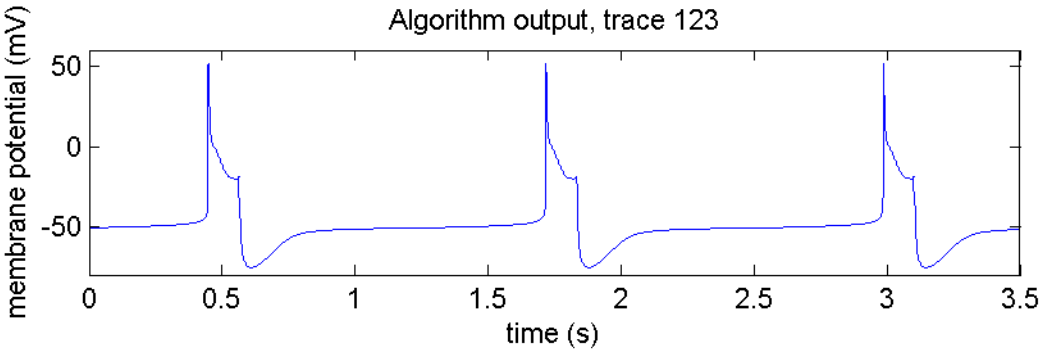

(a) Trace generated by parameters found by inversion algorithm

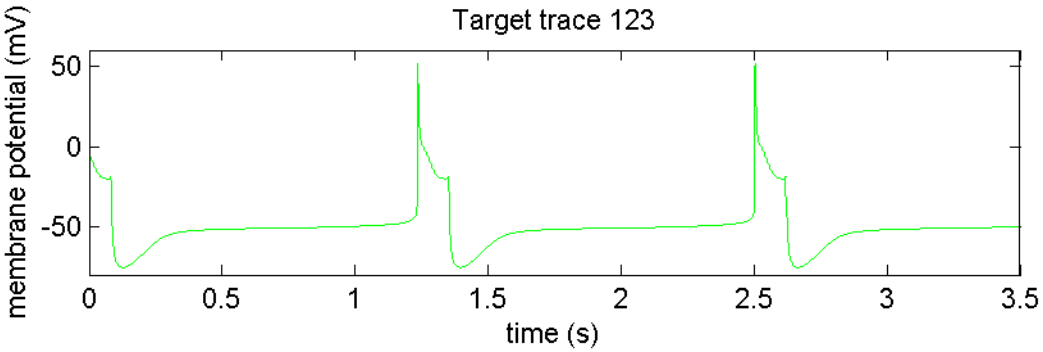

(b) Target trace

Figure 48: Performance of modified inversion algorithm, trace 123

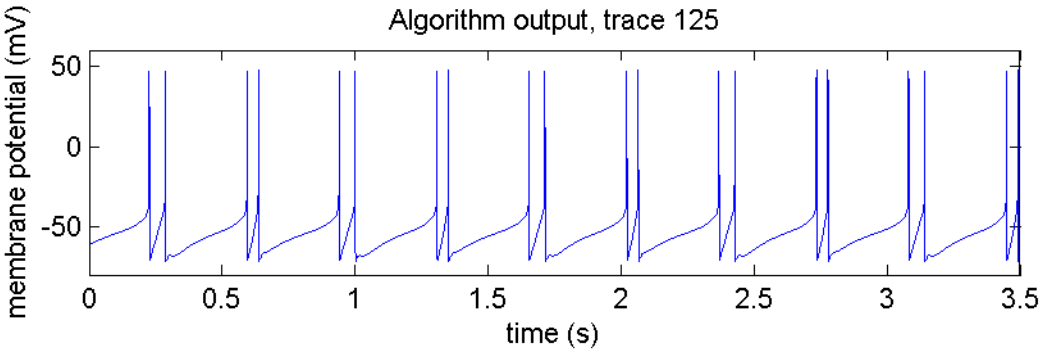

(a) Trace generated by parameters found by inversion algorithm

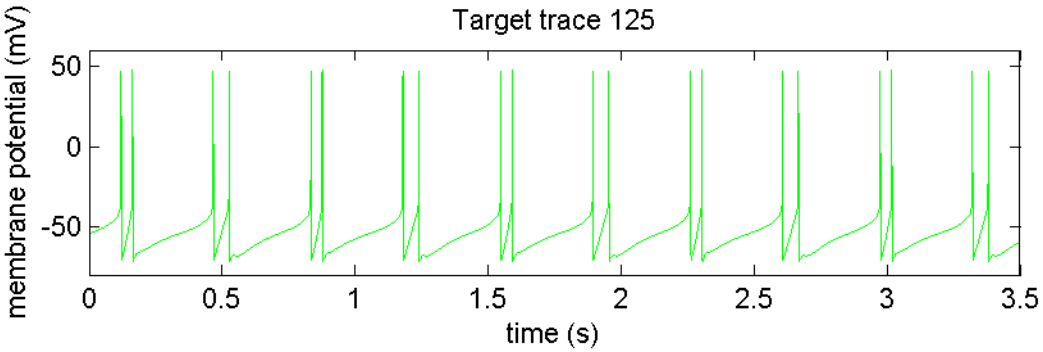

(b) Target trace

Figure 49: Performance of modified inversion algorithm, trace 125

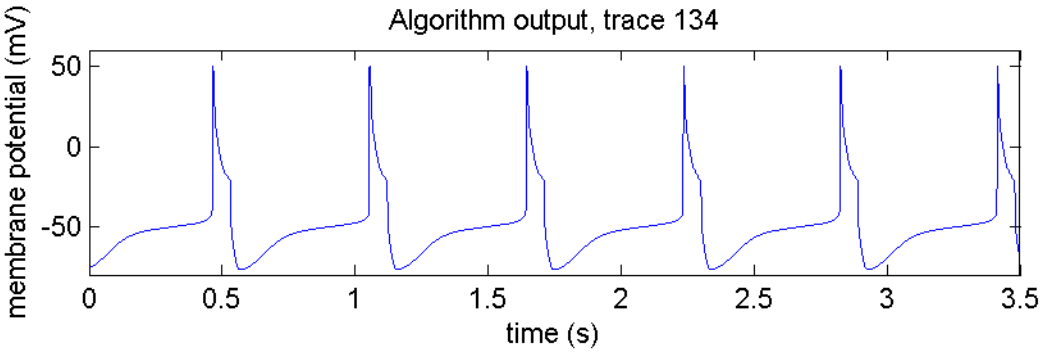

(a) Trace generated by parameters found by inversion algorithm

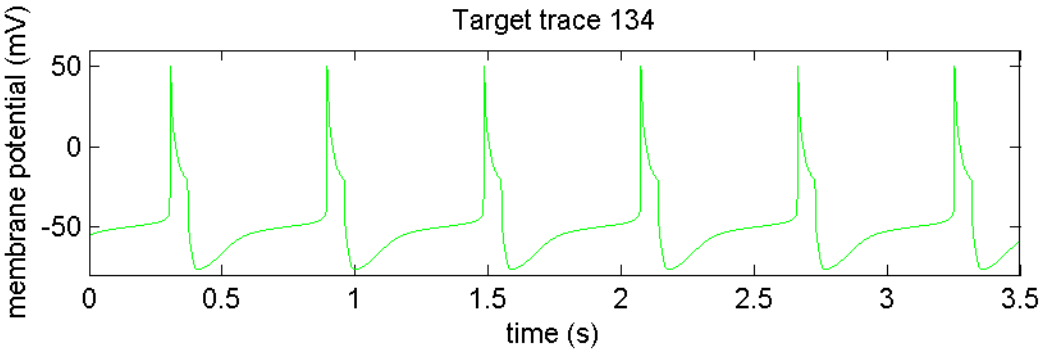

(b) Target trace

Figure 50: Performance of modified inversion algorithm, trace 134

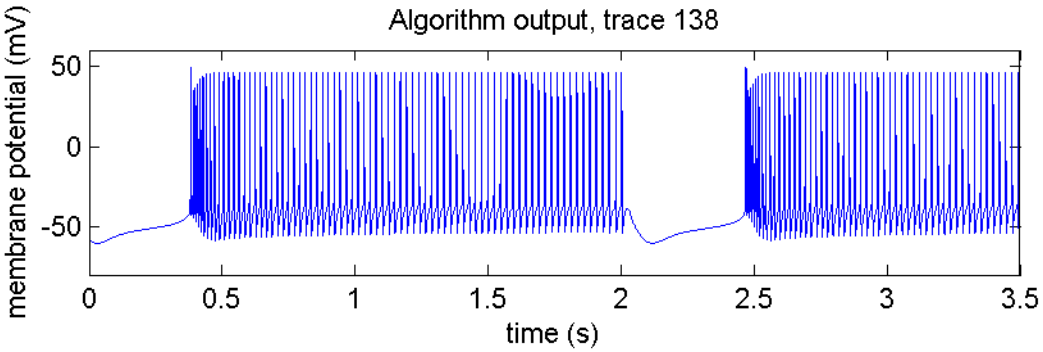

(a) Trace generated by parameters found by inversion algorithm

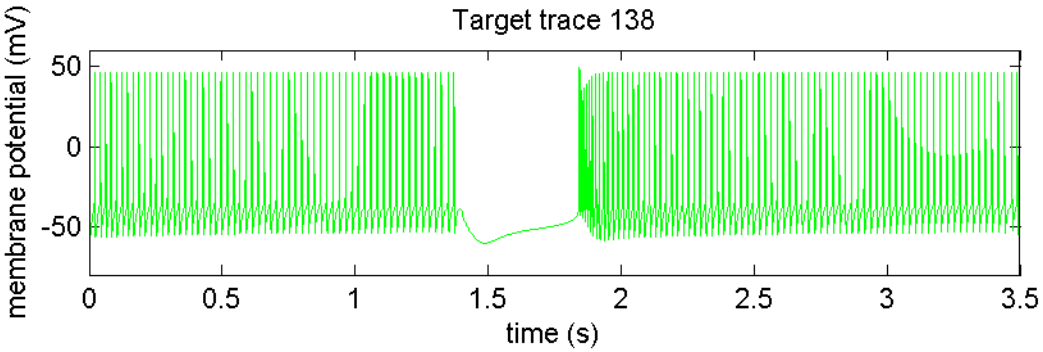

(b) Target trace

Figure 51: Performance of modified inversion algorithm, trace 138

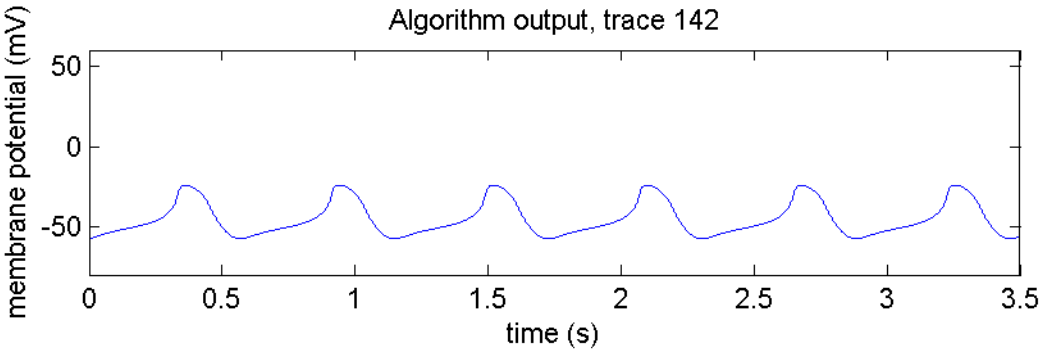

(a) Trace generated by parameters found by inversion algorithm

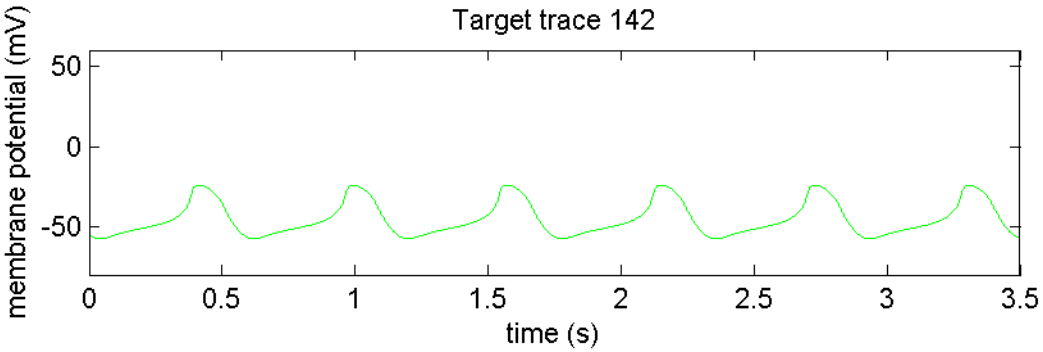

(b) Target trace

Figure 52: Performance of modified inversion algorithm, trace 142

B.2 Challenge traces of type 2: activation/inactivation time constant scaling

Table 13: Maximal conductance parameters found by algorithm. Extension traces of type 2, activation/inactivation time constant scaling. Conductances in mS/cm^2.

Trace	Na	CaS	CaT	A	KCa	Kd	H	L	Tau_m	Tau_h
105	400.00	12.50	8.00	40.00	25.00	50.00	0.01	0.00	0.75	0.75
110	499.64	7.49	6.00	9.99	14.99	124.91	0.05	0.02	0.75	0.75
126	500.26	5.00	7.99	9.99	4.91	100.06	0.00	0.05	0.75	0.75
128	499.91	7.50	4.00	39.99	25.00	124.98	0.02	0.02	0.75	0.75
132	499.92	10.00	4.00	30.00	20.00	99.98	0.00	0.01	0.75	0.75
133	400.00	0.00	2.00	20.00	24.48	50.00	0.01	0.00	0.75	0.75
139	499.97	12.50	0.00	40.00	25.00	50.00	0.02	0.05	0.75	0.75
146	300.00	12.50	2.00	50.00	25.00	75.00	0.00	0.05	0.75	0.75
147	499.97	5.00	6.00	10.00	5.00	25.00	0.02	0.05	0.75	0.75

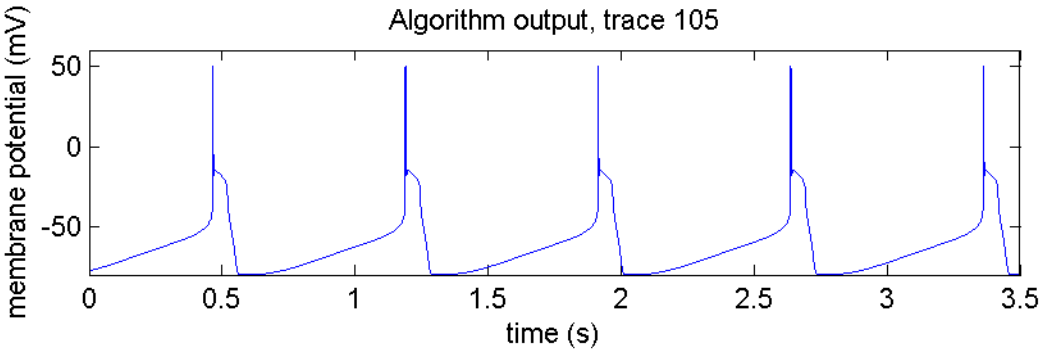

(a) Trace generated by parameters found by inversion algorithm

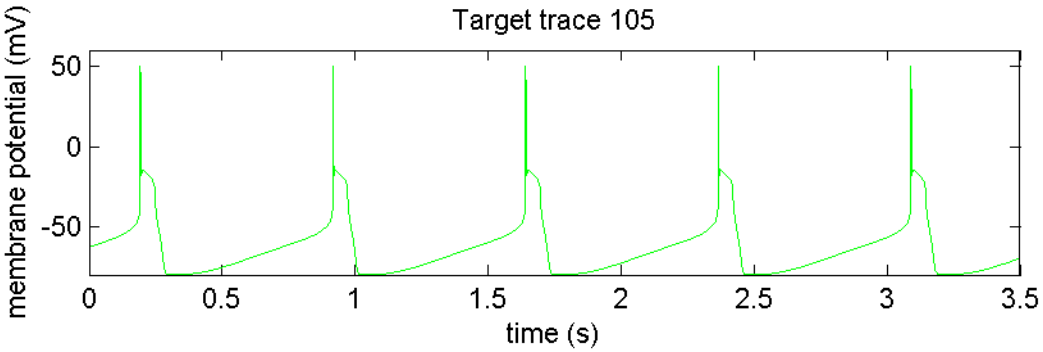

(b) Target trace

Figure 53: Performance of modified inversion algorithm, trace 105

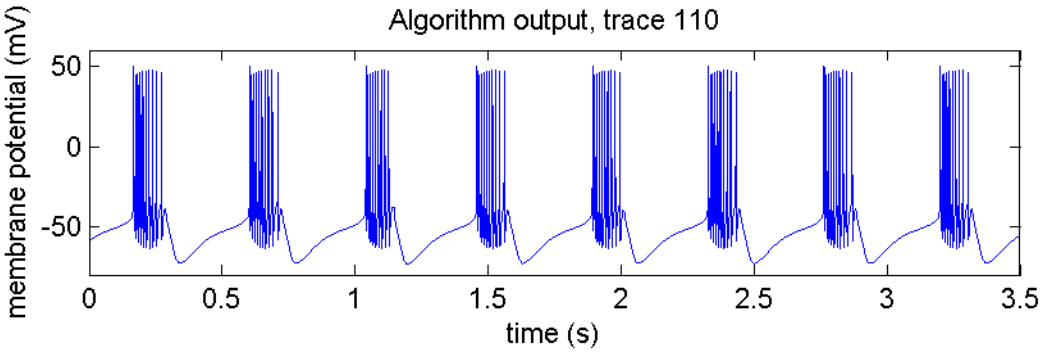

(a) Trace generated by parameters found by inversion algorithm

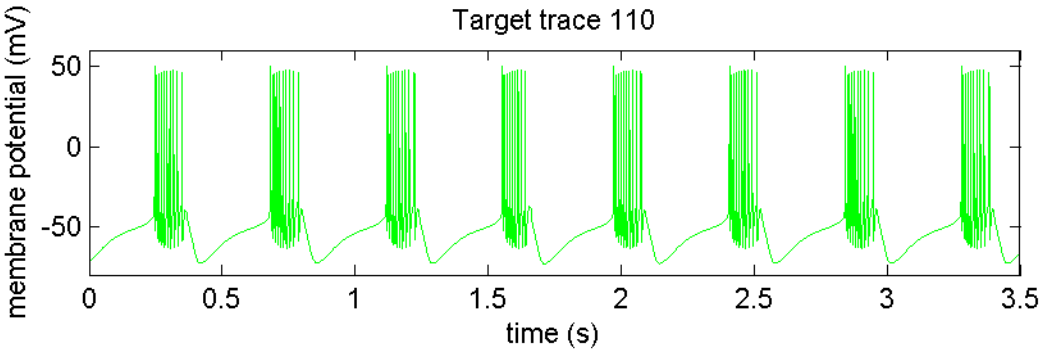

(b) Target trace

Figure 54: Performance of modified inversion algorithm, trace 110

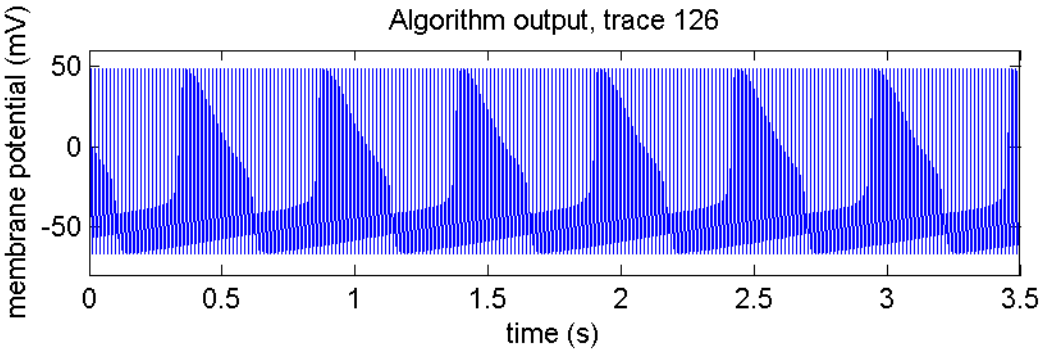

(a) Trace generated by parameters found by inversion algorithm

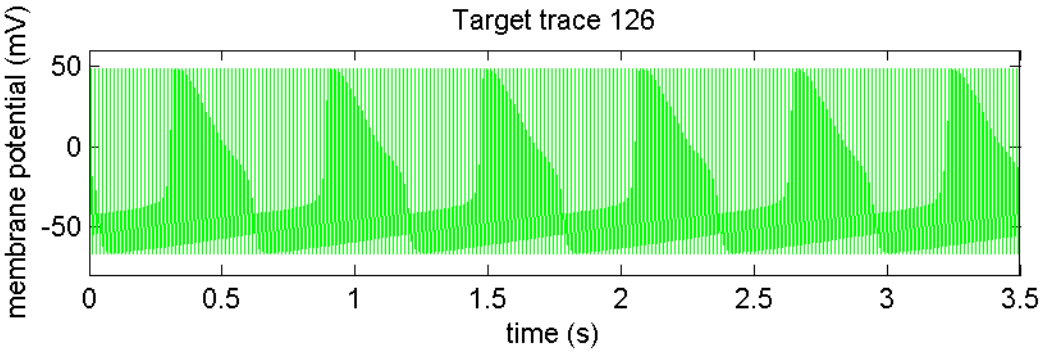

(b) Target trace

Figure 55: Performance of modified inversion algorithm, trace 126

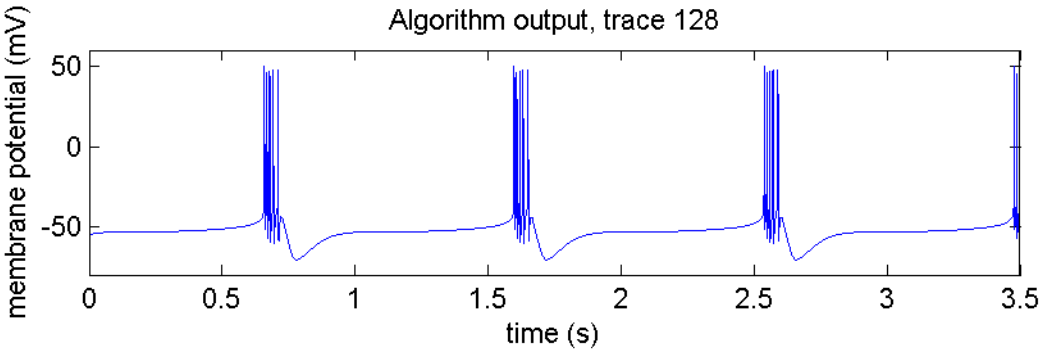

(a) Trace generated by parameters found by inversion algorithm

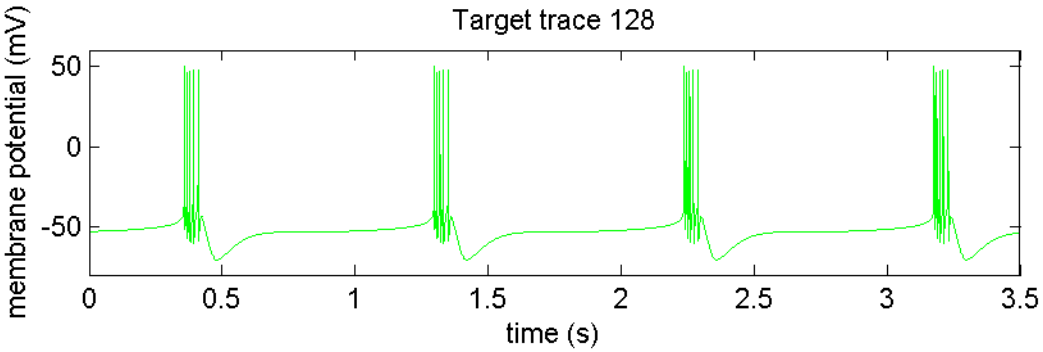

(b) Target trace

Figure 56: Performance of modified inversion algorithm, trace 128

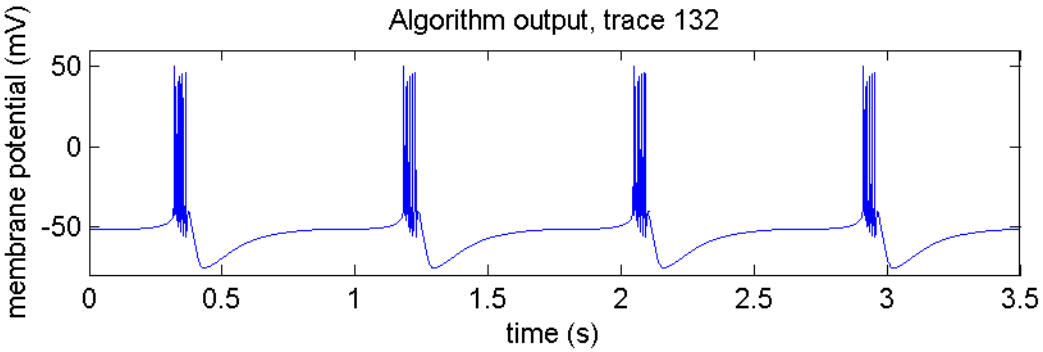

(a) Trace generated by parameters found by inversion algorithm

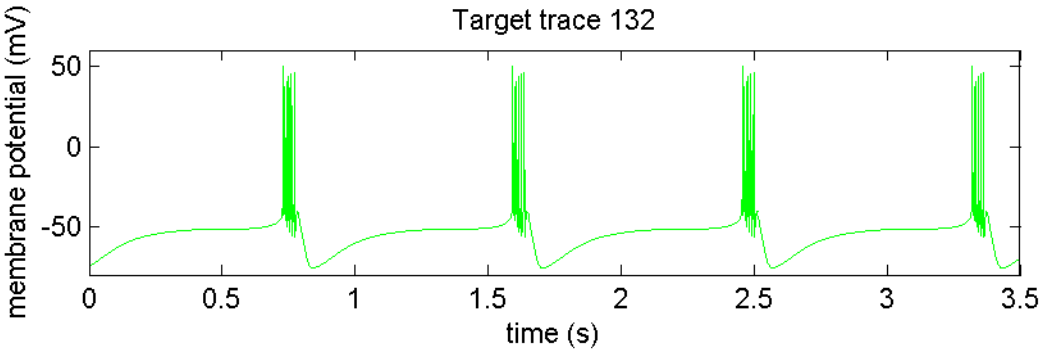

(b) Target trace

Figure 57: Performance of modified inversion algorithm, trace 132

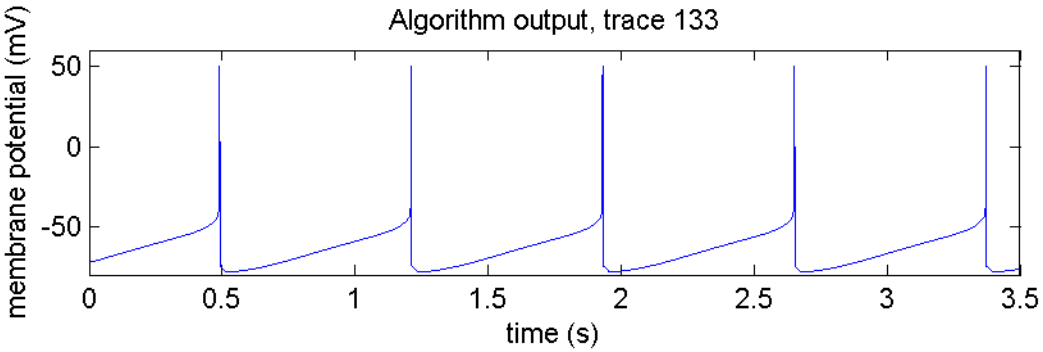

(a) Trace generated by parameters found by inversion algorithm

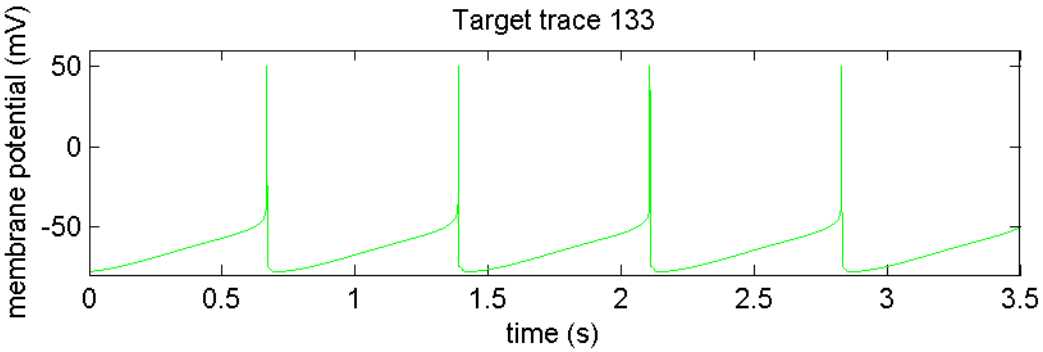

(b) Target trace

Figure 58: Performance of modified inversion algorithm, trace 133

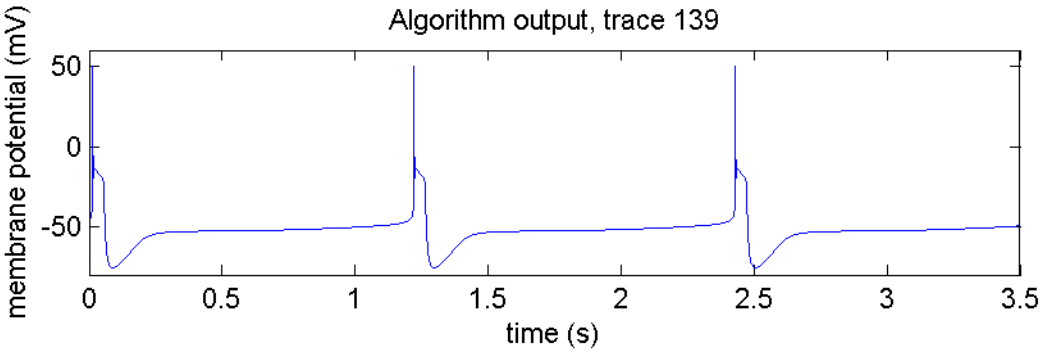

(a) Trace generated by parameters found by inversion algorithm

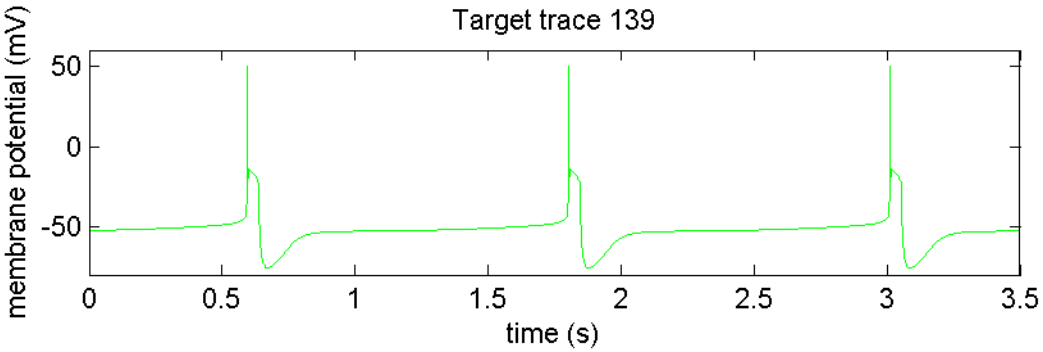

(b) Target trace

Figure 59: Performance of modified inversion algorithm, trace 139

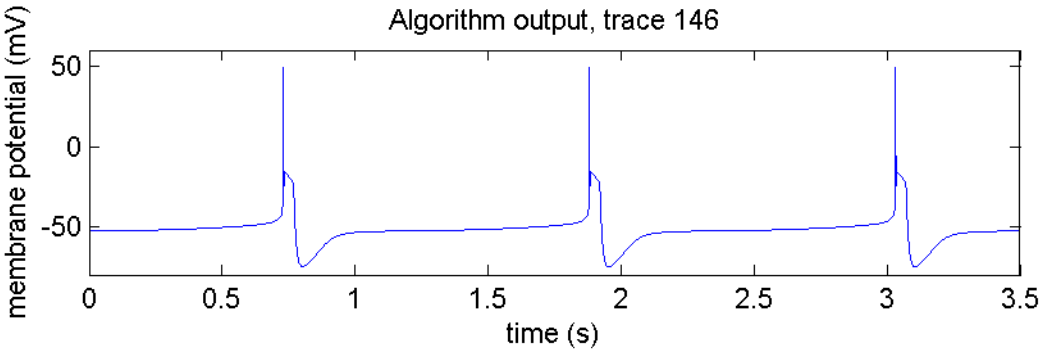

(a) Trace generated by parameters found by inversion algorithm

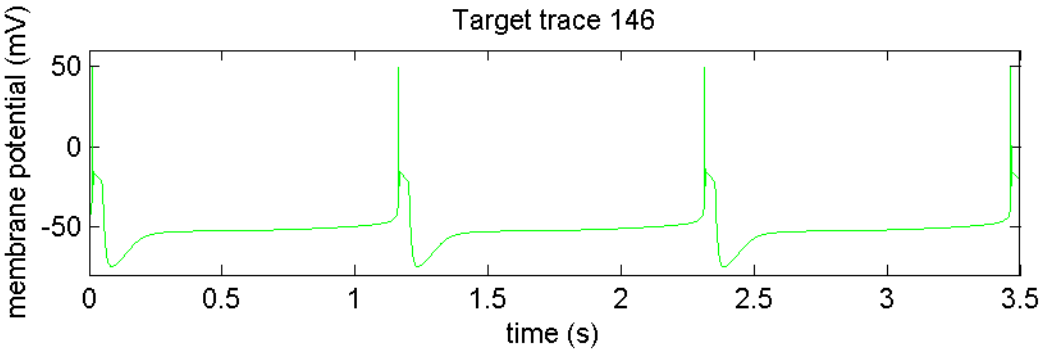

(b) Target trace

Figure 60: Performance of modified inversion algorithm, trace 146

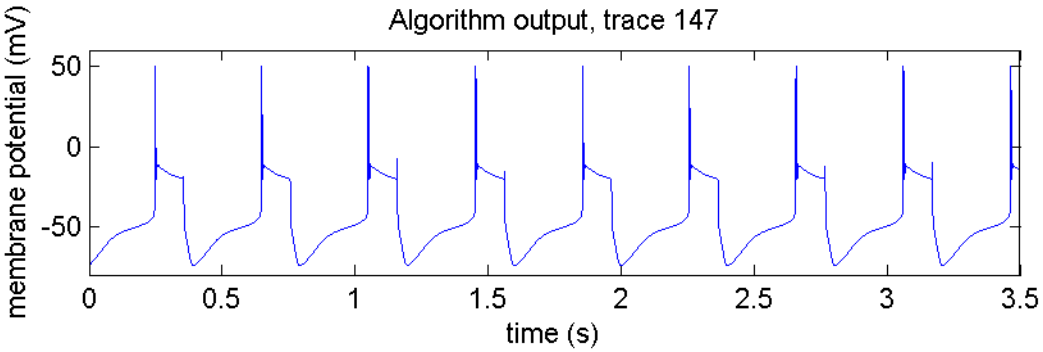

(a) Trace generated by parameters found by inversion algorithm

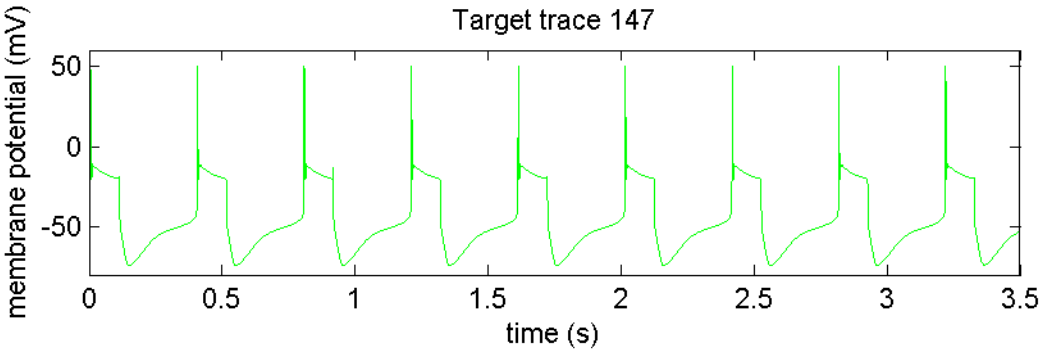

(b) Target trace

Figure 61: Performance of modified inversion algorithm, trace 147

B.3 Extension traces of type 3: constant voltage shift

Table 14: Maximal conductance parameters found by algorithm. Extension traces of type 3, constant voltage shift. Conductances in mS/cm^2.

Trace	Na	CaS	CaT	A	KCa	Kd	H	L	offset (mV)
112	501.14	7.44	6.14	19.69	0.00	125.59	0.00	0.11	10.20
113	499.99	10.00	10.00	39.99	24.99	49.99	0.04	0.03	10.21
115	300.02	10.00	4.00	30.00	15.00	0.00	0.03	0.00	10.21
116	499.96	10.00	6.00	9.98	19.99	99.97	0.01	0.03	10.21
129	499.96	7.50	8.00	29.98	15.00	99.98	0.03	0.04	10.21
135	500.00	10.00	2.00	29.99	20.00	24.99	0.02	0.02	10.21
143	500.01	0.00	4.00	20.02	7.90	99.98	0.04	0.01	10.21
144	300.00	12.50	0.00	49.99	15.00	74.98	0.02	0.05	10.21

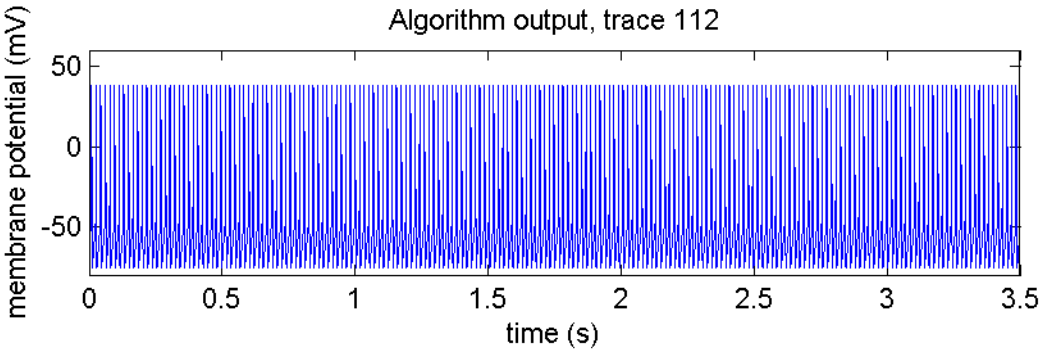

(a) Trace generated by parameters found by inversion algorithm

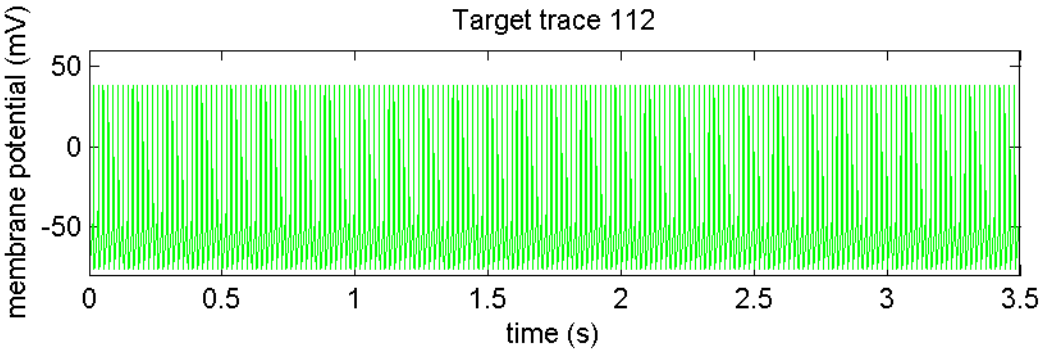

(b) Target trace

Figure 62: Performance of modified inversion algorithm, trace 112

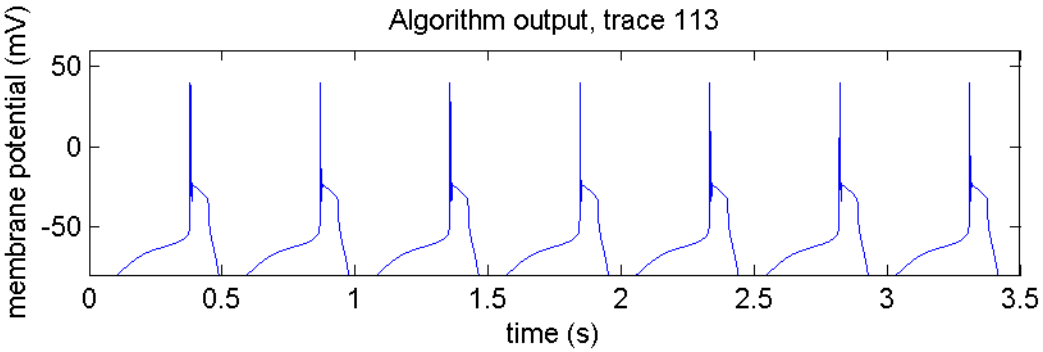

(a) Trace generated by parameters found by inversion algorithm

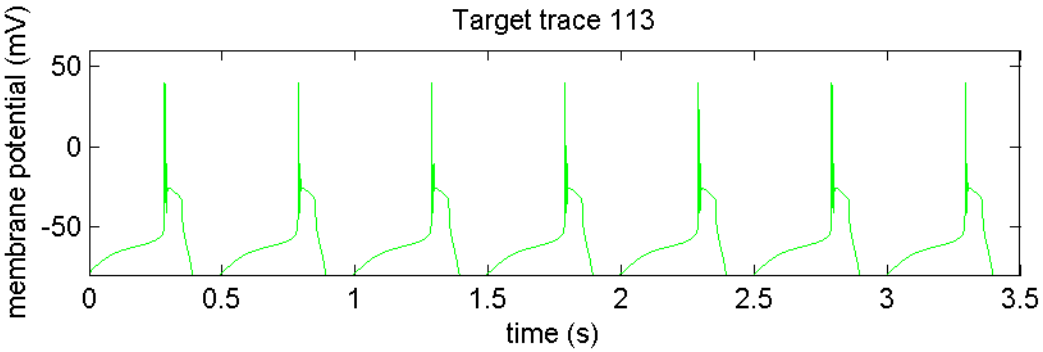

(b) Target trace

Figure 63: Performance of modified inversion algorithm, trace 113

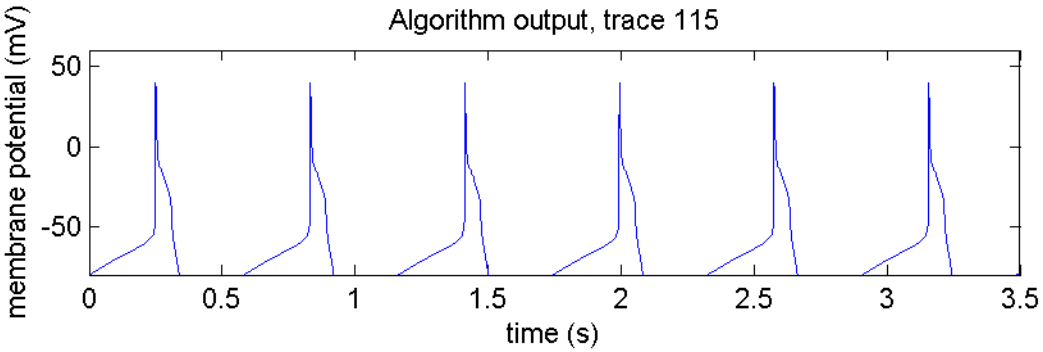

(a) Trace generated by parameters found by inversion algorithm

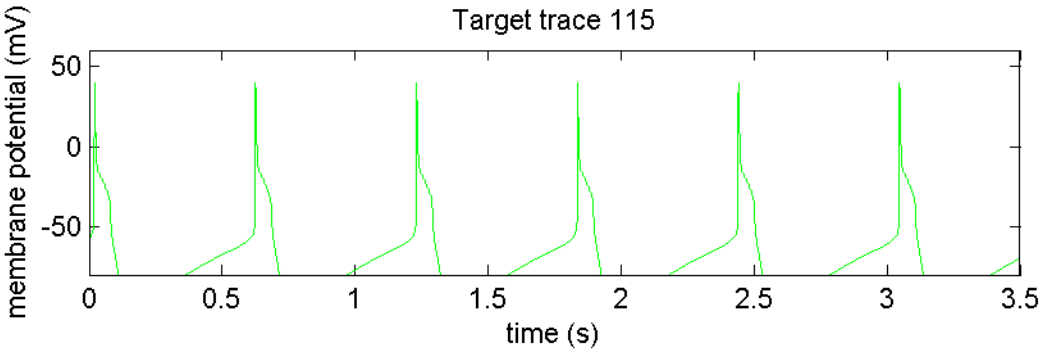

(b) Target trace

Figure 64: Performance of modified inversion algorithm, trace 115

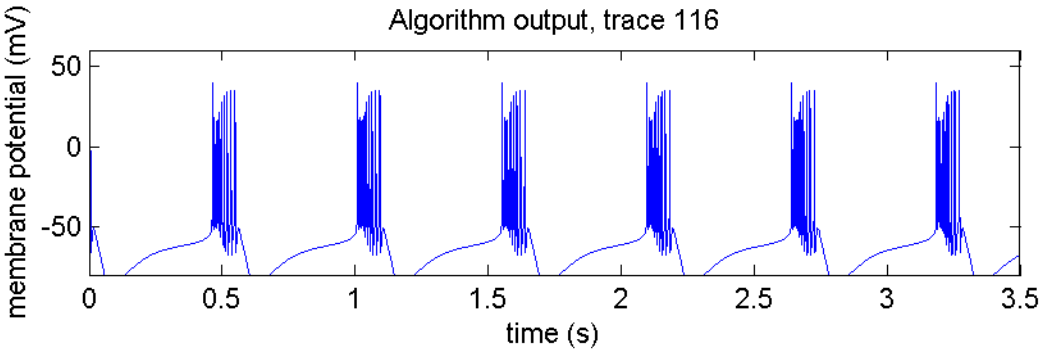

(a) Trace generated by parameters found by inversion algorithm

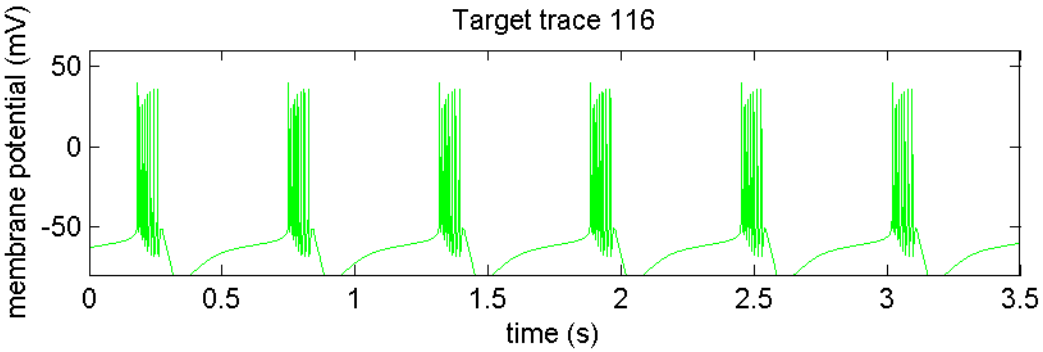

(b) Target trace

Figure 65: Performance of modified inversion algorithm, trace 116

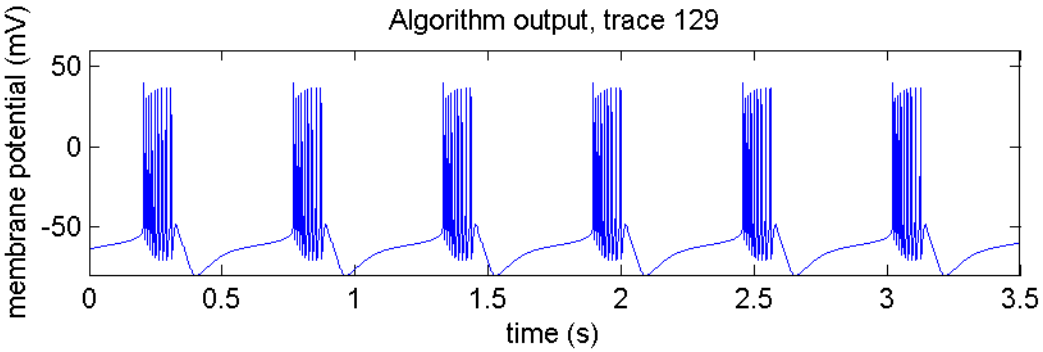

(a) Trace generated by parameters found by inversion algorithm

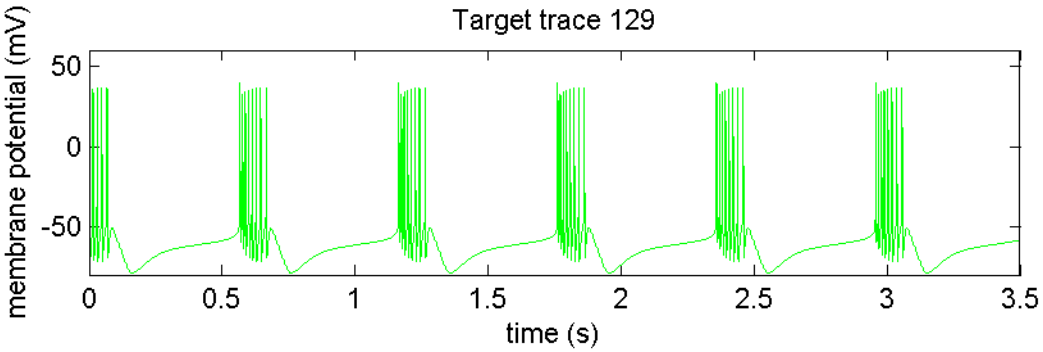

(b) Target trace

Figure 66: Performance of modified inversion algorithm, trace 129

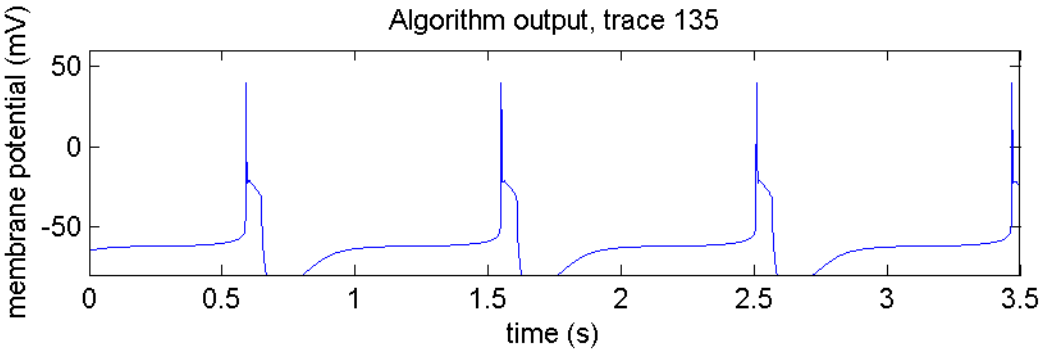

(a) Trace generated by parameters found by inversion algorithm

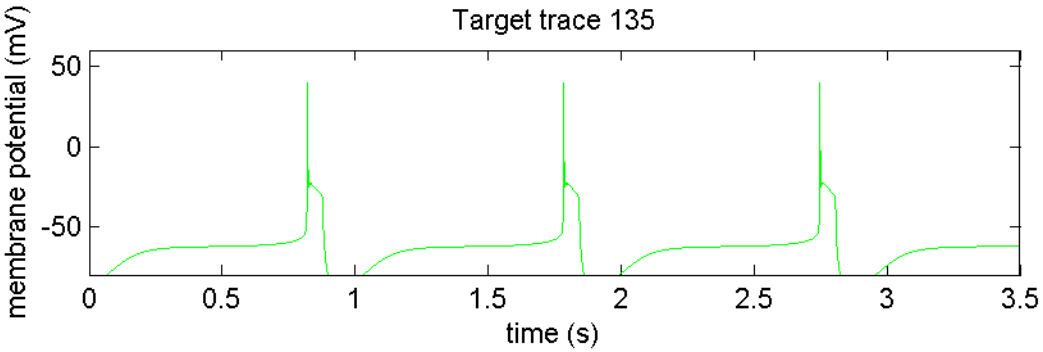

(b) Target trace

Figure 67: Performance of modified inversion algorithm, trace 135

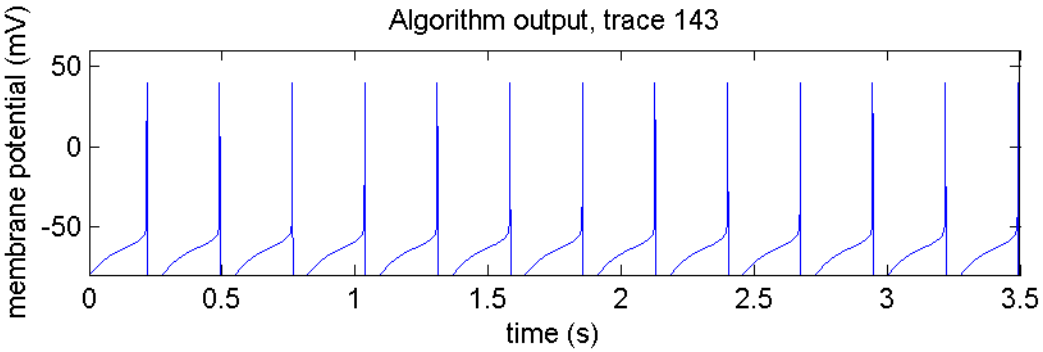

(a) Trace generated by parameters found by inversion algorithm

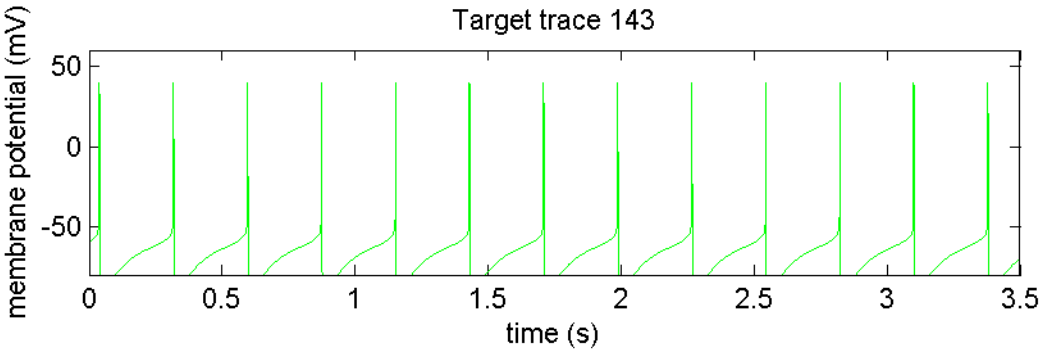

(b) Target trace

Figure 68: Performance of modified inversion algorithm, trace 143

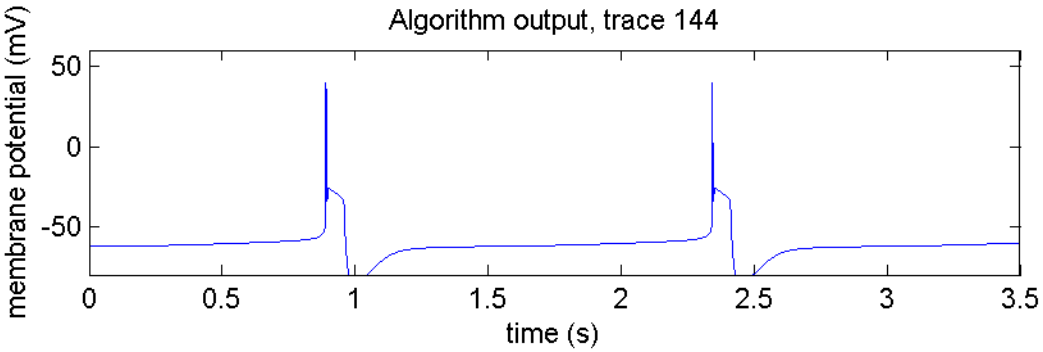

(a) Trace generated by parameters found by inversion algorithm

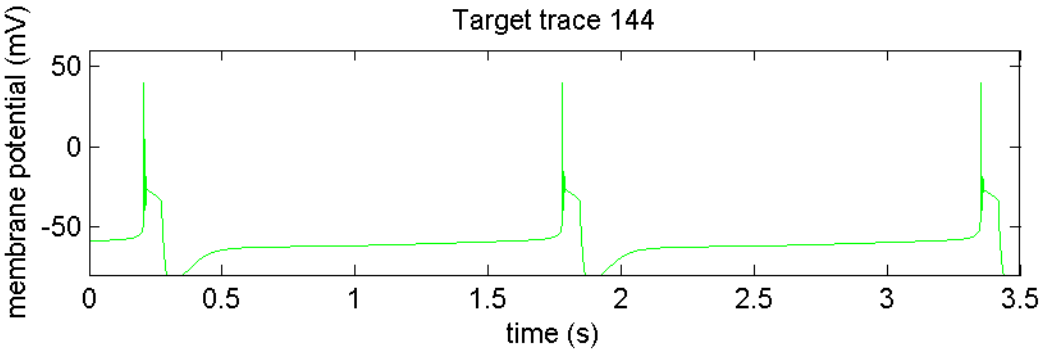

(b) Target trace

Figure 69: Performance of modified inversion algorithm, trace 144

REFERENCES

[1] Achard, P. and De Schutter, E., "Complex parameter landscape for a complex neuron model," *PLoS Comput Biol*, vol. 2, no. 7, pp. 794–804, 2006.

[2] Bhalla, U. and Bower, J., "Exploring parameter space in detailed in single neuron models: simulations of the mitral and granule cells of the olfactory bulb," *J Neurophys*, vol. 69, pp. 1948–1965, 1993.

[3] Butera, R. and McCarthy, M., "Analysis of real-time numerical integration methods applied to dynamic clamp experiments," *J Neural Eng*, vol. 1, pp. 187–194, 2004.

[4] Byrne, J. and Schultz, S., *An introduction to membrane transport and bioelectricity: Foundations of General Physiology and Electrochemical Signaling.* Raven Press, 1994.

[5] Cronin, J., *Mathematics of cell electrophysiology.* Marcel Dekker, Inc., 1981.

[6] Cronin, J., *Mathematical aspects of Hodgkin-Huxley neural theory.* Cambridge University Press, 1987.

[7] Elson, R. and Selverston, A., "Mechanisms of gastric rhythm generation in the isolated stomatogastric ganglion of spiny lobsters: Bursting pacemaker potentials, synaptic interactions, and muscarinic modulation," *J Neurophysiol*, vol. 68, no. 3, pp. 890–907, 1992.

[8] Foster, W., Ungar, L., and Schwaber, J., "Significance of conductances in Hodgkin-Huxley models," *J Neurophysiol*, vol. 70, no. 6, pp. 2502–2518, 1993.

[9] Goldman, M., Golowasch, J., Marder, E., and Abbott, L., "Global structure, robustness, and modulation of neuronal models," *J Neurosci*, vol. 21, pp. 5229–5338, 2001.

[10] Golowasch, J., Goldman, M., Abbott, L., and Marder, E., "Failure of averaging in the construction of a conductance-based neuron model," *J Neurophysiol*, vol. 87, pp. 1129–1131, 2002.

[11] Guckenheimer, J., Gueron, S., and Harris-Warrick, R., "Mapping the dynamics of a bursting neuron," *Phil Trans: Biol Sci*, vol. 341, no. 1298, pp. 345–359, 1993.

[12] Guckenheimer, J., Harris-Warrick, R., Peck, J., and Willms, A., "Bifurcation, bursting, and spike frequency adaptation," *J Comput Neurosci*, vol. 4, pp. 257–277, 1997.

[13] Harris-Warrick, R. and Flamm, R., "Multiple mechanisms of bursting in a conditional bursting neuron," *J Neurosci*, vol. 7, pp. 2113–2128, 1987.

[14] Hausser, M., "The Hodgkin-Huxley theory of the action potential," *Nat Neurosci*, vol. 3, p. 1165, 2000.

[15] Hayes, R., Byrne, J., Cox, S., and Baxter, D., "Estimation of single-neuron parameters from spike train data," *Neurocomputing*, vol. 65, pp. 517–529, 2005.

[16] Hodgkin, A. and Huxley, A., "A quantitative description of membrane current and its application to conduction and excitation in nerve," *J Physiol*, vol. 117, pp. 500–544, 1952.

[17] Isaacson, E. and Keller, H., *Analysis of Numerical Methods*. John Wiley & Sons, 1966.

[18] Jack, J., Noble, D., and Tsien, R., *Electric Current Flow in Excitable Cells*. Clarendon Press, 1975.

[19] Liu, Z., Golowasch, J., Marder, E., and Abbott, L., "A model neuron with activity-dependent conductances regulated by multiple calcium sensors," *J Neurosci*, vol. 18, no. 7, pp. 2309–2320, 1998.

[20] Marder, E. and Goaillard, J.-M., "Variability, compensation and homeostasis in neuron and network function," *Nat Rev Neurosci*, vol. 7, pp. 563–574, 2006.

[21] McCormick, D. and Huguenard, J., "A model of the electrophysiological properties of thalamocortical relay neurons," *J Neurophysiol*, vol. 68, no. 4, pp. 1384–1400, 1992.

[22] Moore, J. and Ramon, F., "On numerical integration of the Hodgkin-Huxley equations for a membrane action potential," *J Theor Biol*, vol. 45, pp. 249–273, 1974.

[23] Prinz, A. A., "Neuronal parameter optimization," *Scholarpedia*, vol. 2, no. 1, p. 1903, 2007.

[24] Prinz, A., Billimoria, C., and Marder, E., "Alternative to hand-tuning conductance-based models: Construction and analysis of databases of model neurons," *J Neurophysiol*, vol. 90, pp. 3998–4015, 2003.

[25] Prinz, A., Bucher, D., and Marder, E., "Similar network activity from disparate circuit parameters," *Nat Neurosci*, vol. 7, pp. 1345–1352, 2004.

[26] Roberge, F., Beaumont, J., and Lemieux, D., "Estimating the parameters of the Hodgkin-Huxley model from peak current voltage-clamp data," *Engineering in Medicine and Biology Society, 1992. Vol.14. Proceedings of the Annual International Conference of the IEEE*, vol. 6, pp. 2322–2324, 1992.

[27] Rush, S. and Larsen, H., "A practical algorithm for solving dynamic membrane equations," *IEEE Trans Biomed Eng*, vol. BME-25, no. 4, pp. 389–392, 1978.

[28] Stewart, G. and Sun, J., *Matrix perturbation theory*. Academic Press, 1990.

[29] Tabak, J., Murphey, C., and Moore, L., "Parameter estimation methods for single neuron models," *J Comput Neurosci*, vol. 9, no. 3, pp. 215–236, 2000.

[30] Tien, J. and Guckenheimer, J., "Parameter estimation for bursting neural models," *J Comput Neurosci*, vol. 24, pp. 358–373, 2008.

[31] Vanier, M. and Bower, J., "A comparative survey of automated parameter-search methods for compartmental neural models," *J Comput Neurosci*, vol. 7, pp. 149–171, 1999.